CHAPTER 27

Filter Banks

Our treatment so far in the book has focused largely on discrete-time systems that operate directly on an input sequence, $x(n)$, and generate an output sequence, $y(n)$. There are applications where it is desirable to decompose the input signal into several subband signals that occupy generally (but not necessarily) minimally overlapping segments of the frequency band. Processing and filtering operations are then performed on the subband signals, and the processed data are combined together to construct the output signal. One key advantage of subband operations is that signal processing can be performed at lower rates within the subbands. Another advantage is that subbands can be emphasized or de-emphasized depending on their contribution to the overall processing task. Subband processing is usually achieved by means of filter banks, which consist of analysis and synthesis components, as we proceed to explain.

27.1 ANALYSIS FILTER BANK

Figure 27.1 shows a general structure for an M-band analysis filter bank. The input signal $x(n)$ is filtered through M filters, $A_k(z)$, to generate M subband signals, $u'_k(n)$. In many instances, but not always, the frequency responses of the analysis filters, $A_k(z)$, tend to be minimally overlapping. In the realization indicated in the figure, each of the subband signals, $u'_k(n)$, will have the same number of samples as the original signal, $x(n)$. In this way, it would appear that the analysis filter bank generates a total number of samples that is M times larger than the original number of samples in $x(n)$. However, as the discussion will reveal, more efficient implementations are possible by modifying the filter bank structure in order to exploit the fact that the bandwidth of each of the analysis filters, $A_k(z)$, is generally M times smaller than the bandwidth of the original sequence, $x(n)$.

27.1.1 Uniform Filter Banks

Figure 27.2 illustrates one example of the frequency responses of minimally overlapping analysis filters, $A_k(z)$. The frequency band $[0, 2\pi]$ is divided into segments of width $2\pi/M$ each. The filter $A_o(e^{j\omega})$ is a low-pass causal filter with cutoff frequency π/M radians/sample and with a transition region extending between ω_p and ω_s radians/sample. Although unnecessary, the magnitude response of $A_o(e^{j\omega})$ can be assumed to be approximately equal to one in its passband region so that when the signal $x(n)$ is filtered by $A_o(e^{j\omega})$, the frequency content of $x(n)$ over the bandwidth of $A_o(e^{j\omega})$ does not undergo significant change in magnitude. If this is not the case, namely, if the magnitude response of $A_o(e^{j\omega})$ ends up scaling the frequency content of $x(n)$ in its passband, then during the reconstruction procedure (described later when we study synthesis filter banks in Sec. 27.2),

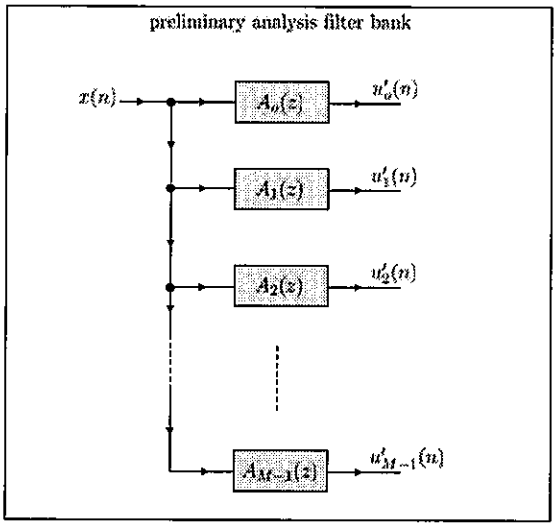

FIGURE 27.1 General structure of an $M-$band analysis filter bank. The input sequence $x(n)$ is separated into M subband signals, $u'_k(n)$. In this structure, the frequency responses of the analysis filters, $A_k(z)$, are chosen to be generally minimally overlapping.

the scaling introduced by the analysis filters will need to be undone by the synthesis filters. For this reason, in the sequel, we will not restrict the magnitude response of $A_o(e^{j\omega})$ to unity in the passband, and will comment later on how the synthesis filters can help adjust for any scaling introduced by the analysis filters (see, e.g., Sec. 27.5 on perfect reconstruction filter banks).

Starting from the low-pass filter $A_o(e^{j\omega})$, the other filters in Fig. 27.2 can be obtained by shifting the frequency response of $A_o(e^{j\omega})$ to the locations $\frac{2\pi k}{M}$ for $k = 1, 2, \ldots, M-1$. In this case, all analysis filters will be uniformly shifted versions of $A_o(e^{j\omega})$, namely,

$$\boxed{A_k(e^{j\omega}) \;=\; A_o\left(e^{j\left(\omega-\frac{2\pi k}{M}\right)}\right)} \tag{27.1}$$

For this reason, we refer to such filter banks as *uniform filter banks*, and the filter $A_o(z)$ is called the *prototype* filter. We also say that the subband filters $A_k(z)$ are modulated versions of the prototype filter $A_o(z)$ for the following reason. Let $a_k(n)$ denote the impulse response sequence of $A_k(z)$. Using the frequency-shift property (14.23) of the DTFT we can relate $a_k(n)$ to $a_o(n)$ as follows:

$$\boxed{a_k(n) \;=\; e^{j\frac{2\pi kn}{M}}\, a_o(n)} \tag{27.2}$$

It also follows from this result that the transfer functions satisfy (recall the scaling property (9.60)):

$$\boxed{A_k(z) = A_o\left(ze^{-j\frac{2\pi k}{M}}\right)} \tag{27.3}$$

Baseband Processing

While the frequency content of the original signal, $x(n)$, may spread over the entire frequency range $[0, 2\pi]$, the frequency bandwidth of each of the filters, $A_k(z)$, is limited to

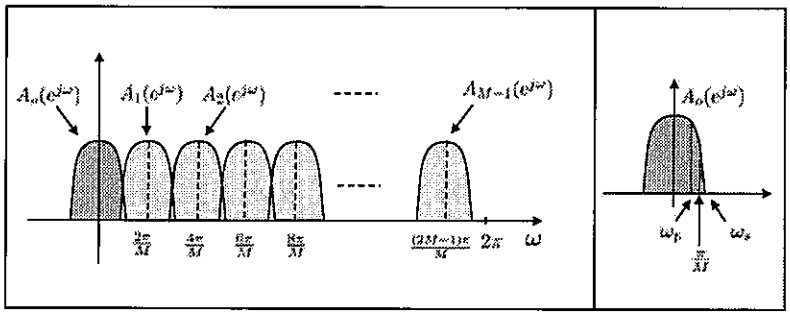

FIGURE 27.2 An illustration of minimally overlapping frequency responses of the analysis filters, $A_k(z)$. The bandwidth of each analysis filter is approximately $\frac{2\pi}{M}$ radians/sample; and the filters are centered at locations $\frac{2\pi k}{M}$ for $k = 0, 1, \ldots, M-1$.

approximately $\frac{2\pi}{M}$ radians/sample and spreads mainly over the region

$$\left[\frac{(2k-1)\pi}{M}, \frac{(2k+1)\pi}{M}\right] \tag{27.4}$$

Accordingly, the frequency content of each of the subband signals, $u'_k(n)$, is largely contained within this same interval. The limited bandwidth of the $\{A_k(z)\}$ can be exploited to reduce the processing rate of the filters appearing in Fig. 27.1 by a factor of M. This objective can be accomplished by replacing the subband signals, $u'_k(n)$, by alternative signals, $u''_k(n)$, whose frequency content is shifted to baseband to lie within the interval $[-\pi/M, \pi/M]$. To see how this is done, assume we modify the analysis filter bank of Fig. 27.1 by scaling the output of each filter, $A_k(z)$, by the factor $e^{-j2\pi kn/M}$, as illustrated in Fig. 27.3; the subband signals are now denoted by $u''_k(n)$ and they are baseband signals.

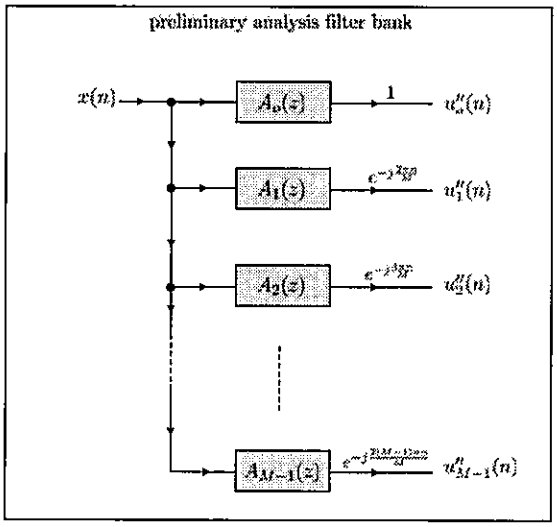

FIGURE 27.3 Analysis filter bank with the frequency responses of the analysis filters shifted to baseband through scaling of their outputs by the factors $e^{-j2\pi kn/M}$, as illustrated in the bottom plot for a generic branch k.

Indeed, consider the $k-$th branch shown on the left-hand side of Fig. 27.4. Then,

$$\begin{aligned} u_k''(n) &= e^{-j\frac{2\pi kn}{M}} \; (x(n) \star a_k(n)) \\ &= e^{-j\frac{2\pi kn}{M}} \; \left(\sum_{m=0}^{\infty} a_k(m) x(n-m) \right) \\ &= \sum_{m=0}^{\infty} \left[\left(a_k(m) e^{-j\frac{2\pi km}{M}} \right) \left(x(n-m) e^{-j\frac{2\pi k(n-m)}{M}} \right) \right] \\ &= \sum_{m=0}^{\infty} \left[a_o(n) \left(x(n-m) e^{-j\frac{2\pi k(n-m)}{M}} \right) \right] \quad \text{(using (27.2))} \\ &= a_o(n) \star x(n) e^{-j\frac{2\pi kn}{M}} \end{aligned} \tag{27.5}$$

The last equality indicates that $u_k''(n)$ can be alternatively obtained by first scaling $x(n)$ by $e^{-j2\pi kn/M}$ and then filtering the result by the baseband filter, $A_o(z)$, as illustrated in the right-hand side of Fig. 27.4.

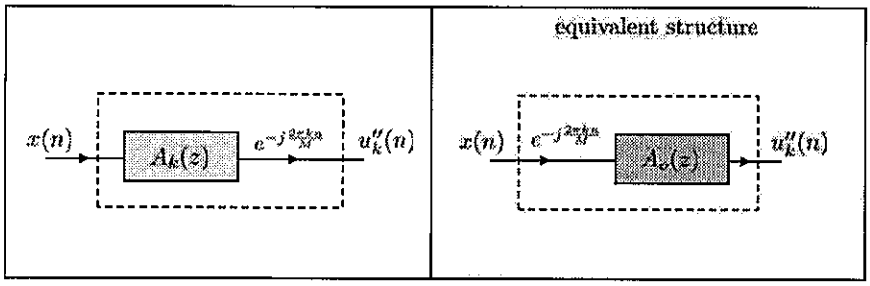

FIGURE 27.4 The two branches are equivalent: scaling by $e^{-j2\pi kn/M}$ followed by filtering by $A_o(z)$ is equivalent to filtering first by $A_k(z)$ and then scaling by $e^{-j2\pi kn/M}$.

Interpretation. Scaling $x(n)$ by $e^{-j2\pi kn/M}$ shifts its frequency content to the left by $2\pi k/M$ radians/sample. In this way, the frequency content of $x(n)$ that is centered around $2\pi k/M$ is shifted down to baseband and centered around $\omega = 0$. By filtering the result by $A_o(z)$ we are, therefore, extracting that portion of the frequency content of $x(n)$ that was originally centered around $2\pi k/M$. This same effect is attained if we first filter $x(n)$ by $A_k(z)$ (which extracts the portion of the frequency content of $x(n)$ that is centered around $2\pi k/M$), and then scale the result by $e^{-j2\pi kn/M}$ in order to shift it down to baseband. Using the equivalence result of Fig. 27.4 we can therefore replace the analysis filter bank of Fig. 27.3 by the revised structure shown in Fig. 27.5.

$\diamond$

Downsampling

We continue for now with the filter bank from Fig. 27.3, which is defined in terms of the analysis filters $\{A_k(z)\}$. Since the bandwidth of the baseband signals $\{u_k''(n)\}$ lies within $[-\frac{\pi}{M}, \frac{\pi}{M}]$ radians/sample, we can downsample them by a factor of M and, therefore, perform processing at a lower rate; recall from Fig. 26.16 that the effect of decimation on the frequency bandwidth of a signal is to expand its bandwidth by a factor of M. Figure 27.6 shows the analysis filter bank with downsampling by a factor of M; the resulting subband

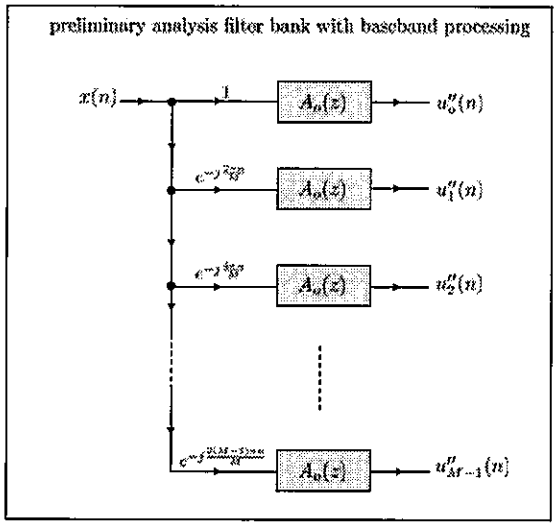

FIGURE 27.5 An equivalent implementation of the analysis filter bank of Fig. 27.3 where the scaling factors $e^{-j2\pi nk/M}$ have been moved before the filters and all filters are replaced by the prototype filter $A_o(z)$.

signals are now denoted by $u_k(n)$ and the bandwidth of each one of them extends over the entire frequency range $[0, 2\pi]$.

Now, recall that a downsampler by a factor of M keeps the samples that occur at time instants that are multiples of M and discards all other samples. Thus, referring to the bottom part of Figure 27.6, which illustrates the $k-$th processing branch of the filter bank, we have

$$\begin{aligned} u_k(n) &= u_k''(nM) \\ &= e^{-j\frac{2\pi nMk}{M}} u_k'(nM) \\ &= e^{-j2\pi nk} u_k'(nM) \\ &= u_k'(nM) \end{aligned} \tag{27.6}$$

This result indicates that the scaling factor $e^{-j2\pi nk/M}$ can be ignored in Fig. 27.6 and the downsampling operation can be applied directly to the output of the analysis filters, $A_k(z)$. In this way, we arrive at the analysis filter bank structure shown in Fig. 27.7.

Example 27.1 (An analysis filter bank)

Assume the low-pass prototype filter is selected as a moving-average filter of order $2M$, i.e.,

$$A_o(z) = \sum_{n=0}^{2M-1} z^{-n} = 1 + z^{-1} + z^{-2} + \ldots + z^{-(2M-1)} \tag{27.7}$$

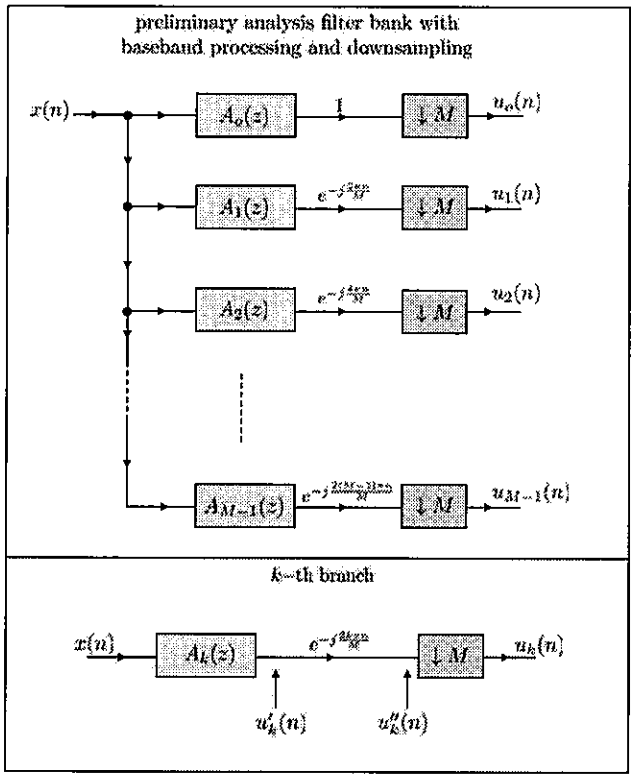

FIGURE 27.6 Analysis filter bank with downsamplers by a factor of M. The bottom part shows the processing that is performing across the $k-$th branch. The output of $A_k(z)$ is denoted by $u'_k(n)$ and the input to the downsampler is denoted by $u''_k(n)$.

This filter has the rectangular window as its impulse response sequence. We already know from (13.20) that the frequency response of $A_o(z)$ is given by

$$A_o(e^{j\omega}) = \begin{cases} 2M, & \omega = 0 \\ e^{-j\omega\frac{2M-1}{2}} \left(\dfrac{\sin(\omega M)}{\sin(\omega/2)}\right), & \text{otherwise} \end{cases} \tag{27.8}$$

The magnitude response of the filter is shown in Fig. 27.8 for the case $M = 8$; in the figure, the maximum magnitude response is normalized to 0 dB. We note that the first zero crossing occurs at $\omega_o = \pi/M$, which is effectively half the width of the main lobe. We thus have that the approximate bandwidth of $A_o(z)$ is $2\pi/M$ radians/sample. The attenuation of the first side lobe is approximately 13 dB relative to the main lobe. Obviously, the prototype filter, $A_o(e^{j\omega})$, is not an ideal low-pass filter; its magnitude response is not flat in the pass-band. Observe also that the frequency gain at $\omega = 0$ is equal to $2M$ (and not unity). Later, when we design the corresponding synthesis filter bank, we will need to account for this amplification.

The frequency responses of all other analysis filters, $A_k(z)$, are obtained from $A_o(e^{j\omega})$ by shifting the latter to the frequency locations $\frac{2\pi k}{M}$, $k = 1, 2, \ldots, M-1$. Since the bandwidths of the filters $A_k(z)$ overlap, and since the side lobe attenuation in each filter is not high enough relative to the main lobe, the bands of the resulting signals $u'_k(n)$ in Fig. 27.7 are not mutually exclusive (or well separated) in this case. Nevertheless, despite these undesirable properties, we will continue to use this simple prototype construction to illustrate several of the concepts in subband decomposition.

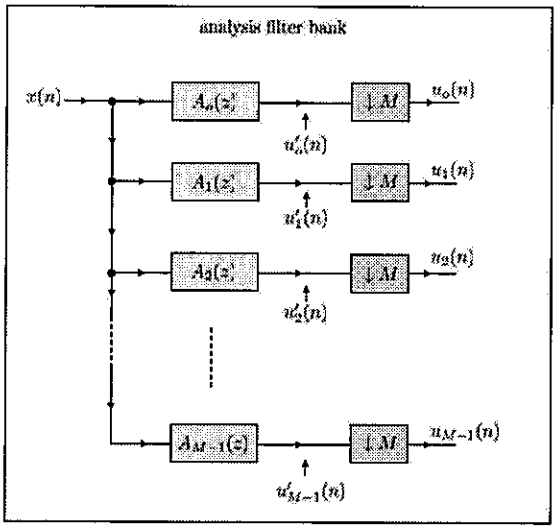

FIGURE 27.7 Structure of the analysis filter bank. It consists of a bank of filters, $A_k(z)$, with frequency responses centered around $\frac{2\pi k}{M}$ and of width $\frac{2\pi}{M}$ radians/sample each, followed by downsampling by a factor of M. The bandwidth of each of the subband signals, $u_k(n)$, extends over the entire range $[0, 2\pi]$. The output signal of each of the subband filters is denoted by $u'_k(n)$.

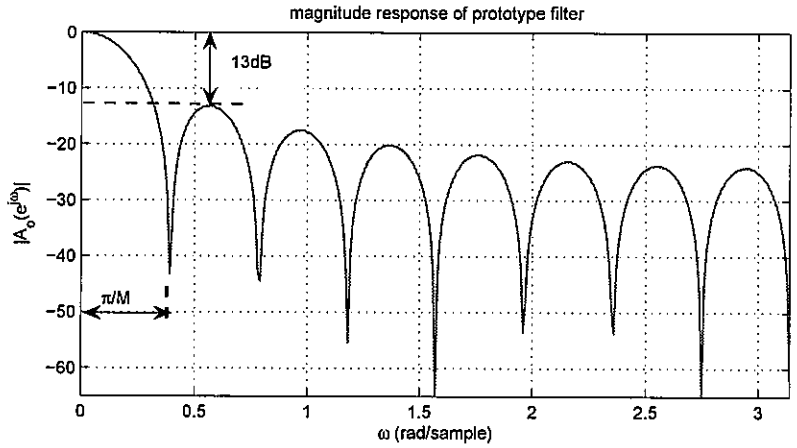

FIGURE 27.8 Magnitude frequency response of the prototype filter $A_o(z)$ defined by (27.7) for $M = 8$. The first zero crossing occurs at $\omega_o = \frac{\pi}{M} \approx 0.3927$ radians/sample.

Analysis filter banks with significantly better performance will be presented later — see Example 27.8.

Let us consider the case $M = 2$, in which case the analysis filter bank of Fig. 27.7 will consist of two branches with analysis filters given by (recall (27.3) and see Fig. 27.9):

$$A_o(z) = 1 + z^{-1} + z^{-2} + z^{-3} \tag{27.9}$$

$$A_1(z) = A_o(-z) = 1 - z^{-1} + z^{-2} - z^{-3} \tag{27.10}$$

Figure 27.10 shows the frequency responses of both filters over the range $[0, \pi]$ radians/sample, with the maximum gain normalized to 0 dB. The bandwidth of each filter is approximately π radi-

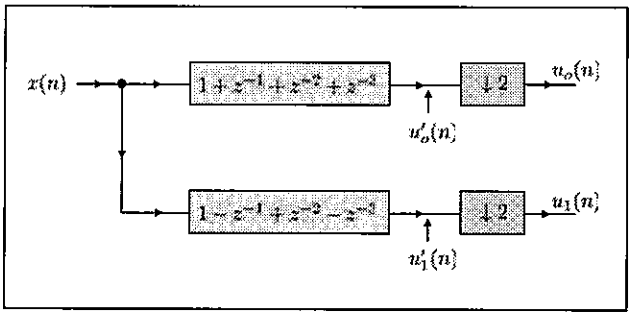

FIGURE 27.9 An analysis filter bank with 2 branches using the prototype filter $A_o(z) = 1 + z^{-1} + z^{-2} + z^{-3}$.

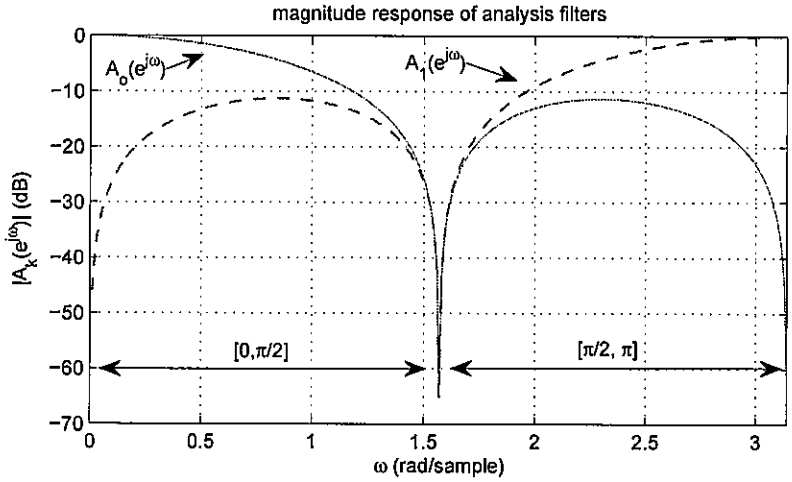

FIGURE 27.10 Magnitude frequency response of the analysis filters $A_o(z) = 1 + z^{-1} + z^{-2} + z^{-3}$ and $A_1(z) = 1 - z^{-1} + z^{-2} - z^{-3}$ from Example 27.1. The maximum magnitude is normalized to 0dB in both cases.

ans/sample; the bandwidth of the filter $A_o(z)$ covers the range of frequencies $[-\frac{\pi}{2}, \frac{\pi}{2}]$, while the bandwidth of the filter $A_1(z)$ covers the range of frequencies $[\frac{\pi}{2}, \pi]$ and $[-\pi, -\frac{\pi}{2}]$.

Figures 27.11 and 27.12 plot the time-domain sequences $x(n)$, $u'_o(n)$, $u'_1(n)$, $u_o(n)$, and $u_1(n)$ that would result from using

$$x(n) = \sin\left(\frac{\pi}{4}n\right) + 0.5\sin\left(\frac{5\pi}{4}n\right) \tag{27.11}$$

Figures 27.13 and 27.14 plot the magnitude frequency content of the same sequences over the interval $[0, \pi]$.

◇

27.1.2 DFT Analysis Filter Bank

Let us return to the analysis filter bank of Fig. 27.7. There are many ways by which the analysis filters, $A_k(z)$, can be implemented. We illustrate one useful technique in this section that is based on the use of the DFT.

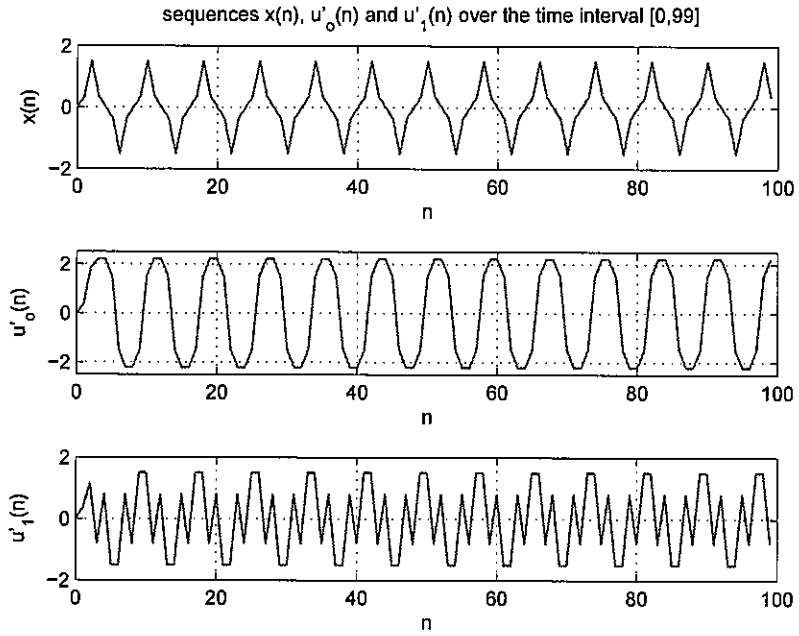

FIGURE 27.11 Original sequence (top) and the outputs, $u_o'(n)$ and $u_1'(n)$, of the analysis filters (middle and bottom) over the interval $n \in [0, 99]$ for Example 27.1.

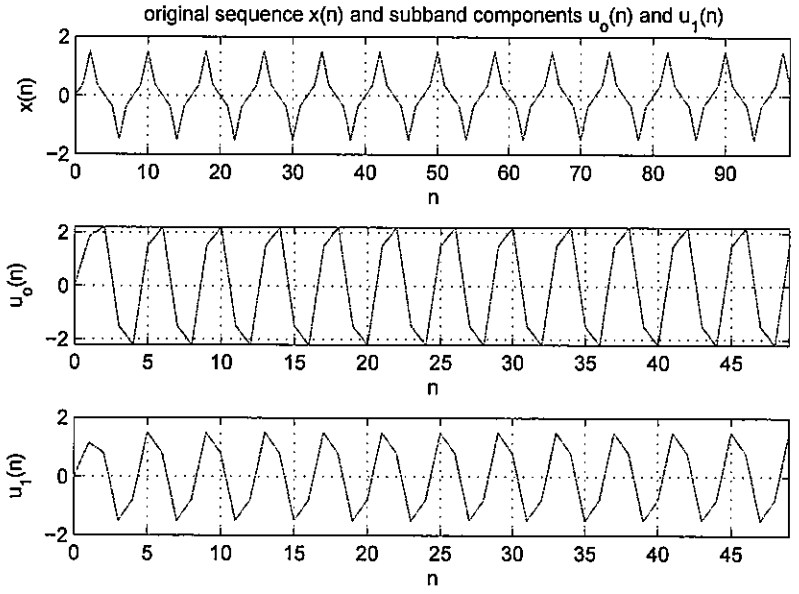

FIGURE 27.12 Original sequence (top) over the interval $n \in [0, 99]$ and the outputs of the downsamplers (middle and bottom) over the interval $n \in [0, 49]$ for Example 27.1.

We resort to the M-th order polyphase decomposition (cf. (26.64)) of the prototype filter $A_o(z)$, say,

$$A_o(z) = \sum_{m=0}^{M-1} z^{-m} E_m(z^M) \tag{27.12}$$

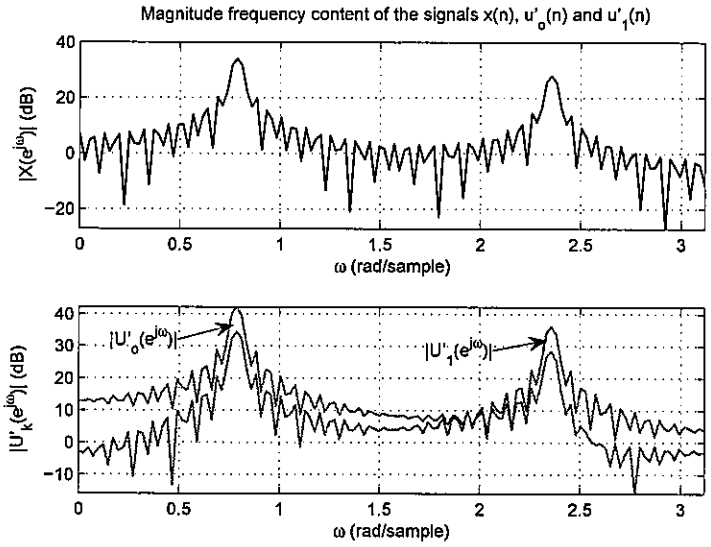

FIGURE 27.13 Magnitude frequency content of the original sequence, $x(n)$ (top), and of the outputs of the analysis filters, $\{u'_o(n), u'_1(n)\}$ (bottom), over the interval $\omega \in [0, \pi]$ for Example 27.1.

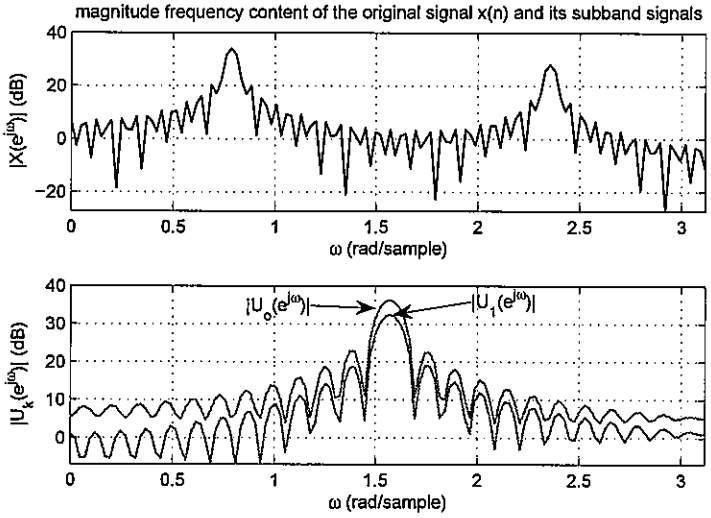

FIGURE 27.14 Magnitude frequency response of the original sequence, $x(n)$ (top), and of the outputs of the downsamplers, $\{u_o(n), u_1(n)\}$ (bottom), over the interval $\omega \in [0, \pi]$ for Example 27.1.

Let W_M denote the $M-$th root of unity, i.e.,

$$W_M \triangleq e^{-j\frac{2\pi}{M}} \tag{27.13}$$

Then, each filter $A_k(z)$ can be expressed in terms of the same $\{E_m(z)\}$ as follows:

$$\begin{aligned} A_k(z) &\triangleq A_o\left(ze^{-j2\pi k/M}\right) \quad \text{(using (27.3))} \\ &= \sum_{m=0}^{M-1} z^{-m} e^{j2\pi km/M} E_m\left(z^M\right) \\ &= \sum_{m=0}^{M-1} z^{-m} W_M^{-mk} E_m\left(z^M\right) \end{aligned} \tag{27.14}$$

Relation (27.14) can be rewritten in the form of an inner product, namely,

$$\boxed{A_k(z) = \begin{bmatrix} 1 & W_M^{-k} & W_M^{-2k} & \ldots & W_M^{-(M-1)k} \end{bmatrix} \begin{bmatrix} E_o(z^M) \\ z^{-1}E_1(z^M) \\ z^{-2}E_2(z^M) \\ \vdots \\ z^{-(M-1)}E_{M-1}(z^M) \end{bmatrix}} \tag{27.15}$$

Let us introduce the DFT matrix of size $M \times M$:

$$F_M \triangleq \begin{bmatrix} 1 & 1 & 1 & 1 & \ldots & 1 \\ 1 & W_M & W_M^2 & W_M^3 & \ldots & W_M^{M-1} \\ 1 & W_M^2 & W_M^4 & W_M^6 & \ldots & W_M^{2(M-1)} \\ \vdots & \vdots & & & \ddots & \\ 1 & W_M^{(M-1)} & W_M^{2(M-1)} & W_M^{3(M-1)} & \ldots & W_M^{(M-1)^2} \end{bmatrix} \tag{27.16}$$

We showed in Sec. 17.5 that F_M satisfies

$$\boxed{F_M F_M^* = M \cdot I_M} \tag{27.17}$$

where I_M denotes the $M \times M$ identity matrix and F_M^* denotes the matrix that is obtained from F_M by complex conjugating its entries and then transposing the matrix. But since

$$\left(W_M^k\right)^* = W_M^{-k} \tag{27.18}$$

we find that F_M^* is given by

$$F_M^* = \begin{bmatrix} 1 & 1 & 1 & 1 & \ldots & 1 \\ 1 & W_M^{-1} & W_M^{-2} & W_M^{-3} & \ldots & W_M^{-(M-1)} \\ 1 & W_M^{-2} & W_M^{-4} & W_M^{-6} & \ldots & W_M^{-2(M-1)} \\ \vdots & \vdots & & & \ddots & \\ 1 & W_M^{-(M-1)} & W_M^{-2(M-1)} & W_M^{-3(M-1)} & \ldots & W_M^{-(M-1)^2} \end{bmatrix} \tag{27.19}$$

where, compared with the expression for F_M, the exponents have been negated. If we now group together expressions (27.15) for $k = 0, 1, \ldots, M-1$, we obtain the revealing relation

$$\begin{bmatrix} A_o(z) \\ A_1(z) \\ A_2(z) \\ \vdots \\ A_{M-1}(z) \end{bmatrix} = F_M^* \begin{bmatrix} E_o(z^M) \\ z^{-1}E_1(z^M) \\ z^{-2}E_2(z^M) \\ \vdots \\ z^{-(M-1)}E_{M-1}(z^M) \end{bmatrix} \tag{27.20}$$

This result indicates that the general analysis filter bank of Fig. 27.7 can be implemented in terms of the polyphase components of $A_o(z)$ as illustrated in Fig. 27.15. In the figure, we are denoting the signals before and after the DFT operation, F_M^*, by $t_k(n)$ and $u'_k(n)$, respectively. These signals are related as follows:

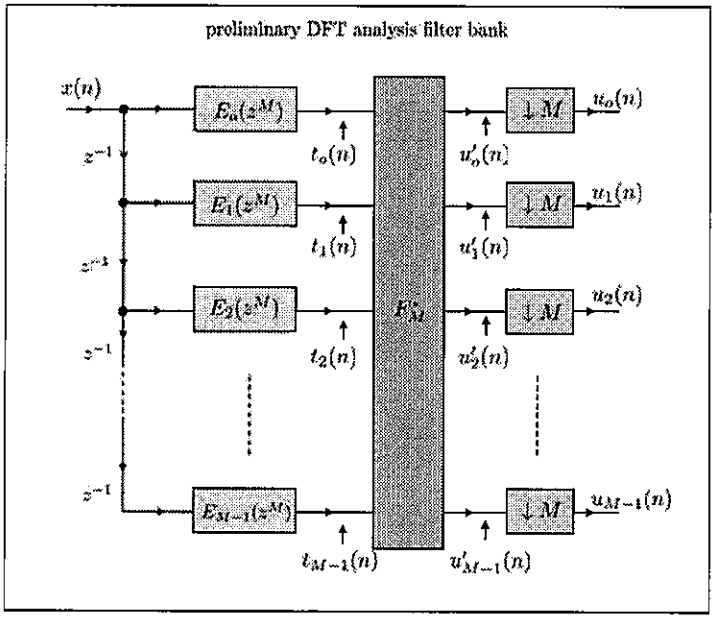

FIGURE 27.15 Uniform DFT analysis filter bank in terms of the $M-$th order polyphase representation of the prototype filter, $A_o(z)$, and where F_M^* denotes the $M \times M$ complex conjugate DFT matrix (27.19).

$$\begin{bmatrix} u'_o(n) \\ u'_1(n) \\ u'_2(n) \\ \vdots \\ u'_{M-1}(n) \end{bmatrix} = F_M^* \begin{bmatrix} t_o(n) \\ t_1(n) \\ t_2(n) \\ \vdots \\ t_{M-1}(n) \end{bmatrix} \tag{27.21}$$

We now argue that the downsamplers can be moved before the DFT operation by first noting that

$$u_k(n) = u'_k(nM) \tag{27.22}$$

so that using (27.21) we have

$$\begin{bmatrix} u_o(n) \\ u_1(n) \\ u_2(n) \\ \vdots \\ u_{M-1}(n) \end{bmatrix} = F_M^* \begin{bmatrix} t_o(nM) \\ t_1(nM) \\ t_2(nM) \\ \vdots \\ t_{M-1}(nM) \end{bmatrix} \tag{27.23}$$

This result shows that we can first downsample the signals $t_k(n)$ to obtain $t_k(nM)$ and then apply the DFT operation, F_M^*, to the signals $t_k(nM)$. This construction is illustrated in Fig. 27.16, where the downsamplers have been moved before the DFT operation.

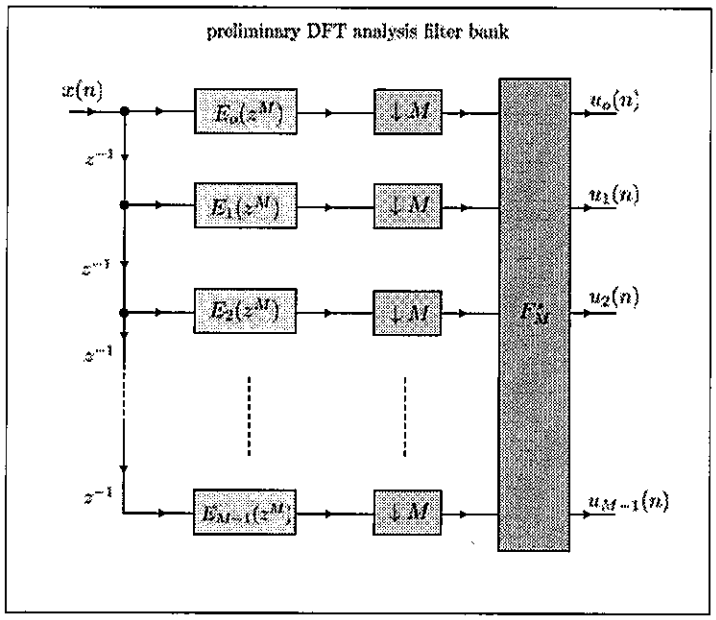

FIGURE 27.16 Equivalent implementation of the uniform DFT analysis filter bank with the downsamplers of Fig. 27.15 now appearing before the DFT operation. .

We can finally invoke the cascade equivalence result shown earlier in Fig. 26.25 to move the downsamplers before the polyphase components and arrive at the DFT filter bank implementation shown in Fig. 27.17.

Example 27.2 (A DFT analysis filter bank)

Let us return to Example 27.1 where the prototype filter was chosen as the moving-average filter (27.7). Let $M = 4$. Then the polyphase components of $A_o(z)$ of order 4 are given by:

$$E_o(z^4) = 1 + z^{-4} \tag{27.24a}$$
$$E_1(z^4) = 1 + z^{-4} \tag{27.24b}$$
$$E_2(z^4) = 1 + z^{-4} \tag{27.24c}$$
$$E_3(z^4) = 1 + z^{-4} \tag{27.24d}$$

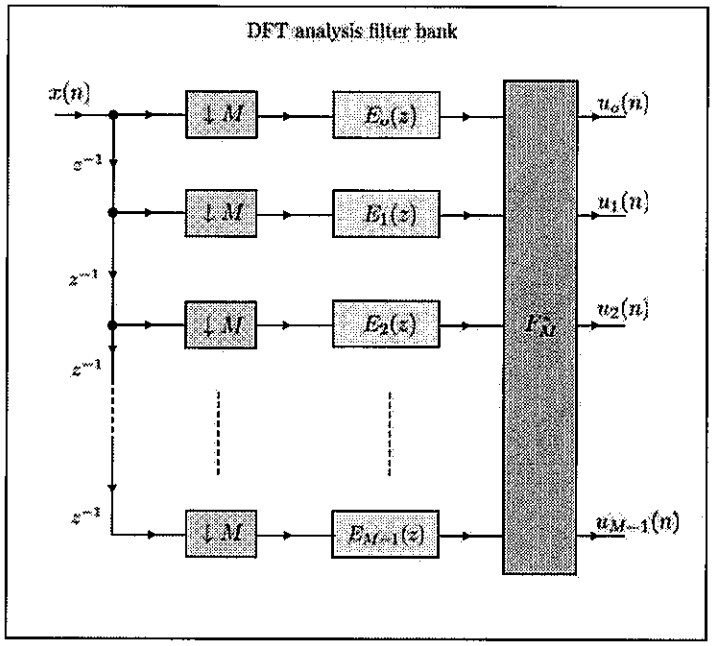

FIGURE 27.17 Efficient implementation of the uniform analysis filter bank of Fig. 27.7 by means of the DFT. The $E_k(z)$ are the $M-$th order polyphase components of the prototype filter, $A_o(z)$.

and the 4×4 DFT matrix is given by

$$F_4^* = \begin{bmatrix} 1 & 1 & 1 & 1 \\ 1 & j & -1 & -j \\ 1 & -1 & 1 & -1 \\ 1 & -j & -1 & j \end{bmatrix} \tag{27.25}$$

The DFT analysis filter bank that corresponds to this choice of $A_o(z)$ is shown in Fig. 27.18.

Let us further consider the case $M = 2$, which was studied in Example. 27.1 and which corresponds to the prototype filter

$$A_o(z) = 1 + z^{-1} + z^{-2} + z^{-3} \tag{27.26}$$

The resulting polyphase filters are

$$E_o(z^2) = 1 + z^{-2}, \quad E_1(z^2) = 1 + z^{-2} \tag{27.27}$$

and the resulting DFT analysis filter bank is shown in Fig. 27.19 where

$$F_2^* = \begin{bmatrix} 1 & 1 \\ 1 & -1 \end{bmatrix} \tag{27.28}$$

$\diamond$

27.2 SYNTHESIS FILTER BANKS

The discussion in the previous section explains how to decompose a signal $x(n)$ into subband signals, $u_k(n)$, e.g., as shown in Figs. 27.7 and 27.17. We now address the reverse construction, namely, given subband signals $u_k(n)$, we study how to reconstruct the signal

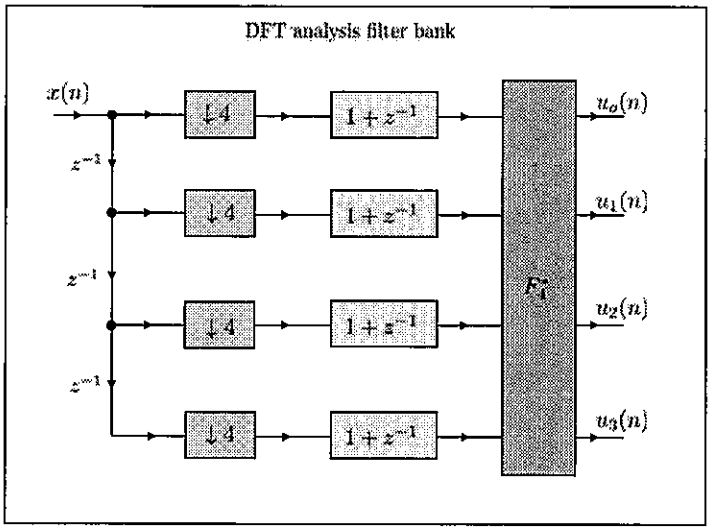

FIGURE 27.18 A DFT analysis filter bank corresponding to a choice of the prototype filter $A_o(z)$ as an 8−th order moving average window of the form (27.7) with a rectangular impulse response sequence — see Example 20.2.

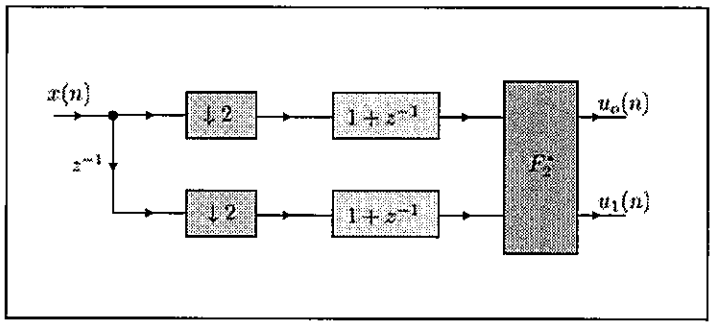

FIGURE 27.19 DFT analysis filter bank with 2 branches corresponding to the prototype filter $A_o(z) = 1 + z^{-1} + z^{-2} + z^{-3}$ from Example 27.2.

$x(n)$. However, we should note that there are several sources of imperfection that will interfere with the fidelity of the reconstruction procedure:

(1) First, the analysis filters $\{A_k(z)\}$ are not ideal filters and they usually overlap in the frequency domain. Interference between adjacent bands in the analysis bank is one source of distortion in the reconstruction procedure.

(2) Second, the analysis filters, as well as the synthesis filters to be discussed in this section, have phase responses and group delays. As such, signals traveling through these filters will be subjected to delay. For this reason, the reconstructed signal will exhibit some delay relative to the original signal, $x(n)$.

(3) Third, if the gain of the analysis filters in their passband regions is not unity, then the synthesis filters will need to compensate for the scaling that was introduced by the analysis filters.

As a result of these imperfections, the synthesis filter bank is generally unable to reproduce the exact original sequence, $x(n)$, but will instead yield some delayed (and sometimes

scaled) approximation for it, say, $x'(n-d)$, for some delay $d > 0$.

27.2.1 Uniform Filter Bank

We motivate a uniform structure for synthesis as follows. Let $S_o(z)$ denote a causal low-pass prototype filter with cutoff frequency $\frac{\pi}{M}$ radians/sample and with a transition region extending between ω_p and ω_s radians/sample, in a manner similar to $A_o(z)$ in Fig. 27.2. In general, the prototype filters used for the analysis and synthesis filter banks need not be the same. For this reason, we are using separate notation to refer to them: $A_o(z)$ in the analysis case and $S_o(z)$ in the synthesis case. The other synthesis filters are obtained by shifting the frequency response of $S_o(e^{j\omega})$ to the locations $\frac{2\pi k}{M}$ for $k = 1, 2, \ldots, M-1$, say,

$$\boxed{S_k(e^{j\omega}) \;=\; S_o\left(e^{j\left(\omega - \frac{2\pi k}{M}\right)}\right)} \tag{27.29}$$

or, equivalently,

$$\boxed{S_k(z) = S_o\left(ze^{-j\frac{2\pi k}{M}}\right)} \tag{27.30}$$

We are again dealing with a uniform filter bank but now for synthesis purposes. We say that the subband filters $S_k(z)$ are modulated versions of the prototype filter $S_o(z)$ for the following reason. If we let $s_k(n)$ denote the impulse response sequence of $S_k(z)$, then using the frequency-shift property (14.23) of the DTFT we can relate $s_k(n)$ to $s_o(n)$ as follows:

$$\boxed{s_k(n) \;=\; e^{j\frac{2\pi kn}{M}} \cdot s_o(n)} \tag{27.31}$$

Now, motivated by the derivation that led to the analysis filter bank of Fig. 27.5, we recognize that the structure shown in Fig. 27.20 can serve as the starting point for our discussion for the following reasons. In this structure, each signal $u_k(n)$, whose frequency band extends over the entire interval $[0, 2\pi]$, is first upsampled by a factor of M. Doing so reduces the signal bandwidth by a factor of M and results in a signal $z_k(n)$ whose frequency band has size $\frac{2\pi}{M}$. However, upsampling introduces spectral images within the range $[0, 2\pi]$, as was already explained earlier in Fig. 26.10 while examining the effect of upsampling on the frequency content of a signal. Therefore, a low-pass filter, $S_o(z)$, is employed to eliminate the spectral images from $z_k(n)$ and to keep only the low-frequency components, which will therefore lie within the range $[-\frac{\pi}{M}, \frac{\pi}{M}]$. This construction leads to the baseband signals $q_k(n)$ with bands extending over $[-\frac{\pi}{M}, \frac{\pi}{M}]$.

The baseband signals $q_k(n)$ are subsequently scaled by $e^{j2\pi kn/M}$ in order to shift and center their frequency bands around $\frac{2\pi k}{M}$. The resulting signals are denoted by $v_k(n)$. The reconstruction $x'(n-d)$ is then obtained by adding the subband signals $v_k(n)$. Now, note

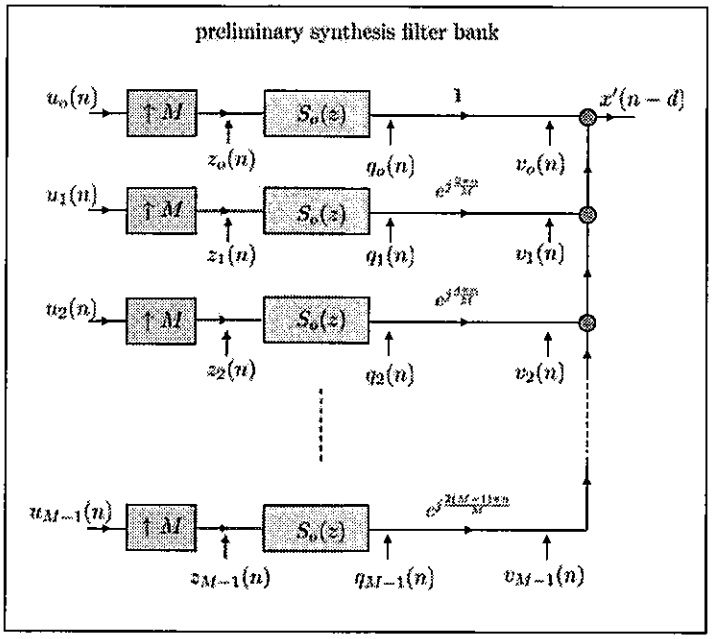

FIGURE 27.20 A structure for synthesizing the signal $x'(n-d)$ from the subband signals $u_k(n)$. An efficient implementation in terms of the polyphase decomposition of the prototype filter, $S_o(z)$, will be derived in the sequel.

that for the $k-$th branch we can write

$$\begin{aligned}
v_k(n) &= [z_k(n) \star s_o(n)] \cdot e^{j\frac{2\pi kn}{M}} \\
&= \sum_{m=0}^{\infty} s_o(m) z_k(n-m) e^{j\frac{2\pi kn}{M}} \\
&= \sum_{m=0}^{\infty} s_o(m) e^{j\frac{2\pi km}{M}} z_k(n-m) e^{j\frac{2\pi k(n-m)}{M}} \\
&= \sum_{m=0}^{\infty} s_k(m) z_k(n-m) e^{j\frac{2\pi k(n-m)}{M}} \quad \text{(using (27.31))} \\
&= s_k(n) \star \left(z_k(m) e^{j\frac{2\pi kn}{M}} \right) \qquad (27.32)
\end{aligned}$$

It follows that the generation of $v_k(n)$ can also be accomplished by first scaling $z_k(n)$ by $e^{j2\pi kn/M}$ and then filtering the result by the synthesis filter, $S_k(z)$, as illustrated in Fig. 27.21. This result allows us to redraw the synthesis structure of Fig. 27.20 in the manner shown in Fig. 27.22 where $S_o(z)$ has been replaced by the subband filters $\{S_k(z)\}$. The signals at both ends of the scaling branches are denoted by $z_k(n)$ and $c_k(n)$.

Now observe that, by definition of the upsampling operation, we have

$$\begin{aligned}
c_k(n) &= e^{j\frac{2\pi kn}{M}} z_k(n) \\
&= \begin{cases} e^{j\frac{2\pi kn}{M}} u_k(\frac{n}{M}), & \text{when } n/M \text{ is an integer} \\ 0, & \text{otherwise} \end{cases} \\
&= \begin{cases} u_k(\frac{n}{M}), & \text{when } n/M \text{ is an integer} \\ 0, & \text{otherwise} \end{cases} \qquad (27.33)
\end{aligned}$$

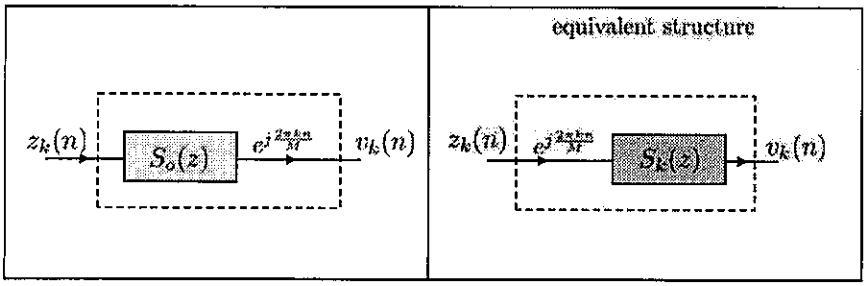

FIGURE 27.21 The two branches are equivalent: filtering by $S_o(z)$ followed by scaling by $e^{j2\pi kn/M}$ is equivalent to scaling first by $e^{j2\pi kn/M}$ and then filtering by $S_k(z)$.

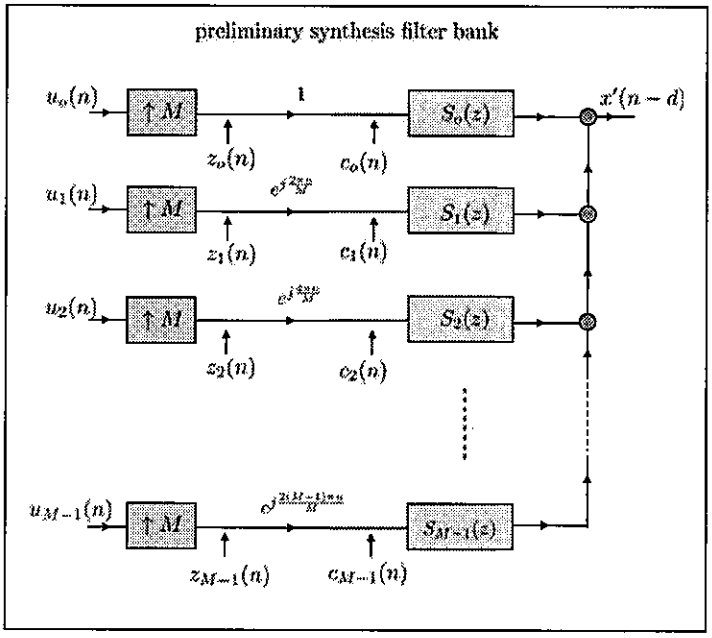

FIGURE 27.22 An equivalent structure to that of Fig. 27.20 for synthesizing the signal $x'(n-d)$ from the subband signals $u_k(n)$ in terms of the synthesis filters, $S_k(z)$.

This result means that the mapping from $u_k(n)$ to $c_k(n)$ can be accomplished by simply upsampling $u_k(n)$ by the factor M and ignoring the scaling by $e^{j2\pi kn/M}$. The construction leads to the equivalent structure of Fig. 27.23.

Example 27.3 (A synthesis filter bank)

Let us reconsider the context of Example 27.1 where we considered the prototype analysis filter

$$A_o(z) = 1 + z^{-1} + z^{-2} + z^{-3} \tag{27.34}$$

In this example, we set $M = 2$ and select a similar prototype synthesis filter, say,

$$S_o(z) = 1 + z^{-1} + z^{-2} + z^{-3} \tag{27.35}$$

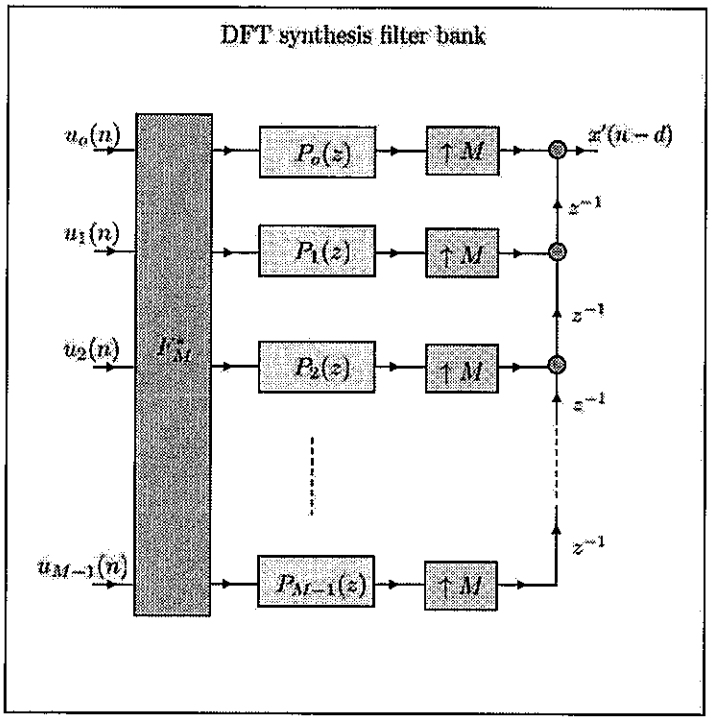

FIGURE 27.23 An equivalent structure to that of Fig. 27.22 for synthesizing the signal $x'(n-d)$ from the subband signals $u_k(n)$ in terms of the synthesis filters, $S_k(z)$, and without the scaling factors $e^{j2\pi nk/M}$.

The second synthesis filter is then given by

$$S_1(z) = S_o(-z) = 1 - z^{-1} + z^{-2} - z^{-3} \tag{27.36}$$

In this way, we end up with the synthesis filter bank of Fig. 27.24 with two branches. The signals that are feeding these branches are the same subband signals, $u_o(n)$ and $u_1(n)$, that were generated by the analysis filter bank of Fig. 27.19. Recall from (27.8) that the prototype filter, $A_o(z)$, used in that figure is not an ideal low-pass filter; in particular, its gain is equal to 4 at $\omega = 0$. The gain of $S_o(z)$ is also 4 at $\omega = 0$. Therefore, in this example, while reconstructing $x'(n-d)$ from $u_o(n)$ and $u_1(n)$, we will need to scale down the output signal by some factor, α, in order to undo the scaling effects through the analysis and synthesis filter banks. The scaling by α is indicated on the right-most side of Fig. 27.24 and its value is determined empirically in this exercise. More generally, the question of how to ensure that the output of the synthesis filter bank is a good match to the original sequence falls within the realm of designing perfect reconstruction banks, which we shall study later in Sec. 27.5.

Figure 27.25 plots the original sequence $x(n)$ and the output of the synthesis filter bank, $x'(n-d)$, when α is set to $\alpha = 1$. It is seen that $x'(n-d)$ is magnified relative to $x(n)$ by a factor of approximately 4. It is also seen that the delay is $d = 2$.

Figure 27.26 plots the original sequence $x(n)$ and the output of the analysis filter bank, $x'(n-d)$, when α is set to $\alpha = 1/4$ and when the output sequence is advanced by 2 samples in order to align it with $x(n)$. The bottom plot in the figure shows the resulting error sequence; obviously, the error is relatively large in this nonideal case since the analysis and synthesis filters do not exhibit good frequency characteristics. Later, in Example 27.8, we shall illustrate a perfect reconstruction filter bank.

◇

27.2.2 DFT Synthesis Filter Bank

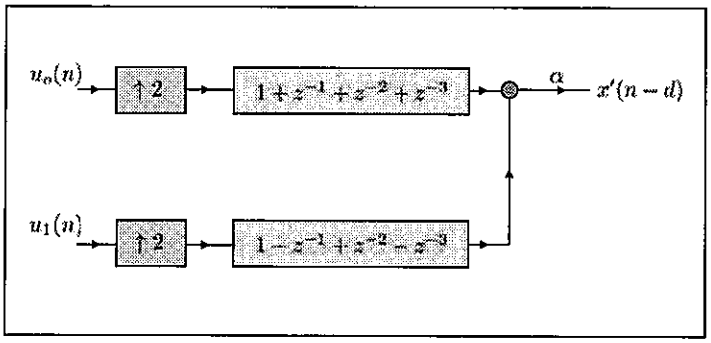

FIGURE 27.24 A synthesis filter bank with two branches and prototype filter $S_o(z) = 1+z^{-1}+z^{-2}+z^{-3}$ from Example 27.3. The output branch is further scaled by α.

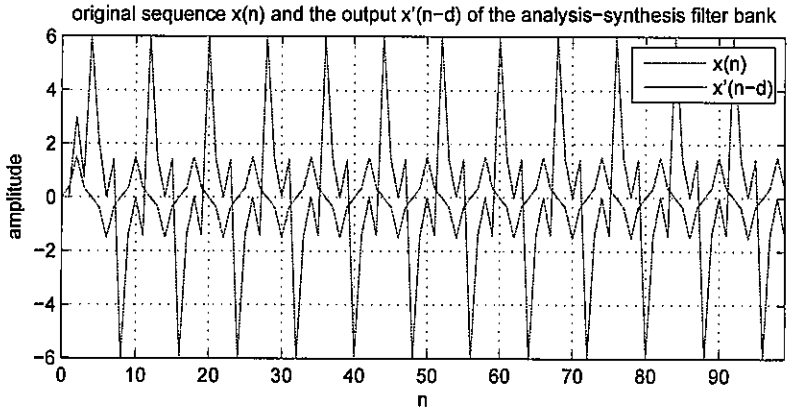

FIGURE 27.25 Original sequence, $x(n)$, and the output of the analysis-synthesis filter bank, $x'(n-d)$, when $\alpha = 1$ in Example 27.3. It is seen that $x'(n)$ is magnified by a factor of approximately 4 relative to $x(n)$ and is also delayed by 2 samples.

As was the case with the analysis filter bank in Sec. 27.1, we can also develop an efficient implementation for the synthesis filter bank of Fig. 27.23 by using the DFT operation and the polyphase representation of the prototype filter, $S_o(z)$. Thus, introduce the $M-$th order polyphase decomposition

$$\boxed{S_o(z) = \sum_{m=0}^{M-1} z^{-m} P_m(z^M)} \tag{27.37}$$

where we are denoting the polyphase components of $S_o(z)$ by $P_m(z)$. Then, as in (27.15), the synthesis filters, $S_k(z)$, can be expressed in terms of the $\{P_m(z)\}$ as follows:

$$\boxed{\begin{bmatrix} S_o(z) \\ S_1(z) \\ S_2(z) \\ \vdots \\ S_{M-1}(z) \end{bmatrix} = F_M^* \begin{bmatrix} P_o(z^M) \\ z^{-1}P_1(z^M) \\ z^{-2}P_2(z^M) \\ \vdots \\ z^{-(M-1)}P_{M-1}(z^M) \end{bmatrix}} \tag{27.38}$$

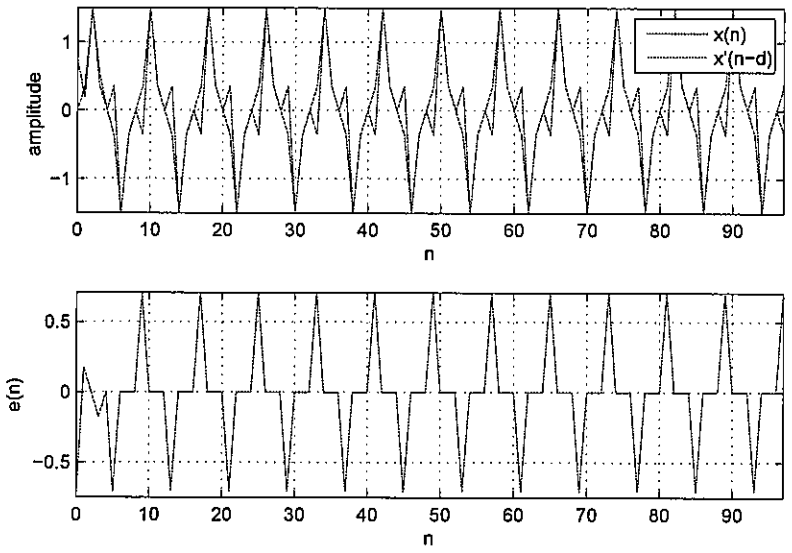

FIGURE 27.26 Original sequence, $x(n)$, and the output of the analysis-synthesis filter bank, $x'(n-d)$, from Example 27.3 after scaling by $\alpha = 1/4$ and after advancing the output by two units of time (top). The bottom plot shows the error sequence, which is large in this contrived example.

If we now refer to Fig. 27.23, and use the $z-$transform representation, we note that

$$\begin{aligned} z^{-d}X'(z) &= C_o(z)S_o(z) + C_1(z)S_1(z) + \ldots + C_{M-1}(z)S_{M-1}(z) \\ &= \begin{bmatrix} C_o(z) & C_1(z) & \ldots & C_{M-1}(z) \end{bmatrix} \begin{bmatrix} S_o(z) \\ S_1(z) \\ S_2(z) \\ \vdots \\ S_{M-1}(z) \end{bmatrix} \\ &= \begin{bmatrix} C_o(z) & C_1(z) & \ldots & C_{M-1}(z) \end{bmatrix} F_M^* \begin{bmatrix} P_o(z^M) \\ z^{-1}P_1(z^M) \\ z^{-2}P_2(z^M) \\ \vdots \\ z^{-(M-1)}P_{M-1}(z^M) \end{bmatrix} \end{aligned} \tag{27.39}$$

This result shows that the output signal $x'(n-d)$ can be generated from the signals $c_k(n)$ by first transforming them by the DFT operation, F_M^*, and then feeding the result into the polyphase filters, $z^{-m}P_m(z)$, as illustrated in Fig. 27.27 where we are denoting the signals on the left and right of the DFT operation by $\{c_k(n), d_k(n)\}$.

We now argue that the upsamplers in Fig. 27.27 can be moved after the DFT operation. Indeed, refer to Fig. 27.28 where we are denoting the signals before and after the upsampler

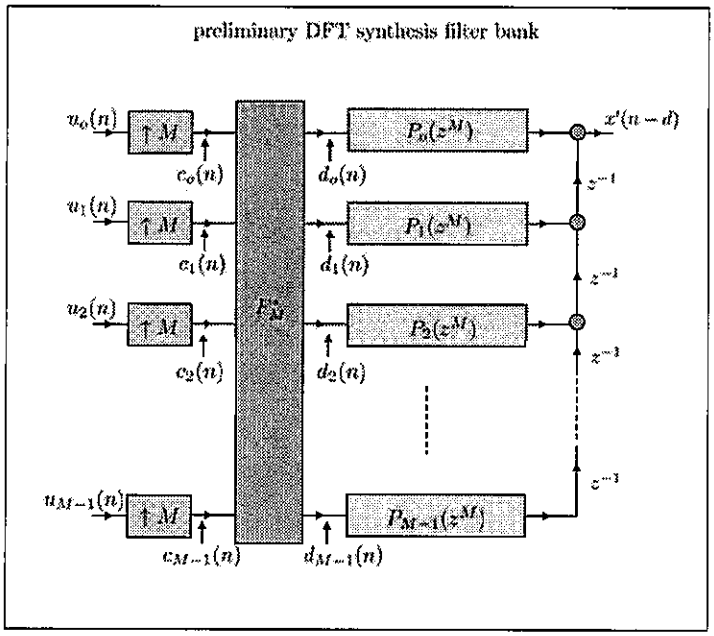

FIGURE 27.27 Uniform DFT synthesis filter bank in terms of the $M-$th order polyphase representation of the prototype filter, $S_o(z)$, and where F_M^* denotes the $M \times M$ complex conjugate DFT matrix (27.19).

by $\ell_k(n)$ and $d_k(n)$, respectively. These signals are related as follows:

$$\begin{bmatrix} d_o(n) \\ d_1(n) \\ d_2(n) \\ \vdots \\ d_{M-1}(n) \end{bmatrix} = \begin{cases} \begin{bmatrix} \ell_o(n/M) \\ \ell_1(n/M) \\ \ell_2(n/M) \\ \vdots \\ \ell_{M-1}(n/M) \end{bmatrix}, & \text{when } n \text{ is multiple of } M \\ 0, & \text{otherwise} \end{cases} \tag{27.40}$$

so that

$$\begin{bmatrix} d_o(n) \\ d_1(n) \\ d_2(n) \\ \vdots \\ d_{M-1}(n) \end{bmatrix} = \begin{cases} F_M^* \begin{bmatrix} u_o(n/M) \\ u_1(n/M) \\ u_2(n/M) \\ \vdots \\ u_{M-1}(n/M) \end{bmatrix}, & \text{when } n \text{ is multiple of } M \\ 0, & \text{otherwise} \end{cases} \tag{27.41}$$

This result shows that the signals $d_k(n)$ in Figs. 27.27 and 27.28 coincide; they are the result of upsampling the $\{u_k(n)\}$ and then transforming them by F_M^*. Therefore, the implementations of Figs. 27.27 and 27.28 are equivalent. We can finally invoke the cascade

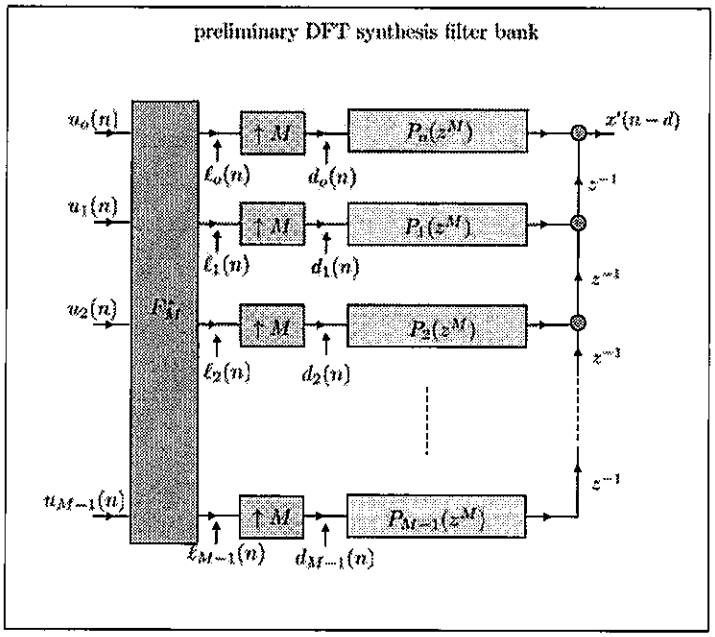

FIGURE 27.28 Equivalent implementation of the uniform DFT synthesis filter bank with the upsamplers of Fig. 27.27 now appearing after the DFT operation.

equivalence result shown in Fig. 26.25 to move the upsamplers behind polyphase components and arrive at the DFT filter bank implementation shown in Fig. 27.29.

27.3 SUBBAND PROCESSING

Combining the general structures for analysis and synthesis filter banks from Figs. 27.7 and 27.23, we arrive at the structure shown in Fig. 27.30. In this structure, a signal $x(n)$ is decomposed into subband signals, $u_k(n)$. The subband signals, $u_k(n)$, are subsequently subjected to some desired processing in order to generate another set of subband signals, say, $r_k(n)$. For example, each signal $r_k(n)$ may be the result of filtering the corresponding subband signal $u_k(n)$ through some filter, $L_k(z)$ (we shall encounter this situation in the next chapter — see Fig. 28.6). The signals $r_k(n)$ are then combined via a synthesis filter bank to reconstruct an output signal $y(n)$. Most of the time, the frequency responses of the analysis filters, $A_k(z)$, are uniformly shifted versions of some prototype filter, $A_o(z)$ (and similarly for the synthesis filters, $S_k(z)$, in terms of a prototype filter $S_o(z)$); though this is not always the case.

When uniform filter banks are used for both analysis and synthesis purposes, then we can call upon the efficient DFT implementations of Figs. 27.17 and 27.29 to arrive at the structure shown in Fig. 27.31. In this structure, the signal $x(n)$ is decomposed into subband signals, which are subsequently subjected to some desired processing before passing

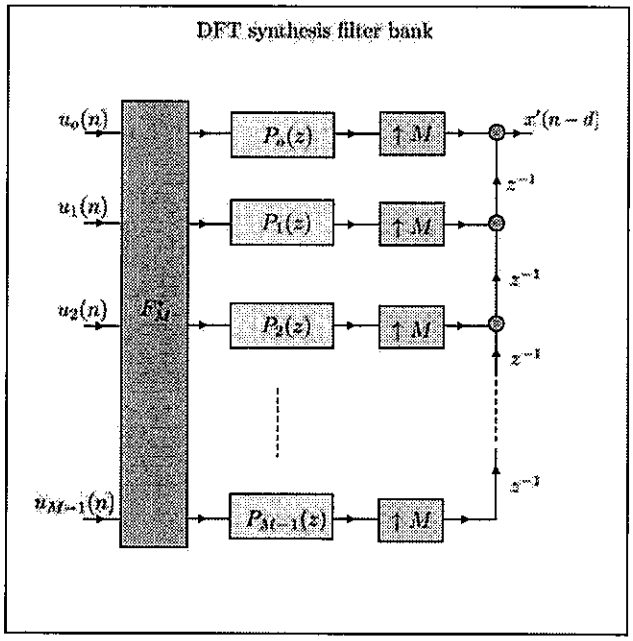

FIGURE 27.29 Efficient implementation of the uniform synthesis filter bank of Fig. 27.23 by means of the DFT. The $P_k(z)$ are the $M-$th order polyphase components of the prototype synthesis filter, $S_o(z)$.

through the DFT synthesis filter bank to reconstruct the output signal $y(n)$.

27.4 OVERSAMPLED FILTER BANKS

More generally, we may consider relaxing the relation between the downsampling and upsampling factors, and the number of analysis and synthesis filters. Assume, for instance, that we select some causal low-pass prototype filter, $A_o(z)$, with bandwidth $\frac{2\pi}{M}$ and use it to define an analysis filter bank with K filters as follows:

$$A_k(z) = A_o\big(ze^{-j2\pi k/K}\big), \qquad k = 0, 1, \ldots, K-1 \tag{27.42}$$

i.e., with frequency responses

$$A_k(e^{j\omega}) = A_o\big(e^{j(\omega - \frac{2\pi k}{K})}\big), \qquad k = 0, 1, \ldots, K-1 \tag{27.43}$$

Note that we are denoting the number of analysis filters by K (instead of restricting it to coincide with M as has been the case so far). Usually, $K \geq M$ so that the shifts in frequency that generate the $A_k(z)$ are smaller than the bands of the filters. In this way, the interval $[0, 2\pi]$ will be covered by K equally spaced filters, $A_k(z)$, whose bands overlap.

Since the signals at the outputs of the analysis filters, $A_k(z)$, have bandwidths that are smaller than the bandwidth of the fullband signal $x(n)$, the outputs of $A_k(z)$ can be downsampled to a lower rate, say, by some factor $D \leq M$, prior to further processing. The resulting structure is shown in Fig. 27.32; the difference now, compared with Fig. 27.7 is

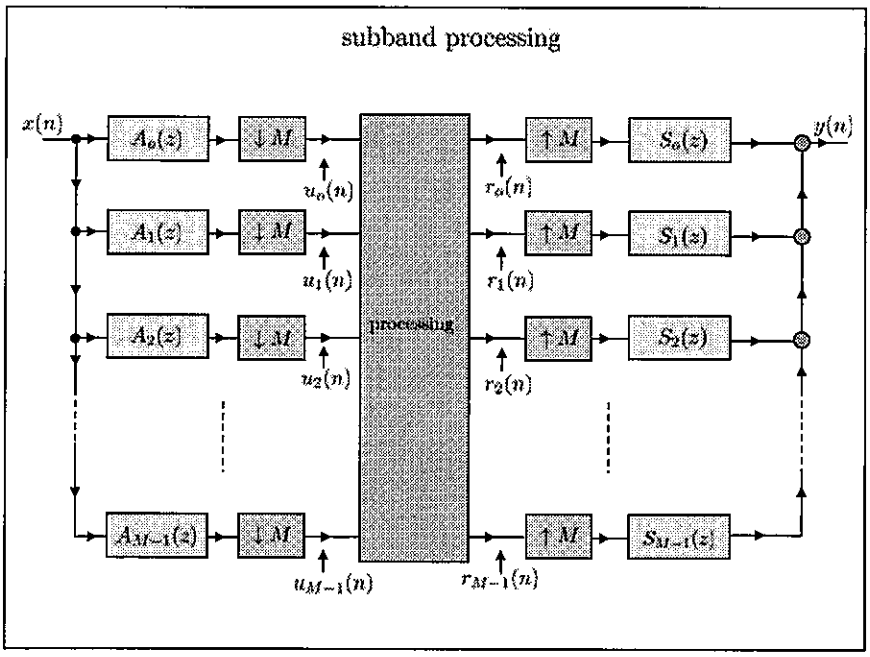

FIGURE 27.30 Structure for subband processing using an analysis filter bank with analysis filters, $A_k(z)$, and a synthesis filter bank with synthesis filters, $S_k(z)$.

that the number of analysis filters, K, and the decimation factor, D, are not necessarily equal as before.

The special choice that corresponds to $D = K$ results in what is called a *maximally* or critically decimated analysis filter bank. In this case, the total number of samples after decimation is the same as the total number of input samples. Thus, observe that N input samples $\{x(n)\}$ lead to N samples at the output of each analysis filter and, therefore, to a total of KN samples at the output of these filters. After decimation by a factor $D = K$, we are left again with N samples. Choices of D such that $D < K$ lead to what are called *oversampled* or noncritically sampled analysis filter banks. In these cases, N input samples generate more than N total samples at the output of the decimators. If $D > K$, then aliasing occurs in the subbands.

The corresponding synthesis filter bank is shown in Fig. 27.33 with synthesis filters, $S_k(z)$, that are defined in terms of some prototype filter, $S_o(z)$, of bandwidth $\frac{2\pi}{M}$, as follows:

$$S_k(z) = S_o\big(ze^{-j2\pi k/K}\big), \qquad k = 0, 1, \ldots, K-1 \tag{27.44}$$

i.e., with frequency responses

$$S_k(e^{j\omega}) = S_o\big(e^{j(\omega - \frac{2\pi k}{K})}\big), \qquad k = 0, 1, \ldots, K-1 \tag{27.45}$$

Example 27.4 (An oversampled filter bank)

Consider a low-pass prototype filter, $A_o(z)$, and let $E_m(z)$ denote its polyphase components of order K, i.e.,

$$A_o(z) = \sum_{m=0}^{K-1} z^{-m} E_m(z^K) \tag{27.46}$$

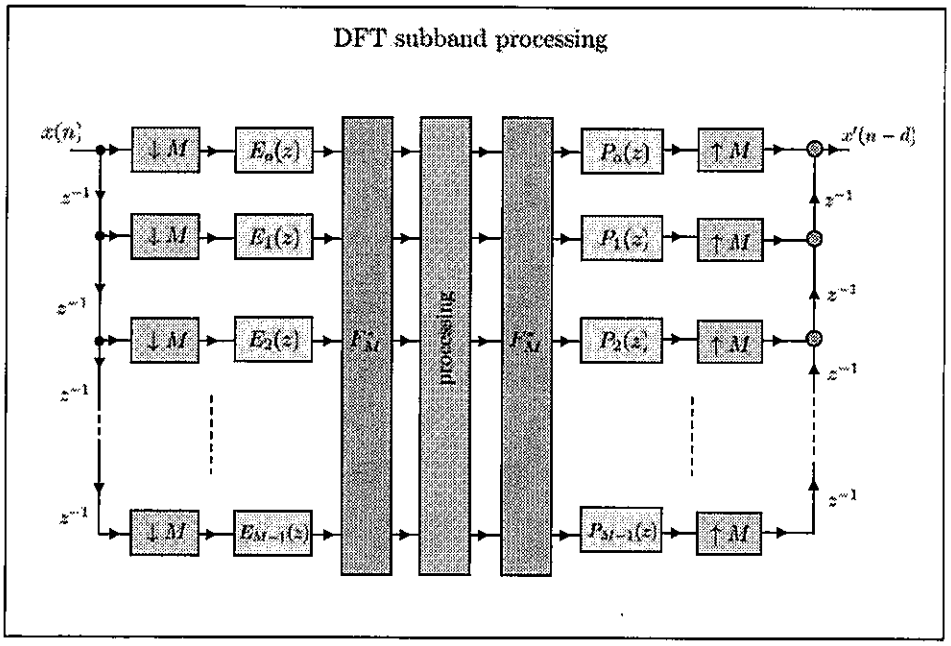

FIGURE 27.31 Efficient structure for subband processing using a DFT analysis filter bank and a DFT synthesis filter bank.

Using the same derivation that led to (27.20) we have

$$\begin{bmatrix} A_o(z) \\ A_1(z) \\ A_2(z) \\ \vdots \\ A_{K-1}(z) \end{bmatrix} = F_K^* \begin{bmatrix} E_o(z^K) \\ z^{-1}E_1(z^K) \\ z^{-2}E_2(z^K) \\ \vdots \\ z^{-(K-1)}E_{K-1}(z^K) \end{bmatrix} \tag{27.47}$$

In this example, we are interested in the analysis filters that would correspond to the following choice of polyphase components:

$$E_m(z^K) = 1, \quad m = 0, 1, \ldots, K-1 \tag{27.48}$$

For this to hold, the prototype filter $A_o(z)$ will obviously need to correspond to a moving average filter of order K:

$$A_o(z) = \sum_{m=0}^{K-1} z^{-m} \tag{27.49}$$

with the rectangular window as its impulse response sequence. Then, the analysis filters will be given by

$$\begin{bmatrix} A_o(z) \\ A_1(z) \\ A_2(z) \\ \vdots \\ A_{K-1}(z) \end{bmatrix} = F_K^* \begin{bmatrix} 1 \\ z^{-1} \\ z^{-2} \\ \vdots \\ z^{-(K-1)} \end{bmatrix} \tag{27.50}$$

In other words, the coefficients of each filter $A_k(z)$ will be given by the $k-$th row of the DFT matrix F_K^*. That is, the analysis filters in this case are defined by the rows of F_K^*.

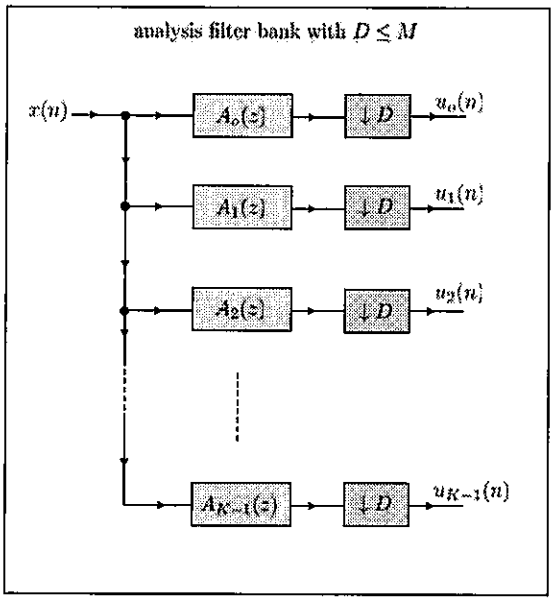

FIGURE 27.32 An analysis filter bank with K analysis filters having bandwidth $\frac{2\pi}{M}$ each with $K \geq M$ and with downsampling factor $D \leq M$.

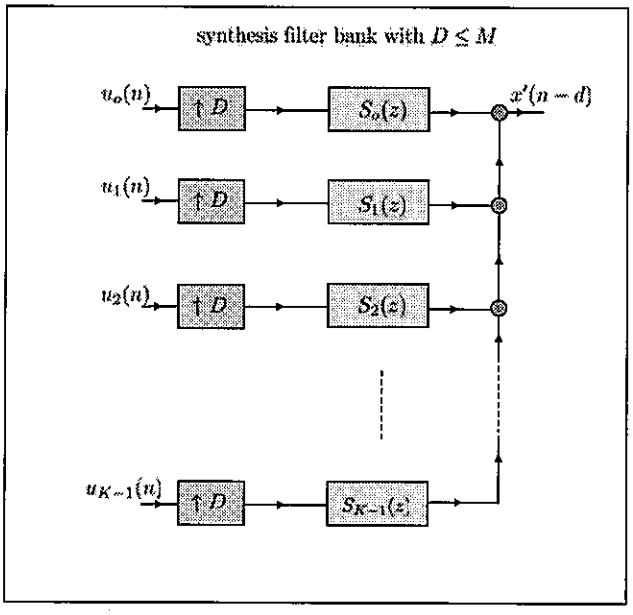

FIGURE 27.33 A synthesis filter bank with K synthesis filters with bandwidth $\frac{2\pi}{M}$ each with $K \geq M$ and using upsampling factor $D \leq M$.

As we saw earlier in Example 27.1, the frequency response of $A_o(z)$ is given by

$$A_o(e^{j\omega}) = \begin{cases} K, & \omega = 0 \\ e^{-j\omega\frac{(K-1)}{2}} \left(\dfrac{\sin(\omega K/2)}{\sin(\omega/2)}\right), & \text{otherwise} \end{cases} \tag{27.51}$$

and its bandwidth is equal to

$$\text{bandwidth} = \frac{4\pi}{K} \triangleq \frac{2\pi}{M} \tag{27.52}$$

where we introduced $M = K/2$. The analysis filters are obtained by shifting the frequency response of the prototype filter by multiples of $\frac{2\pi}{K}$ radians/sample, while the bandwidth of each of the filters is $\frac{2\pi}{M}$ radians/sample. Figure 27.34 illustrates the frequency responses of the analysis filter banks for the case $K = 4$ over the range $[0, 2\pi]$; each filter has bandwidth equal to π radians/sample and its frequency response is centered at multiples of $\pi/2$.

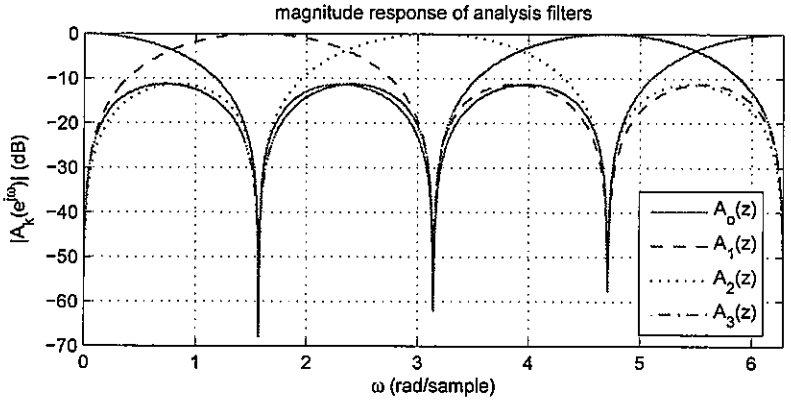

FIGURE 27.34 Frequency responses of the analysis filters that correspond to the case $K = 4$ in Example 27.4 over the range $[0, 2\pi]$. Each filter has bandwidth equal to π radians/sample and the frequency responses are centered at multiples of $\pi/2$.

Since the bandwidth of each analysis filter is $\frac{2\pi}{M}$ radians/sample, we select $D = M$. Following the same argument that was used in Sec. 27.1 to arrive at the efficient DFT implementation of Fig. 27.17, we can similarly justify the oversampled DFT structure of Fig. 27.35 for the example under study. In this case, the signal $x(n)$ is decomposed into $2M$ subband signals. We shall encounter one application for this structure later in Sec. 28.1 when we discuss block filtering methods (see Fig. 28.9).

In a similar vein, Fig. 27.36 shows the oversampled DFT synthesis filter bank that would result if the synthesis filters are selected in manner similar to (27.50), namely,

$$\begin{bmatrix} S_o(z) \\ S_1(z) \\ S_2(z) \\ \vdots \\ S_{K-1}(z) \end{bmatrix} = F_K^* \begin{bmatrix} 1 \\ z^{-1} \\ z^{-2} \\ \vdots \\ z^{-(K-1)} \end{bmatrix} \tag{27.53}$$

◇

27.5 PERFECT RECONSTRUCTION FILTER BANKS

The discussion in the previous sections showed how to decompose an input signal $x(n)$ into a collection of subband signals $\{u_k(n)\}$ by means of an analysis filter bank. The discussion also showed how to aggregate these subband signals into an output signal $x'(n-d)$ by means of a synthesis filter bank. It would be ideal if the analysis and synthesis filters $\{A_k(z), S_k(z)\}$ can be designed such that the reconstructed signal $x'(n-d)$ is related to $x(n)$ by simple transformations involving only delays and scaling by a constant. This task,

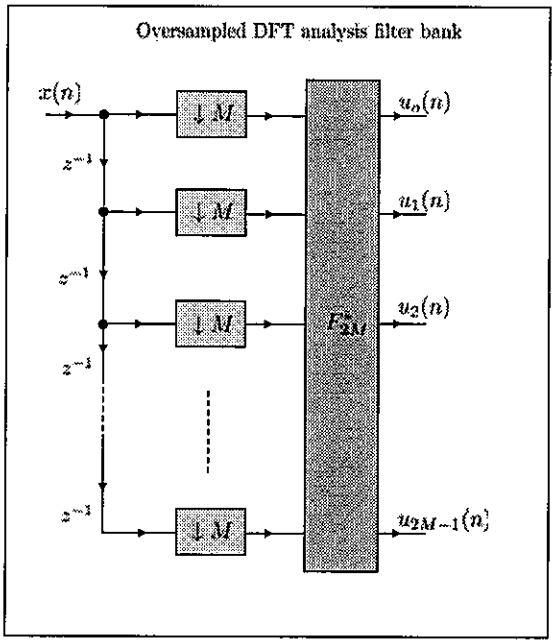

FIGURE 27.35 An oversampled DFT analysis filter bank for the prototype filter of Example 27.4, which corresponds to a rectangular window of width $K = 2M$ samples, i.e., $A_o(z) = 1 + z^{-1} + z^{-2} + \ldots + z^{-(2M-1)}$. The implementation consists of $2M$ branches and employs a DFT of size $2M \times 2M$.

however, is often hindered by the distortions introduced during the analysis and synthesis stages. In this section, we explain how to design filter banks that are able to eliminate aliasing and distortion effects introduced by the downsampling and upsampling stages and by the non-ideal frequency response characteristics of the analysis and synthesis filters.

It is noteworthy that it will be possible to construct filter banks that are able to yield perfect reconstruction of the input signal despite possible aliasing and distortion effects within the filter bank. We hinted at this possibility earlier in Example 27.3. In that example, the analysis and filter banks are non-ideal and have overlapping bands. Yet, Fig. 27.26 showed that it is still possible to recover a reasonable approximation for the input sequence. Obviously, this example does not deal with *perfect* reconstruction because the output sequence appears distorted relative to the input sequence. The presentation in the sequel focuses on the design of filter banks with perfect reconstruction properties, namely, filter banks where the overall transfer function between the input and output terminals, $\{x(n), x'(n-d)\}$ turns out to be a pure delay, say, of the form z^{-d} for some delay d.

We illustrate the main ideas in this section by focusing on a 2–branch filter bank; multi-branch filter banks are considered in Probs. 26.23 and 27.14, and also in Sec. 28.6. Thus, refer to Fig. 27.37. The input signal is denoted by $x(n)$ and the output signal is denoted by $y(n)$. The objective of is to determine conditions on the (causal and stable) analysis and synthesis filters, $A_k(z)$ and $S_k(z)$, such that the transfer function from $x(n)$ to $y(n)$ is equal to the pure delay, z^{-d}, for some integer d. We approach this objective in two steps. First we determine conditions to eliminate aliasing and, subsequently, we determine conditions to enable perfect reconstruction.

27.5.1 Alias-Free Reconstruction Condition

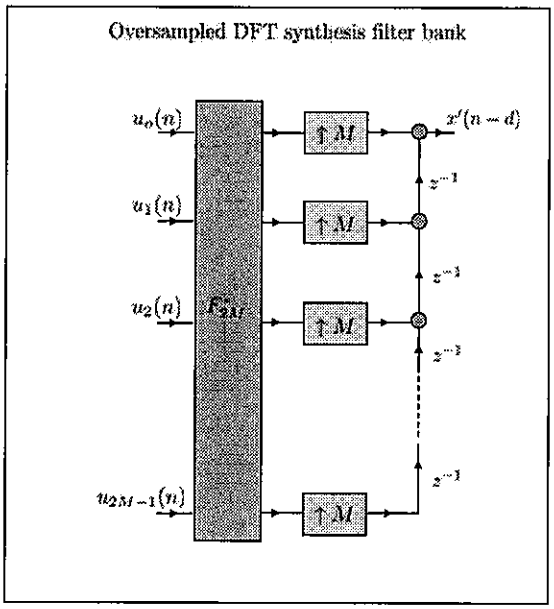

FIGURE 27.36 An oversampled DFT synthesis filter bank for Example 27.4, which corresponds to a rectangular window of width $K = 2M$ samples, i.e., $S_o(z) = 1+z^{-1}+z^{-2}+\ldots+z^{-(2M-1)}$. The implementation consists of $2M$ branches and employs a DFT of size $2M \times 2M$.

Let $u_o(n)$ and $u_1(n)$ denote the signals at the output of the decimators in Fig. 27.37. Using the $z-$transform representation, we have

$$U_o(z) = \frac{1}{2}A_o(z^{1/2})X(z^{1/2}) + \frac{1}{2}A_o(-z^{1/2})X(-z^{1/2}) \tag{27.54}$$

$$U_1(z) = \frac{1}{2}A_1(z^{1/2})X(z^{1/2}) + \frac{1}{2}A_1(-z^{1/2})X(-z^{1/2}) \tag{27.55}$$

and

$$\begin{aligned} Y(z) &= U_o(z^2)S_o(z) + U_1(z^2)S_1(z) \\ &= \frac{1}{2}\left[A_o(z)S_o(z) + A_1(z)S_1(z)\right]X(z) + \\ &\quad \frac{1}{2}\left[A_o(-z)S_o(z) + A_1(-z)S_1(z)\right]X(-z) \end{aligned} \tag{27.56}$$

We may express $Y(z)$ in the equivalent form

$$Y(z) = \frac{1}{2}\begin{bmatrix} X(z) & X(-z) \end{bmatrix} \underbrace{\begin{bmatrix} A_o(z) & A_1(z) \\ A_o(-z) & A_1(-z) \end{bmatrix}}_{\mathcal{A}(z)} \begin{bmatrix} S_o(z) \\ S_1(z) \end{bmatrix} \tag{27.57}$$

where we are introducing the 2×2 transfer matrix, $\mathcal{A}(z)$, whose entries are defined in terms of the analysis filters $\{A_o(z), A_1(z)\}$.

It is clear from (27.57) that the output signal $Y(z)$ contains a contribution from $X(z)$ and a contribution from $X(-z)$. The terms involving $X(-z^{-1/2})$ and $X(-z)$ in the expressions for $U_o(z), U_1(z)$, and $Y(z)$ are due to the aliasing effect that arises from the

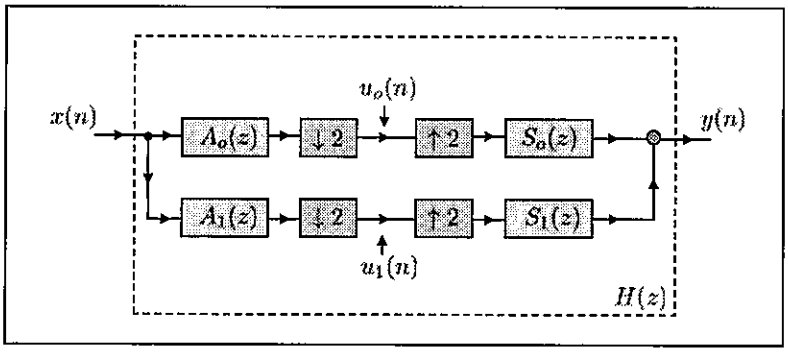

FIGURE 27.37 A 2−branch multi-rate filter bank.

downsampling operation. In order to cancel the effect of aliasing from $Y(z)$ we see from (27.56) that the analysis and synthesis filters must satisfy the condition:

$$\boxed{A_o(-z)S_o(z) + A_1(-z)S_1(z) = 0} \quad \text{(alias-free condition)} \tag{27.58}$$

or, equivalently,

$$\frac{S_1(z)}{S_o(z)} = -\frac{A_o(-z)}{A_1(-z)} \tag{27.59}$$

This relation can also be rewritten as

$$-\frac{S_1(z)}{A_o(-z)} = \frac{S_o(-z)}{A_1(-z)} \tag{27.60}$$

which can be interpreted to mean that the analysis and synthesis filters should be related as

$$\boxed{S_o(z) = G(z)A_1(-z) \quad \text{and} \quad S_1(z) = -G(z)A_o(-z)} \tag{27.61}$$

for some rational transfer function $G(z)$. These relations show how the synthesis filters, $\{S_o(z), S_1(z)\}$, can be chosen in terms of the analysis filters, $\{A_o(z), A_1(z)\}$, in order to ensure an alias-free filter bank implementation. Substituting into (27.56), the resulting alias-free transfer function from $x(n)$ to $y(n)$, which simplifies to

$$H(z) = \frac{1}{2}\left[A_o(z)S_o(z) + A_1(z)S_1(z)\right] \tag{27.62}$$

is then given by

$$\boxed{H(z) = \frac{1}{2}\left[A_o(z)A_1(-z) - A_1(z)A_o(-z)\right]G(z)} \tag{27.63}$$

Example 27.5 (Alias-free filter bank)

Consider a 2−branch filter bank with the selections

$$A_o(z) = 2 + z^{-1}, \quad A_1(z) = 2 - z^{-1}, \quad G(z) = \frac{1}{4 + z^{-1}} \tag{27.64}$$

so that the corresponding synthesis filters are

$$S_o(z) = \frac{2+z^{-1}}{4+z^{-1}}, \quad S_1(z) = -\frac{2-z^{-1}}{4+z^{-1}} \tag{27.65}$$

The analysis and synthesis filters so chosen satisfy the alias-free condition (27.58). The resulting transfer function from $x(n)$ to $y(n)$ is given by

$$\begin{aligned} H(z) &= \frac{1}{2}\left[A_o(z)S_o(z) + A_1(z)S_1(z)\right] \\ &= \frac{1}{2}\left[(2+z^{-1})^2 - (2-z^{-1})^2\right]\frac{1}{4+z^{-1}} \\ &= \frac{4z^{-1}}{4+z^{-1}} \end{aligned} \tag{27.66}$$

We therefore find that, in this case, the signal $x(n)$ continues to be distorted by the filter bank since

$$Y(z) = \frac{4z^{-1}}{4+z^{-1}} \cdot X(z) \tag{27.67}$$

In other words, an alias-free filter bank is still not a distortionless filter bank.

◇

27.5.2 Perfect Reconstruction Condition

To remove the distortion, in addition to aliasing, we observe from expression (27.62) that in order to ensure that the transfer function from $x(n)$ to $y(n)$ is a pure delay, the analysis and synthesis filters need to satisfy additionally the following condition:

$$A_o(z)S_o(z) + A_1(z)S_1(z) = 2z^{-d} \tag{27.68}$$

for some integer delay $d > 0$. In this way, the transfer function from $x(n)$ to $y(n)$ ends up being

$$Y(z) = z^{-d}X(z)$$

and we say that the filter bank has accomplished perfect reconstruction, apart from a pure delay, of the input signal. Alternatively, using (27.63), we conclude that perfect reconstruction requires the analysis filters $\{A_o(z), A_1(z)\}$ to satisfy the condition

$$\boxed{\left[A_o(z)A_1(-z) \;-\; A_1(z)A_o(-z)\right]G(z) \;=\; 2z^{-d}} \quad \text{(perfect reconstruction)} \tag{27.69}$$

for some $G(z)$ and delay d. When perfect reconstruction is attained, it will hold that $H(z) = z^{-d}$.

In summary, the design of a perfect reconstruction 2−branch filter bank of the form shown in Fig. 27.37 can be accomplished by selecting filters $A_o(z)$, $A_1(z)$, and $G(z)$ that satisfy (27.69) for some some integer delay $d > 0$. The synthesis filters are then set as in (27.61). Furthermore, the analysis and synthesis filters, $A_k(z)$ and $S_k(z)$, are required to be causal and stable filters.

Example 27.6 (Perfect reconstruction filter bank)

Consider a 2−branch filter bank with the selections

$$A_o(z) = 1+z^{-1}, \quad A_1(z) = 1-z^{-1} \tag{27.70}$$

$$S_o(z) = \frac{1}{2}(1+z^{-1}), \quad S_1(z) = -\frac{1}{2}(1-z^{-1}) \tag{27.71}$$

It is straightforward to verify that these filters satisfy the perfect reconstruction condition (27.69) with $G(z) = 1/2$ and $d = 1$. Moreover, the resulting transfer function from $x(n)$ to $y(n)$ is

$$\begin{aligned} H(z) &= \frac{1}{2}\left[A_o(z)S_o(z) + A_1(z)S_1(z)\right] \\ &= \frac{1}{4}\left[(1+z^{-1})^2 - (1-z^{-1})^2\right] \\ &= z^{-1} \end{aligned} \tag{27.72}$$

◇

27.5.3 Perfect Reconstruction with FIR Filters

It is often desirable to meet the perfect reconstruction condition (27.69) by requiring the analysis and synthesis filters to be causal FIR filters. Example 27.6 above illustrated one such situation.

Condition (27.69) implies that the transfer function $G(z)$ satisfies

$$G(z) = \frac{2z^{-d}}{A_o(z)A_1(-z) - A_1(z)A_o(-z)} \tag{27.73}$$

Substituting into (27.61), we find that the synthesis filters should be chosen in terms of the analysis filters as follows:

$$S_o(z) = \frac{2z^{-d}A_1(-z)}{A_o(z)A_1(-z) - A_1(z)A_o(-z)} \tag{27.74}$$

(27.75)

$$S_1(z) = \frac{-2z^{-d}A_o(-z)}{A_o(z)A_1(-z) - A_1(z)A_o(-z)} \tag{27.76}$$

These expressions reveal that for general FIR analysis filters, $A_o(z)$ and $A_1(z)$, and in order for $S_o(z)$ and $S_1(z)$ to be FIR as well, the denominator expression must evaluate to a pure delay, say,

$$A_o(z)A_1(-z) - A_1(z)A_o(-z) = z^{-\delta}/\beta \tag{27.77}$$

for some nonzero constant β and delay $\delta > 0$. When this holds, we would obtain

$$S_o(z) = 2\beta z^{(\delta-d)}A_1(-z) \tag{27.78}$$

$$S_1(z) = -2\beta z^{(\delta-d)}A_o(-z) \tag{27.79}$$

Generally, the leading coefficient of the FIR analysis filters $A_o(z)$ and $A_1(z)$ are nonzero. We set $\delta = d$ to obtain causal filters $S_o(z)$ and $S_1(z)$. These choices lead to the selections:

$$\boxed{S_o(z) = 2\beta A_1(-z), \quad S_1(z) = -2\beta A_o(-z)} \tag{27.80}$$

In this way, we arrive at causal FIR synthesis filters that guarantee perfect reconstruction.

In summary, starting from causal FIR analysis filters $A_o(z)$ and $A_1(z)$ satisfying the condition

$$\boxed{A_o(z)A_1(-z) - A_1(z)A_o(-z) = \frac{1}{\beta}z^{-d}} \tag{27.81}$$

we select the synthesis filters according to (27.80). In this way, the synthesis filters will be causal and FIR as well, and the filter bank will enable perfect reconstruction with transfer function from $x(n)$ to $y(n)$ given by

$$H(z) = z^{-d} \tag{27.82}$$

Substituting condition (27.81) into (27.73) we find that it amounts to setting $G(z) = 2\beta$ in (27.61). The filter bank in Example 27.6 is a perfect reconstruction filter bank with FIR analysis and synthesis filters that result from the choices $d = 1$ and $\beta = 1/4$.

We further remark that condition (27.81) can be restated in terms of an equivalent condition on the determinant of the 2×2 matrix $\mathcal{A}(z)$ introduced in (27.57), namely, that it should hold:

$$\boxed{\det \mathcal{A}(z) = \frac{1}{\beta} z^{-d}} \tag{27.83}$$

More generally, when $A_o(z)$ and $A_1(z)$ are not necessarily FIR filters but still satisfy (27.81) or (27.83), we get $G(z) = 2\beta$ in (27.61) and continue to select the synthesis filters according to (27.80). In this case, the analysis and synthesis filters need not be FIR but the filter bank will still possess the perfect reconstruction property, $H(z) = z^{-d}$, as long as the analysis and synthesis filters are causal and stable.

27.5.4 Quadrature Mirror Filter Banks

The quadrature mirror filter (QMF) bank is an alias-free filter bank where the analysis filters are related as follows

$$\boxed{A_1(z) = A_o(-z)} \tag{27.84}$$

We assume that the prototype filter, $A_o(z)$, is a low-pass filter with a real-valued impulse response sequence so that its magnitude frequency response, $|A_o(e^{j\omega})|$, is symmetric about the vertical axis, i.e., $|A_o(e^{j\omega})| = |A_o(e^{-j\omega})|$. It then follows from (27.84) that the frequency responses of the analysis filters are related as follows:

$$\begin{aligned} |A_1(e^{j\omega})| &= |A_o(-e^{j\omega})| \\ &= |A_o(e^{j(\omega-\pi)})| \\ &= |A_o(e^{-j(\omega-\pi)})| \\ &= |A_o(e^{j(\pi-\omega)})| \end{aligned} \tag{27.85}$$

That is,

$$\boxed{|A_1(e^{j\omega})| = \left|A_o\left(e^{j(\pi-\omega)}\right)\right|} \tag{27.86}$$

If we introduce the change of variables $\theta = \omega - \frac{\pi}{2}$, then the above equality becomes

$$\left|A_1(e^{j(\theta+\frac{\pi}{2})})\right| = \left|A_o\left(e^{j(\frac{\pi}{2}-\theta)}\right)\right| \tag{27.87}$$

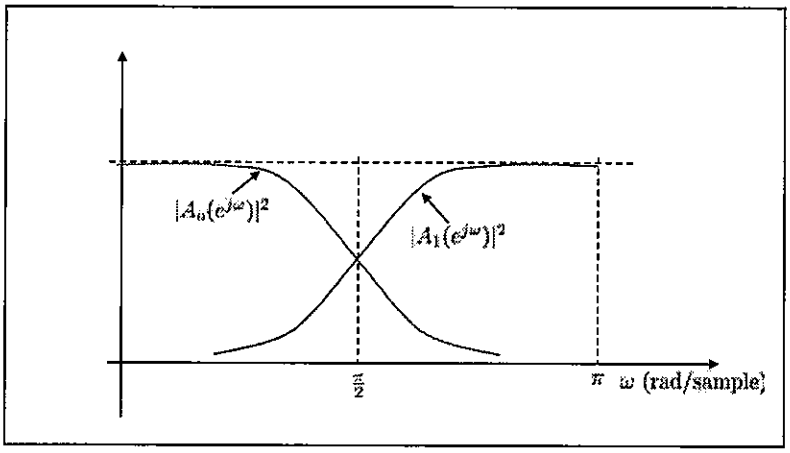

FIGURE 27.38 The magnitude responses of the analysis filters of a QMF are symmetric about $\omega = \pi/2$.

which means that the magnitude responses of the analysis filters, $A_o(z)$ and $A_1(z)$, are symmetric about the quadrature frequency, $\omega = \pi/2$, as illustrated in Fig. 27.38 and, hence, the name Quadrature Mirror Filter Bank.

Setting $G(z) = 2$ in (27.61), the alias-free condition of the QMF filter bank is met by selecting the synthesis filters as

$$\boxed{S_o(z) = 2A_1(-z) = 2A_o(z), \quad S_1(z) = -2A_o(-z)} \tag{27.88}$$

Thus, note that all filters in the QMF implementation are defined in terms of the prototype filter, $A_o(z)$. Using (27.63), we find that the resulting transfer function from $x(n)$ to $y(n)$ is

$$\boxed{H(z) = A_o^2(z) - A_o^2(-z)} \tag{27.89}$$

Perfect Reconstruction QMF with FIR Filters

The selection (27.88) ensures alias-free operation. In addition, we would like to select the prototype filter $A_o(z)$ to be an FIR filter than guarantees perfect reconstruction. Substituting (27.84) into (27.81) we find that $A_o(z)$ should be chosen to satisfy

$$A_o^2(z) - A_o^2(-z) = \frac{1}{\beta} z^{-d} \tag{27.90}$$

for some delay $d > 0$ and nonzero scalar β. Let us introduce the second-order polyphase decomposition of $A_o(z)$, say,

$$A_o(z) = E_o(z^2) + z^{-1}E_1(z^2) \tag{27.91}$$

Then condition (27.90) translates into the requirement that

$$E_o(z^2)E_1(z^2) = \frac{1}{4\beta} \cdot z^{-(d-1)} \tag{27.92}$$

which we rewrite as

$$E_o(z)E_1(z) \;=\; \frac{1}{4\beta}\cdot z^{-\frac{(d-1)}{2}} \tag{27.93}$$

Since $E_o(z)$ and $E_1(z)$ are FIR filters, the above equality is satisfied when

$$E_o(z) = a_o z^{-d_o} \quad \text{and} \quad E_1(z) = a_1 z^{-d_1} \tag{27.94}$$

for some constants $\{a_o, a_1\}$ and integer delays $\{d_o, d_1\}$ such that

$$a_o a_1 = \frac{1}{4\beta}, \qquad d_o + d_1 = \frac{d-1}{2} \tag{27.95}$$

Note that if $d > 0$ is selected as an odd integer, then d_o and d_1 can be selected as integers. It follows from (27.91) that the prototype filter is of the form:

$$A_o(z) = a_o z^{-2d_o} \;+\; a_1 z^{-2d_1-1} \tag{27.96}$$

which corresponds to a filter with only two nonzero taps. As a result, $A_o(z)$ will have poor selectivity in frequency and the subband signals $u_o(n)$ and $u_1(n)$ in Fig. 27.37 will not be well separated in the frequency domain. For this reason, perfect reconstruction QMF filter banks with 2 branches only involving FIR analysis and synthesis filters are generally undesirable.

Johnston QMF with FIR Filters

One way to address the poor performance of the perfect reconstruction QMF filter bank with FIR filters is to relax the condition of perfect reconstruction.

We continue to seek an alias-free QMF filter bank with FIR filters. Let $A_o(z)$ be a causal FIR filter with piecewise linear phase characteristics and with impulse response sequence of length N, say,

$$A_o(z) = \alpha(0) + \alpha(1)z^{-1} + \ldots + \alpha(N-1)z^{-(N-1)} \tag{27.97}$$

for some coefficients $\{\alpha(k)\}$. We studied linear phase FIR filters earlier in Sec. 16.2, where we showed that when the sequence $\alpha(n)$ is real-valued and symmetric, the frequency response of the filter $A_o(z)$ can be expressed in the form

$$A_o(e^{j\omega}) = e^{-j\omega\left(\frac{N-1}{2}\right)}\,\Gamma(\omega) \tag{27.98}$$

where $\Gamma(\omega)$ is some real-valued function of ω (see Table 16.1). Using the fact that

$$A_o(-e^{j\omega}) = A_o(e^{j(\omega-\pi)}) \tag{27.99}$$

and substituting (27.98) into the transfer function $H(z)$ in (27.89), we find that the frequency response of the filter bank in this case will be

$$\begin{aligned} H(e^{j\omega}) &= e^{-j\omega(N-1)}\Gamma^2(\omega) \;-\; e^{-j(\omega-\pi)(N-1)}\Gamma^2(\omega-\pi) \\ &= e^{-j\omega(N-1)}\Big[\Gamma^2(\omega) \;-\; e^{j\pi(N-1)}\Gamma^2(\omega-\pi)\Big] \\ &= e^{-j\omega(N-1)}\Big[\Gamma^2(\omega) \;-\; (-1)^{(N-1)}\Gamma^2(\omega-\pi)\Big] \end{aligned} \tag{27.100}$$

The length N of the prototype filter cannot be odd since otherwise the frequency response, $H(e^{j\omega})$, is annihilated at $\omega = \frac{\pi}{2}$, which is undesirable. Indeed, assume N is odd. Then,

$$H(e^{j\pi/2}) \;=\; e^{-j\frac{\pi(N-1)}{2}}\left[\Gamma^2(\pi/2) \;-\; \Gamma^2(-\pi/2)\right] \;=\; 0 \qquad (27.101)$$

since, from the expressions given for $\Gamma(\omega)$ in Table 16.1 for FIR filters of types I and II, we note that $\Gamma(\omega) = \Gamma(-\omega)$. We therefore select N to be even. In this case, the frequency response of the filter bank will be given by

$$H(e^{j\omega}) = e^{-j\omega(N-1)}\left[\Gamma^2(\omega) + \Gamma^2(\omega-\pi)\right] \qquad (27.102)$$

or, equivalently,

$$\boxed{H(e^{j\omega}) = e^{-j\omega(N-1)}\left[\;|A_o(e^{j\omega})|^2 \;+\; |A_o(e^{j(\omega-\pi)})|^2\;\right]} \qquad (27.103)$$

Thus, observe that the transfer function from $x(n)$ to $y(n)$ has linear phase, with delay $N-1$, and the magnitude response of $H(z)$ is not flat. That is, distortion occurs. However, if we can select the prototype FIR filter, $A_o(z)$, such that

$$|A_o(e^{j\omega})|^2 \;+\; |A_o(e^{j(\omega-\pi)})|^2 \;\approx\; 1 \qquad (27.104)$$

then the QMF filter will approach the performance of a perfect reconstruction filter bank. In other words, rather than impose the exact condition (27.90), we are now imposing the approximate condition (27.104). Johnston's method is based on the idea of designing a low-pass filter, $A_o(z)$, by means of a numerical (computer-aided) procedure that penalizes a weighted measure of two components: (a) the deviation from (27.104) and (b) the attenuation of the filter in its stop-band region. Specifically, let us introduce the cost function:

$$J \;\triangleq\; \lambda\int_{\omega_s}^{\pi}|A_o(e^{j\omega})|^2 d\omega \;+\; (1-\lambda)\int_0^{\pi}\left[\;1 - |A_o(e^{j\omega})|^2 \;-\; |A_o(e^{j(\omega-\pi)})|^2\;\right]d\omega \qquad (27.105)$$

where $0 < \lambda < 1$ is a convex combination parameter that is used to penalize both components of the cost function. Moreover, ω_s is the stopband frequency of the low-pass filter, $A_o(z)$. A numerical procedure can be used to minimize J over the coefficients $\{\alpha(k)\}$ of the filter $A_o(z)$. Tabulations exist for the resulting filters.

Example 27.7 (A Johnston filter)

The following filter coefficients correspond to the case $N = 12$ and are obtained by minimizing (27.105):

$$\begin{aligned} A_o(z) \;=\; & -0.006444 + 0.02746z^{-1} - 0.007582z^{-2} - 0.09138z^{-3} + 0.09809z^{-4} \\ & 0.4808z^{-5} + 0.4808z^{-6} + 0.09809z^{-7} - 0.09138z^{-8} - 0.007582z^{-9} \\ & 0.02746z^{-10} - 0.006444z^{-11} \end{aligned} \qquad (27.106)$$

Figure 27.39 plots the magnitude responses of the analysis filters $A_o(z)$ and $A_1(z) = A_o(-z)$. From (27.88), the corresponding synthesis filters are given by

$$S_o(z) = 2A_o(z), \qquad S_1(z) = -2A_o(-z) \qquad (27.107)$$

Figure 27.40 shows how close the magnitude response of the resulting QMF filter bank, $|H(e^{j\omega})|$, is to the desired value of unity.

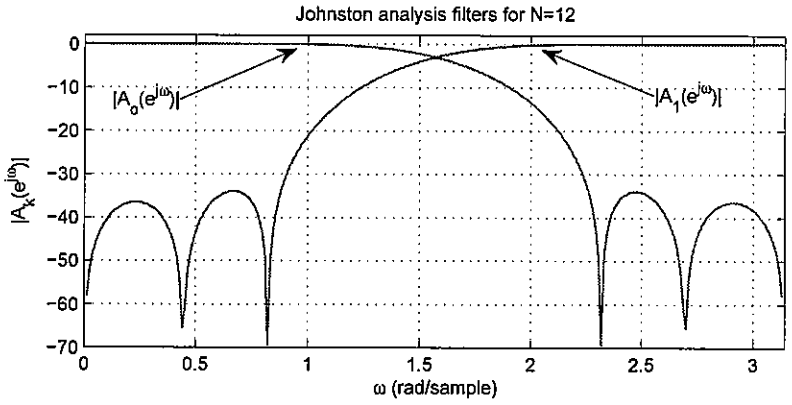

FIGURE 27.39 Magnitude responses of the Johnston analysis filters, $A_o(z)$ and $A_1(z)$, for $N = 12$ from Example 20.7.

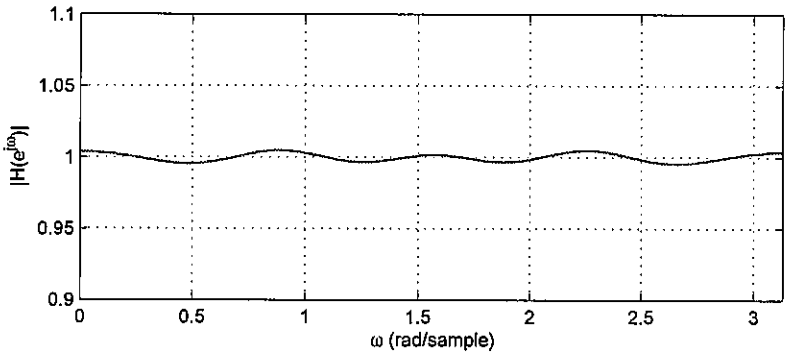

FIGURE 27.40 Resulting magnitude response of the Johnston QMF filter bank from Example 20.7; observe how the values of $|H(e^{j\omega})|$ are clustered around one.

◇

27.5.5 Orthogonal Perfect Reconstruction Filter Banks

Motivated by the discussion on Johnston filter banks, and by the approximate flat magnitude response (27.104), we now describe *orthogonal* filter banks that meet perfect reconstruction requirements. Thus, referring to the 2–branch filter bank in Fig. 27.37, we first note that the analysis filters of an orthogonal bank are causal real-valued FIR filters of the same form (27.97) with even duration N. Moreover, the filters $A_o(z)$ and $A_1(z)$ are chosen to satisfy the following two conditions:

$$\begin{aligned} 1 &= A_o(z)A_o(z^{-1}) + A_o(-z)A_o(-z^{-1}) \\ A_1(z) &= z^{-(N-1)}A_o(-z^{-1}) \end{aligned} \tag{27.108}$$

Observe that we are not dealing with a QMF bank any longer since $A_1(z)$ is not required to satisfy $A_1(z) = A_o(-z)$, as was the case earlier in (27.84).

Now, recall the definition of the 2×2 transfer matrix $\mathcal{A}(z)$ introduced in (27.57), and which is defined in terms of the analysis filters:

$$\mathcal{A}(z) \triangleq \begin{bmatrix} A_o(z) & A_1(z) \\ A_o(-z) & A_1(-z) \end{bmatrix} \tag{27.109}$$

Recall further the definition of the complex-conjugate reversed polynomial notation from (24.112) where, for example, $A_o^{\#}(z)$ is obtained from $A_o(z)$ by replacing z in $A_o(z)$ by $1/z$ and by complex-conjugating the impulse response sequence of $A_o(z)$. For instance, for an FIR filter $A_o(z)$ with real coefficients of the form (27.97) we get

$$A_o^{\#}(z) = \alpha(0) + \alpha(1)z + \ldots + \alpha(N-1)z^{N-1} \tag{27.110}$$

Likewise, for $A_1(z)$ and $A_1^{\#}(z)$. Then, it is straightforward to verify from the requirement (27.108) that the transfer matrix $\mathcal{A}(z)$ satisfies

$$\mathcal{A}(z)\left[\mathcal{A}\left(\frac{1}{z^*}\right)\right]^* = I_2 \tag{27.111}$$

where I_2 denotes the 2×2 identity matrix. In this case, we say that $\mathcal{A}(z)$ is a para-unitary transfer matrix. It is for this reason that filter banks that satisfy (27.108) are referred to as orthogonal filter banks.

Power Symmetry Properties

The first condition in (27.108) implies that the frequency response of the prototype filter, $A_o(z)$, is required to satisfy:

$$|A_o(e^{j\omega})|^2 + |A_o(e^{j(\omega-\pi)})|^2 \;=\; 1 \tag{27.112}$$

which should be compared with the approximate condition used in the Johnston QMF case (27.104). Furthermore, since $A_o(z)$ has a real-valued impulse response sequence, it follows that its magnitude response is symmetric about the vertical axis, i.e.,

$$|A_o(e^{j\omega})| \;=\; |A_o(e^{-j\omega})| \tag{27.113}$$

so that

$$\begin{aligned} |A_o(e^{j(\omega-\pi)})| &= |A_o(e^{j(\omega+\pi)})| \\ &= |A_o(e^{-j(\omega+\pi)})| \\ &= |A_o(e^{j(\pi-\omega)})| \end{aligned} \tag{27.114}$$

where, in the first and last equalities, we used the fact that $A_o(e^{j\omega})$ has period 2π. It follows that (27.112) can be rewritten as

$$\boxed{|A_o(e^{j\omega})|^2 + |A_o(e^{j(\pi-\omega)})|^2 \;=\; 1} \qquad \text{(power symmetry)} \tag{27.115}$$

Filters that satisfy this normalization condition are said to be power symmetric filters. Figure 27.41 illustrates condition (27.115) by plotting the squared magnitude response of $A_o(e^{j\omega})$ and $A_o(e^{j(\pi-\omega)})$; the latter is a reflection of the former about the vertical line at $\omega = \pi/2$. The sum of the squared magnitude responses evaluates to one.

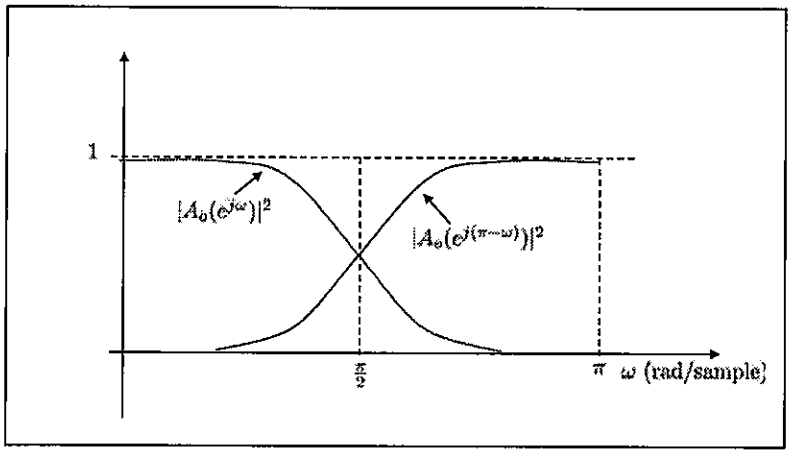

FIGURE 27.41 Illustration of the power symmetry property of the filter $A_o(z)$ in an orthogonal perfect reconstruction filter bank. The squared magnitude responses of $A_o(e^{j\omega})$ and its reflection about the vertical axis $\omega = \pi/2$ add up to one.

If we refer to the second condition in (27.108) we conclude that

$$|A_1(e^{j\omega})| = |A_o(e^{j(\pi-\omega)})| \tag{27.116}$$

so that we also have that the frequency responses of $A_o(z)$ and $A_1(z)$ satisfy

$$\boxed{|A_o(e^{j\omega})|^2 + |A_1(e^{j\omega})|^2 = 1} \quad \text{(power complimentary property)} \tag{27.117}$$

Filters that satisfy this property are said to be power complimentary since their squared magnitude responses add up to one, as illustrated again in Fig. 27.42.

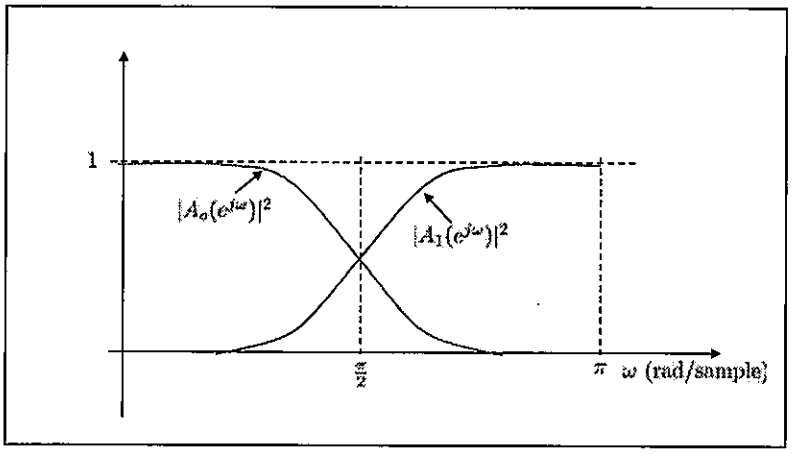

FIGURE 27.42 Illustration of the power complimentary property of the filters $A_o(z)$ and $A_1(z)$ in an orthogonal perfect reconstruction filter bank. The squared magnitude responses of $A_o(e^{j\omega})$ and $A_1(e^{j\omega})$ add up to one.

Perfect Reconstruction Properties

Let us now verify that conditions (27.108) lead to analysis filters $\{A_o(z), A_1(z)\}$ satisfy the perfect reconstruction condition (27.81) or, equivalently, (27.83). Indeed, using the fact that $N-1$ is odd,

$$\begin{aligned}
\det A(z) &= A_o(z)A_1(-z) - A_1(z)A_o(-z) \\
&= -z^{-(N-1)}A_o(z)A_o(z^{-1}) - z^{-(N-1)}A_o(-z^{-1})A_o(-z) \\
&= -z^{-(N-1)}\left[A_o(z)A_o(z^{-1}) + A_o(-z^{-1})A_o(-z)\right] \\
&= -z^{-(N-1)} \quad \text{(using (27.108))}
\end{aligned} \tag{27.118}$$

This result is of the form (27.83) with $\beta = -1$ and $d = N-1$. Therefore, using (27.80), we may select the synthesis filters as

$$S_o(z) = -2A_1(-z) \quad \text{and} \quad S_1(z) = 2A_o(-z) \tag{27.119}$$

so that

$$\boxed{S_o(z) = 2z^{-(N-1)}A_o(z^{-1}) \quad \text{and} \quad S_1(z) = 2A_o(-z)} \tag{27.120}$$

We still need to show how to determine a prototype filter, $A_o(z)$, that satisfies (27.115). Once $A_o(z)$ is determined, we can then construct the remaining filters, $A_1(z)$, $S_o(z)$, and $S_1(z)$ using (27.108) and (27.120).

Design via Spectral Factorization

We seek a causal low-pass FIR filter, $A_o(z)$, with even duration N, of the form (27.97) and that satisfies the power symmetry condition (27.115). One way to design such a filter is to design an auxiliary half-band filter (recall Sec. 26.4) followed by a spectral factorization step.

Specifically, let $r = N-1$ and $N_h = 2r+1$. Using the design procedure outlined in Sec. 26.4, and which was illustrated in Example 26.5, we already know how to design a half-band filter, $H(z)$, of duration N_h and whose impulse response sequence, $h(n)$, is real-valued and symmetric about the point $n = (N_h-1)/2$; the resulting filter will be FIR of type I. Moreover, in view of (26.125) and Example 26.5, the transfer function of the resulting half-band filter will satisfy

$$H(z) + H(-z) = z^{-r} \tag{27.121}$$

or, equivalently,

$$\boxed{z^r H(z) + z^r H(-z) = 1} \tag{27.122}$$

Now, the filter $H(z)$ has the form

$$H(z) = \sum_{n=0}^{2r} h(n)z^{-n} \tag{27.123}$$

in terms of its impulse response sequence. Let $H'(z) = z^r H(z)$ so that

$$H'(z) = \sum_{n=-r}^{r} h(n)z^{-n} \tag{27.124}$$

with positive and negative powers of z^{-1}. Using (27.122), we conclude that the frequency response of $H'(z)$ satisfies

$$H'(e^{j\omega}) + H'(e^{j(\pi-\omega)}) = 1 \tag{27.125}$$

In view of property (16.51) for type-I FIR filters, we know that the frequency response of $H(z)$ has the form

$$H(e^{j\omega}) = e^{-j\omega\left(\frac{N_h-1}{2}\right)} \cdot \Gamma(\omega) \tag{27.126}$$

for some real-valued function $\Gamma(\omega)$. Therefore, $H'(e^{j\omega}) = \Gamma(\omega)$, and we conclude that the frequency response of $H'(z)$ is real-valued. This frequency response can still assume negative values at some frequencies. For this reason, we modify it as follows:

$$P'(z) = H'(z) + \epsilon \tag{27.127}$$

where ϵ is a nonnegative number that is chosen large enough to ensure

$$P'(e^{j\omega}) > 0 \quad \text{for all } \omega \in [0, 2\pi] \tag{27.128}$$

Then, using (27.125), we have that

$$P'(e^{j\omega}) + P'(e^{j(\pi-\omega)}) = 1 + 2\epsilon \tag{27.129}$$

Let

$$\boxed{P(z) \triangleq \frac{z^r H(z) + \epsilon}{1 + 2\epsilon}} \tag{27.130}$$

Then, using (27.129), the transfer function $P(z)$ has a nonnegative real-valued frequency response that satisfies

$$\boxed{P(e^{j\omega}) + P(e^{j(\pi-\omega)}) = 1 \quad \text{and} \quad P(e^{j\omega}) > 0} \tag{27.131}$$

Since $P(e^{j\omega})$ is nonnegative, we can also write

$$|P(e^{j\omega})| + |P(e^{j(\pi-\omega)})| = 1 \tag{27.132}$$

Now observe from (27.124) and (27.130) that $P(z)$ has the form

$$P(z) = \sum_{n=-r}^{r} p(n) z^{-n} \tag{27.133}$$

for some real-valued impulse response sequence $\{p(n)\}$ and with both positive and negative powers of z^{-1}. Moreover, since $h(n)$ is symmetric around the point $n = (N_h - 1)/2$, we conclude that the coefficients $\{p(n),\ -r \le n \le r\}$ are symmetric around $n = 0$. The fact that the coefficients of $P(z)$ are real-valued and symmetric about $p(0)$ translates into conditions on the locations of the roots of $P(z) = 0$.

To begin with, since $P(e^{j\omega}) > 0$, then $P(z)$ does not have roots on the unit circle. Moreover, let z_i denote a zero of $P(z)$. Since $P(z)$ has real coefficients, then z_i^* should also be a zero of $P(z)$. In other words, the zeros of $P(z)$ occur in complex conjugate pairs. Likewise, if z_i is a root of $P(z)$ then $1/z_i$ is also a root of $P(z)$ due to the symmetry in the

coefficients $\{p(n)\}$. In this way, if $P(z)$ has a root outside the unit circle, then it will also have a root inside the unit circle. We can then factor $P(z)$ in the form

$$\boxed{P(z) \;=\; \gamma \cdot \prod_{i=1}^{r} \left(1 - z_i z^{-1}\right)\left(1 - z_i^* z\right)} \tag{27.134}$$

for some scalar $\gamma > 0$ and where we are using z_i to denote the roots of $P(z)$ that lie inside the unit circle ($|z_i| \leq 1$). We then choose $A_o(z)$ as follows:

$$\boxed{A_o(z) \;=\; \sqrt{\gamma} \cdot \prod_{i=1}^{r} (1 - z_i z^{-1})} \tag{27.135}$$

where the roots used in the construction of $A_o(z)$ will appear in complex conjugate pairs and will ensure real-coefficients for the prototype filter, $A_o(z)$. Then, $A_o(z)$ is a causal FIR filter and it satisfies

$$|A_o(e^{j\omega})|^2 \;=\; |P(e^{j\omega})| \tag{27.136}$$

We say that $A_o(z)$ is the canonical spectral factor of $P(z)$; such factors also arise in the study of estimation problems — see future Secs. ?? and ??. Note that by (27.132), the filter $A_o(z)$ that is found in this manner satisfies the desired power normalization property (27.108). We illustrate the above design procedure by means of an example.

Example 27.8 (Orthogonal perfect reconstruction)

We illustrate the construction of an orthogonal perfect reconstruction filter bank with $L = 2$ branches. We assume for this example that we desire a filter $A_o(z)$ of duration $N = 6$. Let $r = N - 1 = 5$ and set $N_h = 2r + 1 = 11$.

(1) The first step is to design a half-band filter, $H(z)$, of duration $N_h = 11$. We do so by following the procedure outlined earlier in Example 26.5. The filter coefficients are given by

$$h(n) = \frac{\sin\left(\frac{\pi(n-3)}{2}\right)}{\pi(n-3)} \cdot \left[0.54 - 0.46\cos\left(\frac{2\pi n}{N-1}\right)\right], \quad 0 \leq n \leq 10 \tag{27.137}$$

so that

$$H(z) = 0.0051 - 0.0422z^{-2} + 0.2903z^{-4} + 0.5z^{-5} + 0.2903z^{-6} - 0.0422z^{-8} + 0.0051z^{-10} \tag{27.138}$$

(2) Let $H'(z) = z^r H(z) = z^5 H(z)$, i.e.,

$$H'(z) = 0.0051z^5 - 0.0422z^3 + 0.2903z + 0.5 + 0.2903z^{-1} - 0.0422z^{-3} + 0.0051z^{-5} \tag{27.139}$$

The frequency response of $H'(z)$ is real-valued and its minimum value can be verified to be $H'_{\min}(e^{j\omega}) = -0.0065$. We select

$$\epsilon = 0.1 \;>\; H'_{\min}(e^{j\omega}) \tag{27.140}$$

and define

$$P'(z) = H'(z) + \epsilon \tag{27.141}$$

so that $P'(e^{j\omega}) > 0$. Then,

$$P'(z) = 0.0051z^5 - 0.0422z^3 + 0.2903z + 0.6 + 0.2903z^{-1} - 0.0422z^{-3} + 0.0051z^{-5} \tag{27.142}$$

Let

$$P(z) = \frac{P'(z)}{1+2\epsilon} = \frac{P'(z)}{1.2} \tag{27.143}$$

Then,

$$P(z) = 0.0043z^5 - 0.0352z^3 + 0.2419z + 0.5 + 0.2419z^{-1} - 0.0352z^{-3} + 0.0043z^{-5} \tag{27.144}$$

The roots of $P(z)$ are found to be:

$$\begin{aligned} z_1 &= -0.4381 && \text{(27.145a)} \\ z_2 &= -0.3870 + j0.3761 && \text{(27.145b)} \\ z_3 &= -0.3870 - j0.3761 && \text{(27.145c)} \\ z_4 &= 0.2723 + j0.1515 && \text{(27.145d)} \\ z_5 &= 0.2723 - j0.1515 && \text{(27.145e)} \end{aligned}$$

and

$$\begin{aligned} 1/z_1 &= -2.2825 && \text{(27.146a)} \\ 1/z_2 &= -1.3290 - j1.2914 && \text{(27.146b)} \\ 1/z_3 &= -1.3290 + j1.2914 && \text{(27.146c)} \\ 1/z_4 &= 2.8040 - j1.5599 && \text{(27.146d)} \\ 1/z_5 &= 2.8040 + j1.5599 && \text{(27.146e)} \end{aligned}$$

where the roots $\{z_1, z_2, z_3, z_4, z_5\}$ are all inside the unit circle. Moreover, $\gamma = 0.3425$ in the factorization

$$P(z) = \gamma \cdot \prod_{i=1}^{r} \left(1 - z_i z^{-1}\right)\left(1 - z_i^* z\right) \tag{27.147}$$

Note that the value of γ in this case can be determined as follows

$$\gamma = \frac{P(z)|_{z=1}}{\prod_{i=1}^{5}(1 - z_i)(1 - z_i^*)} \tag{27.148}$$

where the value of $P(z)$ at $z = 1$ is the sum of the coefficients of $P(z)$.

(3) Finally, we construct the canonical spectral factor $A_o(z)$ by retaining all the roots of $P(z)$ that lie inside the unit circle and by making sure that complex-conjugate roots are included in $A_o(z)$. This step gives

$$\begin{aligned} A_o(z) = {} & 0.5852 \times \\ & [1 + (0.3870 + j0.3760)z^{-1}][1 + (0.3870 - j0.3760)z^{-1}] \times \\ & (1 + 0.4381z^{-1}) \times \\ & [1 - (0.2723 + j0.1515)z^{-1}][1 - (0.2723 - j0.1515)z^{-1}] \end{aligned} \tag{27.149}$$

which translates into a filter $A_o(z)$ with real coefficients:

$$\begin{aligned} A_o(z) = {} & 0.5852 \times \\ & (1 + 0.7740z^{-1} + 0.2911z^{-2}) \times \\ & (1 + 0.4381z^{-1}) \times \\ & (1 - 0.5446z^{-1} + 0.0971z^{-2}) \end{aligned} \tag{27.150}$$

(4) Using (27.108) and (27.120), the filter $A_1(z)$ and the synthesis filters, $S_o(z)$ and $S_1(z)$ are given by

$$A_1(z) = z^{-5}A_o(-z^{-1}) \tag{27.151}$$
$$S_o(z) = 2z^{-5}A_o(z^{-1}) \tag{27.152}$$
$$S_1(z) = 2A_o(-z) \tag{27.153}$$

Figure 27.43 plots the squared magnitude frequency responses of $A_o(z)$ and $A_1(z)$, and their sum (which evaluates to one). Figure 27.44 plots the magnitude frequency responses of the filters $\{A_o(z), A_1(z), S_o(z), S_1(z)\}$.

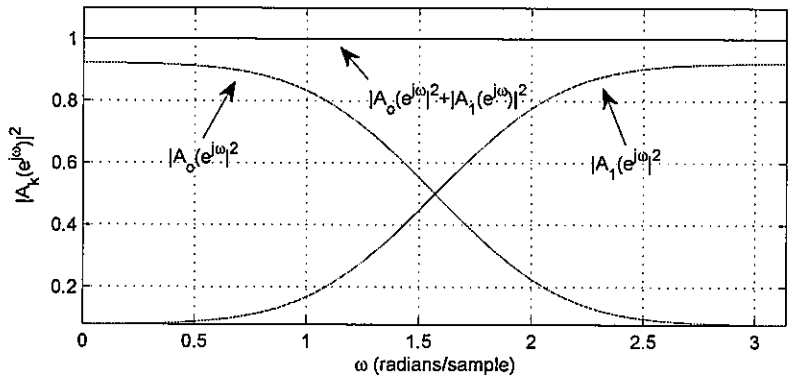

FIGURE 27.43 Squared magnitude responses of the analysis filters, $A_o(z)$ and $A_1(z)$, and their sum from Example 27.8.

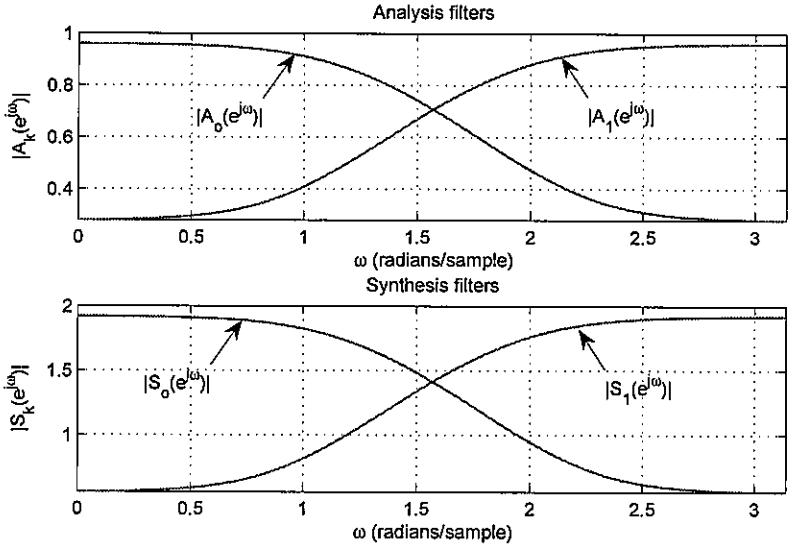

FIGURE 27.44 Magnitude responses of the analysis and synthesis filters for a 2−branch orthogonal perfect reconstruction filter bank from Example 27.8.

Figure 27.45 plots the sequences $x(n)$ and $y(n)$ at the input and output of the filter bank, and which result from using

$$x(n) = \sin\left(\frac{\pi}{4}n\right) + 0.5\sin\left(\frac{5\pi}{4}n\right)$$

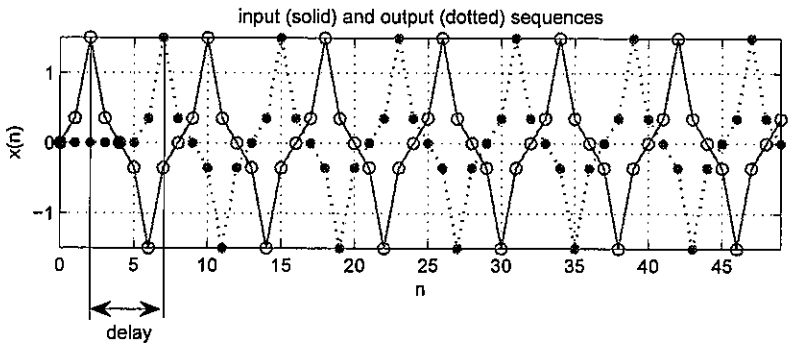

FIGURE 27.45 Original sequence, $x(n)$, and the output sequence, $y(n)$, for the 2−branch orthogonal perfect reconstruction filter bank from Example 27.8 — see Fig. 27.37. Note that there is a delay of $N-1=5$ samples at the output of the filter bank, as anticipated by the design procedure.

◇

Table 27.1 summarizes the main features of the various design methods described in this section for prefect (or close-to-perfect) reconstruction for 2−branch multi-rate filter banks of the form shown earlier in Fig. 27.37.

TABLE 27.1 Features of several design techniques for perfect (or close-to-perfect) reconstruction for 2−branch multi-rate filter banks of the form shown earlier in Fig. 27.37. In each case, the objective is to design causal and stable analysis and synthesis filters. In the table, the symbols PR and QMF stand for perfect reconstruction and quadrature mirror filters.

procedure	analysis filters	synthesis filters
PR (general)	select $\{A_o(z), A_1(z), G(z)\}$ such that $(A_o(z)A_1(-z) - A_1(z)A_o(-z))G(z) = z^{-d}$	$S_o(z) = G(z)A_1(-z)$ $S_1(z) = -G(z)A_o(-z)$
PR (FIR)	select causal FIR $\{A_o(z), A_1(z)\}$ such that $A_o(z)A_1(-z) - A_1(z)A_o(-z) = \frac{1}{\beta}z^{-d}$	$S_o(z) = 2\beta A_1(-z)$ $S_1(z) = -2\beta A_o(-z)$
QMF	$A_o(z) = a_o z^{-2d_o} + a_1 z^{-2d_1-1}$ $A_1(z) = A_o(-z)$ a_o, a_1 real	$S_o(z) = 2A_o(z)$ $S_1(z) = -2A_o(-z)$
Johnston QMF	$\min_{A_o(z)} J$ from (27.105), with N even and real symmetric causal impulse response sequence $A_1(z) = A_o(-z)$	$S_o(z) = 2A_o(z)$ $S_1(z) = -2A_o(-z)$
orthogonal PR	select causal FIR $A_o(z)$ to satisfy (e.g., (27.135)): $A_o(z)A_o(z^{-1}) + A_o(-z)A_o(-z^{-1}) = 1$ $A_1(z) = z^{-(N-1)}A_o(-z^{-1})$ $A_o(z)$ has N even and real symmetric impulse response	$S_o(z) = -2A_1(-z)$ $S_1(z) = 2A_o(-z)$

27.6 APPLICATION: TRANSMULTIPLEXERS IN COMMUNICATIONS

The discussion in this section complements and expands the earlier presentation from Sec. 18.4 on OFDM communications. The material serves as a good illustration of multirate concepts in the context of data communications. The key idea is to employ synthesis and analysis filter bank structures to transmit the data over narrower subbands. One main advantage is that the channel frequency response can be assumed to be practically flat over these subbands. When this occurs, recovery of the transmitted data is facilitated and can often be accomplished by means of single-tap equalization, as was the case with OFDM communications.

Before discussing transmultiplexer structures, we first revisit the OFDM transceiver from Fig. 18.32 and show how it can be recast in the form of a filter bank structure. Once this equivalent representation is established, we shall then use it to motivate a more general transceiver architecture, a special case of which will be OFDM. Clearly, the topic of multirate transmultiplexers is broad and the purpose of this section is to highlight some of the main ideas. The presentation is not meant to be comprehensive.

Transmitter Side

To begin with, let us refer to Fig. 18.32. The first step in the OFDM transceiver consists in forming a block vector of size N and processing it by the inverse DFT matrix, F^*:

$$\underbrace{\begin{bmatrix} \bar{s}(nN) \\ \bar{s}(nN-1) \\ \vdots \\ \bar{s}((n-1)N+1) \end{bmatrix}}_{\triangleq \bar{s}} \triangleq F^* \underbrace{\begin{bmatrix} s(nN) \\ s(nN-1) \\ \vdots \\ s((n-1)N+1) \end{bmatrix}}_{\triangleq s} \tag{27.154}$$

The process of forming the vector s is called blocking or *de-interleaving*. As was already explained in Example 26.1, it is straightforward to verify that the operation of blocking followed by the IDFT step can be accomplished by the multirate structure shown in Fig. 27.46. The structure consists of N branches, each with a downsampler by a factor of N. Feeding $s(n)$ through these branches results in the signals denoted by $\{t_k(n)\}$, which correspond to the entries of the successive block vectors s. The signals after transformation by F^* are denoted by $\{u_k(n)\}$ and they correspond to the entries of the successive block vectors $\bar{s}$.

The second step at the OFDM transmission side in Fig. 18.32 consists in adding a cyclic prefix of length P to the vector $\bar{s}$ and then sending the resulting $N+P$ modulated symbols $\{\bar{s}(m)\}$ through the channel, one symbol at a time. This unblocking, also called *interleaving*, operation followed by transmission over the channel can be accomplished by the multirate structure shown in Fig. 27.47, where we introduced the integer:

$$L \triangleq N+P \tag{27.155}$$

The L branches with upsamplers in them, followed by the series of delays and adders, perform the interleaving process. The $N+P$ entries

$$\{\underbrace{u_o(n), u_1(n), \ldots, u_{N-1}(n)}_{N \text{ entries}}, \quad \underbrace{u_o(n), \ldots, u_{P-1}(n)}_{P \text{ cyclic prefix entries}}\} \tag{27.156}$$

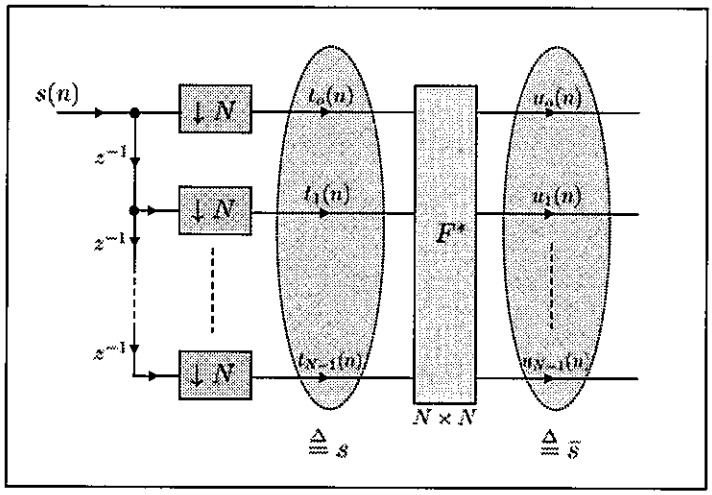

FIGURE 27.46 In an OFDM implementation, the input sequence $s(n)$ is de-interleaved to form the entries $\{t_k(n)\}$ at the input of the IDFT operation. These entries are transformed into the signals $\{u_k(n)\}$. The figure shows the blocking operation and the IDFT transformation from s to $\bar{s}$.

are then transmitted through the channel, one entry at a time, starting with $u_o(n)$.

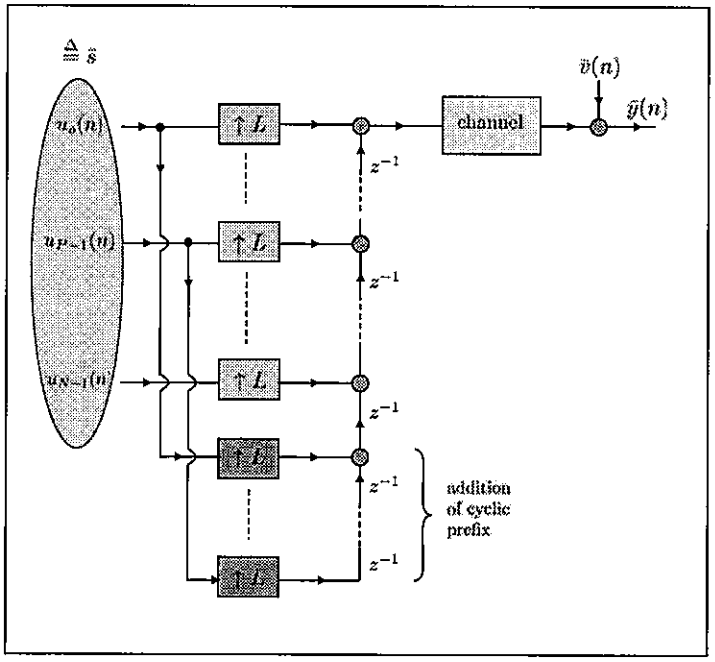

FIGURE 27.47 In an OFDM implementation, a cyclic prefix of size P is added to the transformed data $\{u_k(n)\}$, which amounts to repeating the top P entries and transmitting the resulting $N + P$ entries through the channel.

Figures 27.46 and 27.47 can be cascaded and combined into a single multirate structure. In this process, we can move the upsamplers that would appear after the IDFT operation F^* and place them before F^*; this step is already incorporated into the combined transmitter

structure shown in Fig. 27.48. Observe that the structure consists of a blocking operation followed by a synthesis filter bank with upsampling factor L.

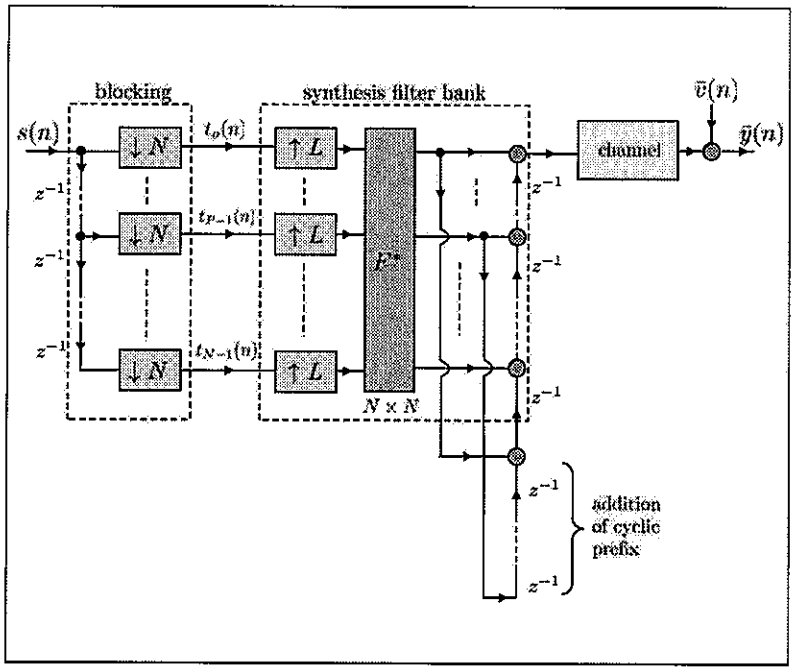

FIGURE 27.48 A multirate filter bank implementation of the OFDM transmission structure. The implementation consists of a blocking operation (by a factor N) followed by a synthesis filter bank with upsampling factor L.

Receiver Side

We can similarly analyze the receiver side of the OFDM structure of Fig. 18.32. The first step consists in forming a block vector of size $L = N + P$, shown below, from the received data $\{\bar{y}(n)\}$ and removing the cyclic prefix (namely, the last P entries):

$$\begin{bmatrix} \bar{y}(nN+P) \\ \bar{y}(nN+P-1) \\ \vdots \\ \bar{y}((n-1)N+P+1) \\ \hline \bar{y}((n-1)N+P) \\ \vdots \\ \bar{y}((n-1)N+1) \end{bmatrix} \xrightarrow{\text{remove prefix}} \underbrace{\begin{bmatrix} \bar{y}(nN+P) \\ \bar{y}(nN+P-1) \\ \vdots \\ \bar{y}((n-1)N+P+1) \end{bmatrix}}_{\triangleq \bar{y}} \tag{27.157}$$

The resulting vector $\bar{y}$ is subsequently processed by the DFT matrix, F, to generate the vector y:

$$\underbrace{\begin{bmatrix} y(nN+P) \\ y(nN+P-1) \\ \vdots \\ y((n-1)N+P+1) \end{bmatrix}}_{\triangleq y} = F \underbrace{\begin{bmatrix} \bar{y}(nN+P) \\ \bar{y}(nN+P-1) \\ \vdots \\ \bar{y}((n-1)N+P+1) \end{bmatrix}}_{\triangleq \bar{y}} \tag{27.158}$$

The blocking operation to form $\bar{y}$ followed by the DFT operation can be accomplished by the analysis multirate structure shown in Fig. 27.49. The structure consists of L branches, each with a downsampler by a factor of L. In the figure, we are denoting the signals at the input and output of the DFT operation generically by $\{c_k(n), d_k(n)\}$. The collection of the top N signals $\{c_k(n)\}$ constitute the entries of the successive block vectors $\bar{y}$. Likewise, the collection of N signals $\{d_k(n)\}$ corresponds to the entries of the successive vectors y.

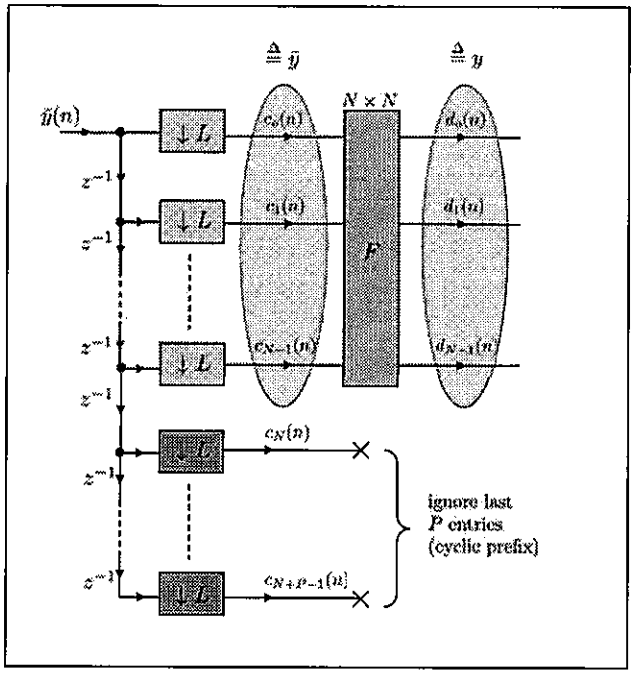

FIGURE 27.49 An OFDM analysis filter bank used at the receiver side. The received sequence $\bar{y}(n)$ is de-interleaved to form the entries $\{c_k(n)\}$ at the input of the DFT operation. These entries are transformed into the signals $\{d_k(n)\}$, which will be subsequently used by the detector module to recover the transmitted data.

The second step at the OFDM receiver side consists in scaling the entries $\{d_k(n)\}$ of the vector y by the corresponding factors $\{1/\lambda_k\}$ and then recovering the estimated symbols $\{\hat{s}(n-P)\}$. This step can be accomplished by the multirate structure shown in Fig. 27.50. In the figure we are denoting the scaled signals generically by $\{e_k(n)\}$. Recall, however, that the data $\{\bar{y}(n)\}$ up to time $N+P-1$ are collected into the block vector $\bar{y}$ in the process of recovering $\hat{s}(N-P)$. For this reason, there will be a delay of P samples and the output signal in Fig. 27.50 is denoted by $\hat{s}(n-P)$ (since the input to the transmitter block in Fig. 27.48 is $s(n)$).

Figures 27.49 and 27.50 can be cascaded and combined into a single multirate structure. In this process, we can move the upsamplers that appear after the DFT operation and place them before F; this step is already incorporated into the combined transmitter structure shown in Fig. 27.51.

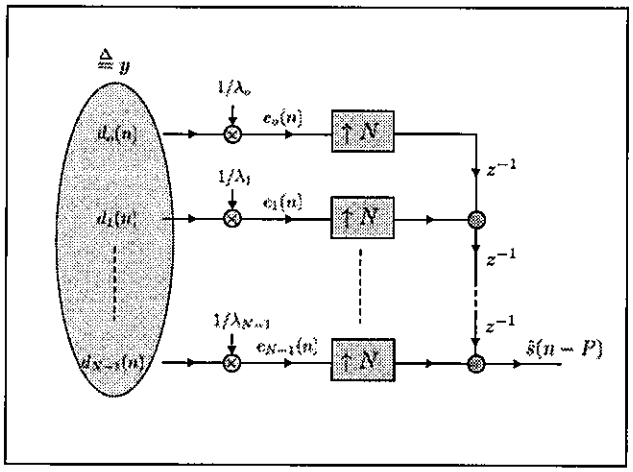

FIGURE 27.50 At the OFDM receiver, the signals $\{d_k(n)\}$ are scaled by $\{1/\lambda_k\}$ and the data are interleaved to result in the output sequence $\hat{s}(n-P)$.

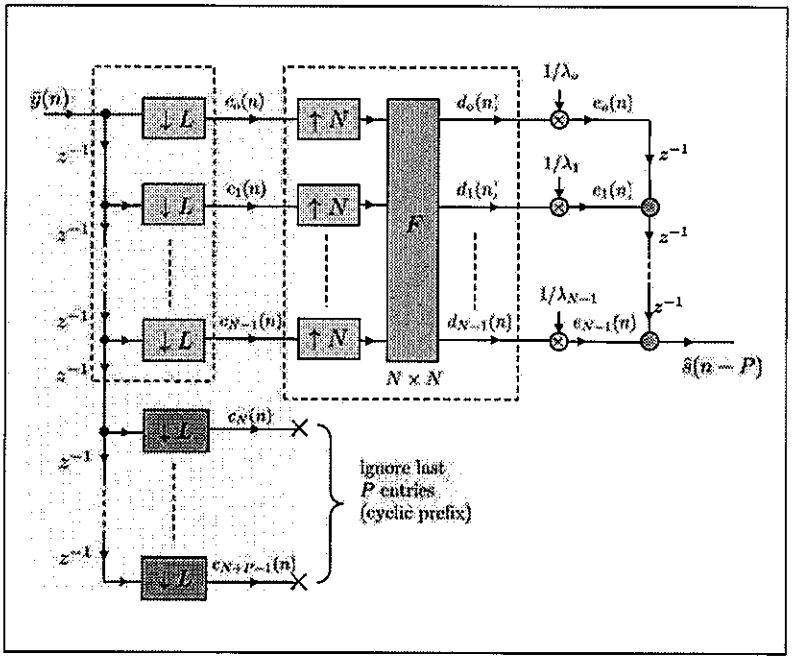

FIGURE 27.51 A multirate filter bank implementation of the OFDM receiver structure.

Transmultiplexers

Our objective now is to use the filter bank implementations derived in Figs. 27.48 and 27.51 to motivate more general transceiver structures. One notable difference will arise in the treatment of filter banks in this section in relation to what was done in the earlier sections of this chapter. Recall from Figs. 27.30 and 27.31 that in traditional subband processing, we start from an input sequence and decompose it into subbands using an analysis filter bank. Subsequently, after processing, the subband signals are synthesized together using a synthesis filter bank. This type of decomposition, where the synthesis filter bank follows the analysis filter bank, is useful in several applications. The subband coding procedure

discussed in Sec. 26.5 is one prime example where this traditional point of view has proven extremely successful in practice.

However, as the discussion will reveal, in the study of transmultiplexers for communications, the stages corresponding to the analysis and synthesis filter banks are reversed. The synthesis filter bank will come first and will reside at transmitter side, while the analysis filter bank will reside at the receiver side. This placement is already evident in the OFDM case if we examine Figs. 27.48 and 27.51 closely, although the discussion that follows will help make this observation clearer.

Prototype synthesis filter. Starting with an input sequence $s(n)$, we first assume that the data are blocked (or de-interleaved) into blocks of size N, as was the case in Fig. 27.46. Now, however, rather than feed the de-interleaved data into the inverse DFT operation, F^*, we feed them into a more general synthesis filter bank with N subband filters $\{S_k(z)\}$. This situation is illustrated in Fig. 27.52 — compare with Fig. 27.48 in the OFDM case. In the figure, $S_o(z)$ denotes some low-pass prototype filter. Although possible, we shall not deal with general synthesis filter banks. Instead, we shall select the subband filters $\{S_k(z)\}$ to be modulated versions of $S_o(z)$, as explained further ahead (see (27.169)), and as already seen in the body of the chapter when discussing uniform filter banks. We will establish later that the OFDM filter bank of Fig. 27.48 is a special case of Fig. 27.52 when we select $S_o(z)$ as:

$$S_o(z) = 1 + z^{-1} + z^{-2} + z^{-3} + \ldots + z^{-(L-1)} \quad \text{(a special case)} \tag{27.159}$$

In this case, the impulse response sequence of $S_o(z)$ corresponds to a rectangular window of duration L. We shall not restrict $S_o(z)$ to be of the above form. More generally, we shall assume that the impulse response sequence of the prototype filter is real-valued and has some length Q; we denote its samples by $s_o(n)$ so that:

$$\boxed{S_o(z) = s_o(0) + s_o(1)z^{-1} + s_o(2)z^{-2} + \ldots + s_o(Q-1)z^{-(Q-1)}} \tag{27.160}$$

Allowing for more general prototype filters $S_o(z)$, in lieu of the rectangular window (27.159), gives the designer better control over the amount of spectral overlap among adjacent subbands. For example, the designer can select subband filters that result in better frequency selectivity and less overlap than the subband filters that arise from the choice (27.159) (which is used in the OFDM case).

We proceed to derive a more efficient filter bank implementation in terms of the DFT operation for the structure shown in Fig. 27.52. To do so, we decompose the prototype filter, $S_o(z)$, into polyphase components of some order $L \geq N$. Using polyphase components of order $L > N$ results in the addition of redundancy into the transmitted data. We note in passing that we studied in Sec. 27.2) the derivation of DFT synthesis filter banks when the order of the polyphase components coincided with N; the argument in this section extends the derivation to the more general case $L \geq N$.

Thus, let $P_m(z)$ denote the polyphase components of $S_o(z)$ of order $L \geq N$ so that:

$$S_o(z) = \sum_{m=0}^{L-1} z^{-m} P_m(z^L) \tag{27.161}$$

For convenience of presentation, and without loss of generality, we can assume that Q is a multiple of both L and N (by appending zero entries to the impulse response sequence of $S_o(z)$, as necessary). As we already know from (26.64), the polyphase components $P_m(z)$

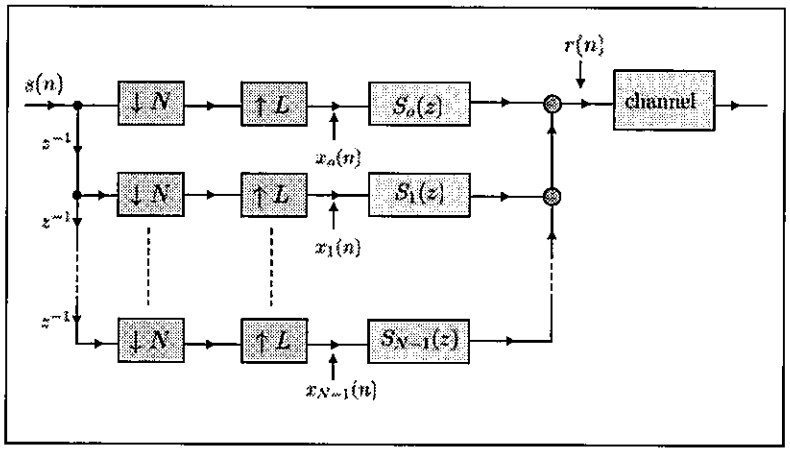

FIGURE 27.52 Transmitter module in a communications transmultiplexer. The input sequence $s(n)$ is de-interleaved to form block vectors of size N; the resulting signals feed into a synthesis filter bank with upsampling factor L to generate the signal $r(n)$ that is transmitted over the channel. The signals at the input of the subband filters are being denoted by $\{x_k(n)\}$. Compare this structure with the transmission structure for OFDM in Fig. 27.48. The main difference is that we are now allowing for a more general prototype filter, $S_o(z)$ and, correspondingly, for more general subband filters, $\{S_k(z)\}$. The OFDM structure of Fig. 27.48 will be seen to correspond to the special choice (27.159) for the prototype filter $S_o(z)$. In the sequel we will be showing how the subband filters in the above figure can be implemented in terms of a DFT-based structure, which will get us closer to Fig. 27.48.

are defined in terms of the impulse response coefficients $\{s_o(n)\}$ as follows:

$$P_m(z) = \sum_{n=0}^{\frac{Q}{L}-1} s_o(nL+m)z^{-n} \tag{27.162}$$

It follows that we can express the polyphase components in terms of the impulse response sequence $\{s_o(n)\}$ through the following matrix-vector relation:

$$\underbrace{\begin{bmatrix} P_o(z) & P_1(z) & \dots & P_{L-1}(z) \end{bmatrix}}_{1\times L \text{ (polyphase components)}} = \tag{27.163}$$

$$\underbrace{\begin{bmatrix} s_o(0) & s_o(1) & \dots & s_o(Q-1) \end{bmatrix}}_{1\times Q \text{ (impulse response sequence)}} \underbrace{\begin{bmatrix} I_L \\ z^{-1}I_L \\ \vdots \\ z^{-(Q/L)+1}I_L \end{bmatrix}}_{Q\times L\ (\triangleq B(z))}$$

where we are denoting the right-most $Q \times L$ matrix by $B(z)$; it consists of $L \times L$ diagonal blocks with z^{-m} on their diagonal, for $m = 0, 1, \dots, \frac{Q}{L} - 1$. The notation I_L denotes the

$L \times L$ identify matrix with ones on the diagonal and zeros elsewhere:

$$I_L \triangleq \begin{bmatrix} 1 & & & \\ & 1 & & \\ & & \ddots & \\ & & & 1 \end{bmatrix} \quad (L \times L) \tag{27.164}$$

Note that the matrix $B(z)$ has the following structure (illustrated for $L = 3$):

$$B(z) = \left[\begin{array}{ccc} 1 & & \\ & 1 & \\ & & 1 \\ \hline z^{-1} & & \\ & z^{-1} & \\ & & z^{-1} \\ \hline z^{-2} & & \\ & z^{-2} & \\ & & z^{-2} \\ \hline \vdots & \vdots & \vdots \end{array}\right] \quad \text{(diagonal blocks multiplied by } z^{-m}\text{)} \tag{27.165}$$

For example, for the numerical values $L = 2$ and $Q = 4$, relation (27.163) takes the form:

$$\begin{bmatrix} P_o(z) & P_1(z) \end{bmatrix} = \begin{bmatrix} s_o(0) & s_o(1) & s_o(2) & s_o(3) \end{bmatrix} \left[\begin{array}{cc} 1 & 0 \\ 0 & 1 \\ \hline z^{-1} & 0 \\ 0 & z^{-1} \end{array}\right] \tag{27.166}$$

which is consistent with the expected expressions for $P_o(z)$ and $P_1(z)$:

$$P_o(z) = s_o(0) + s_o(2)z^{-1} \tag{27.167}$$

$$P_1(z) = s_o(1) + s_o(3)z^{-1} \tag{27.168}$$

Synthesis filter bank. Using the prototype filter $S_o(z)$ defined by (27.160) we now construct a synthesis filter bank consisting of N subband filters $\{S_k(z)\}$ that are chosen as the following modulated versions of $S_o(z)$:

$$\boxed{S_k(z) = S_o\left(ze^{\frac{j2\pi k}{N}}\right), \quad k = 0, 1, \ldots, N-1} \tag{27.169}$$

Observe that, in contrast to the development earlier in Sec. 27.2 when we studied the DFT synthesis filter bank, the factor N that is now used in the modulation factor $e^{j2\pi k/N}$ in (27.169) is smaller than the order L of the polyphase decomposition in (27.161). This fact influences the argument that was used earlier to arrive at (27.20) and (27.38) while deriving the DFT analysis and synthesis filter banks; the argument will need to be adjusted. The modified argument will help explain, for example, how the difference between L and N leads to the introduction of the cyclic prefix step into the filter bank construction in the OFDM case.

Let again W_N denote the $N-$th root of unity, i.e.,

$$W_N \triangleq e^{-j\frac{2\pi}{N}} \tag{27.170}$$

In view of (27.169), the impulse response sequences of the subband filters $S_k(z)$ are related to the impulse response sequence of the prototype filter $S_o(z)$ as follows:

$$\boxed{s_k(n) = W^{-kn} \cdot s_o(n), \quad \begin{cases} k = 0, 1, \ldots, N-1 \\ n = 0, 1, \ldots, Q-1 \end{cases}} \tag{27.171}$$

We can express this relation in vector form as:

$$\begin{bmatrix} s_k(0) & s_k(1) & \ldots & s_k(Q-1) \end{bmatrix} = \tag{27.172}$$

$$\begin{bmatrix} 1 & W^{-k} & W^{-2k} & \ldots & W^{-(Q-1)k} \end{bmatrix} \cdot \begin{bmatrix} s_o(0) & & & & \\ & s_o(1) & & & \\ & & & \ddots & \\ & & & & s_o(Q-1) \end{bmatrix}$$

This relation can be simplified by exploiting the fact that Q is a multiple of N and W is the $N-$th root of unity. This fact implies that the row vector

$$\begin{bmatrix} 1 & W^{-k} & W^{-2k} & \ldots & W^{-(Q-1)k} \end{bmatrix} \tag{27.173}$$

actually consists of Q/N repeated blocks:

$$\begin{bmatrix} 1 & W^{-k} & \ldots & W^{-(N-1)k} & | & 1 & W^{-k} & \ldots & W^{-(N-1)k} & | & \ldots \end{bmatrix} \tag{27.174}$$

It follows that (27.172) can be written as

$$\boxed{\begin{bmatrix} s_k(0) & s_k(1) & \ldots & s_k(Q-1) \end{bmatrix} = \underbrace{\begin{bmatrix} 1 & W^{-k} & \ldots & W^{-(N-1)k} \end{bmatrix}}_{1\times N} \cdot \mathcal{J} \cdot \mathcal{S}} \tag{27.175}$$

where

$$\boxed{\mathcal{J} \triangleq \begin{bmatrix} I_N & I_N & \ldots & I_N \end{bmatrix} \qquad (N \times Q)} \tag{27.176}$$

and

$$\boxed{\mathcal{S} \triangleq \begin{bmatrix} s_o(0) & & & \\ & s_o(1) & & \\ & & \ddots & \\ & & & s_o(Q-1) \end{bmatrix} \quad (Q \times Q)} \tag{27.177}$$

Using (27.175), we can relate the polyphase components of the subband filters $S_k(z)$ to the prototype impulse response sequence $\{s_o(n)\}$, just like we did earlier in (27.163). Thus, let $P_{k,m}(z)$ denote the polyphase components of $S_k(z)$ of order L so that:

$$S_k(z) = \sum_{m=0}^{L-1} z^{-m} P_{k,m}(z^L) \tag{27.178}$$

These polyphase components are defined in terms of the impulse response coefficients $\{s_k(n)\}$ as follows:

$$P_{k,m}(z) = \sum_{n=0}^{\frac{Q}{L}-1} s_k(nL+m)z^{-n} \tag{27.179}$$

As was done to arrive at (27.163), it is again straightforward to verify that, for the $k-$th subband filter:

$$\begin{bmatrix} P_{k,o}(z) & P_{k,1}(z) & \dots & P_{k,L-1}(z) \end{bmatrix} = \begin{bmatrix} s_k(0) & s_k(1) & \dots & s_k(Q-1) \end{bmatrix} \cdot B(z) \tag{27.180}$$

for the same matrix $B(z)$ as in (27.163). But since we know from (27.171) how to relate the impulse response sequence $\{s_k(n)\}$ to that of the prototype filter, we can re-work expression (27.180) into a form that depends on the prototype impulse response sequence. Thus, using (27.171) and (27.180) we can write

$$\begin{bmatrix} P_{k,o}(z) & P_{k,1}(z) & \dots & P_{k,L-1}(z) \end{bmatrix} = \begin{bmatrix} 1 & W^{-k} & \dots & W^{-(N-1)k} \end{bmatrix} \cdot \mathcal{J} \cdot \mathcal{S} \cdot B(z) \tag{27.181}$$

Collecting relation (27.181) for $k = 0, 1, \dots, N-1$ gives

$$\begin{bmatrix} P_o(z) & P_1(z) & \dots & P_{L-1}(z) \\ P_{1,o}(z) & P_{1,1}(z) & \dots & P_{1,L-1}(z) \\ P_{2,o}(z) & P_{2,1}(z) & \dots & P_{2,L-1}(z) \\ \vdots & \vdots & & \vdots \\ P_{N-1,o}(z) & P_{N-1,1}(z) & \dots & P_{N-1,L-1}(z) \end{bmatrix} = F^* \cdot \mathcal{J} \cdot \mathcal{S} \cdot B(z) \tag{27.182}$$

where F^* is the $N \times N$ inverse DFT matrix, e.g., for $N = 4$:

$$F^* = \begin{bmatrix} 1 & 1 & 1 & 1 \\ 1 & W_4^{-1} & W_4^{-2} & W_4^{-3} \\ 1 & W_4^{-2} & W_4^{-4} & W_4^{-6} \\ 1 & W_4^{-3} & W_4^{-6} & W_4^{-9} \end{bmatrix} \tag{27.183}$$

Using (27.178), we conclude that the subband filters $\{S_k(z)\}$ satisfy:

$$\boxed{\begin{bmatrix} S_o(z) \\ S_1(z) \\ S_2(z) \\ \vdots \\ S_{N-1}(z) \end{bmatrix} = F^* \cdot \mathcal{J} \cdot \mathcal{S} \cdot B(z^L) \cdot \begin{bmatrix} 1 \\ z^{-1} \\ z^{-2} \\ \vdots \\ z^{-(L-1)} \end{bmatrix}} \tag{27.184}$$

If we now refer back to Fig. 27.52, the signal $r(n)$ is given by (in the transform domain):

$$\begin{aligned} R(z) &= X_o(z)S_o(z) + X_1(z)S_1(z) + \ldots + X_{N-1}(z)S_{N-1}(z) \\ &= \begin{bmatrix} X_o(z) & X_1(z) & \ldots & X_{N-1}(z) \end{bmatrix} \cdot F^* \cdot \mathcal{J} \cdot \mathcal{S} \cdot B(z^L) \cdot \begin{bmatrix} 1 \\ z^{-1} \\ z^{-2} \\ \vdots \\ z^{-(L-1)} \end{bmatrix} \end{aligned} \tag{27.185}$$

This result shows that the signal $r(n)$ can be generated from the signals $\{x_k(n)\}$ by first transforming them by the inverse DFT operation, F^*, and then duplicating the resulting signals and feeding combinations thereof into the polyphase filters. The corresponding multirate structure is illustrated in Fig. 27.53 for the case $N = 4$, $Q = 12$, and $L = 6$. The adders and delays to the right of the inverse DFT operation can be combined together into a simpler equivalent structure, which is shown in Fig. 27.54. It is now immediate to verify that when $S_o(z)$ is chosen as in (27.159), with $P = 2$ and $s_o(6) = \ldots = s_o(11) = 0$, then the structure of Fig. 27.54 reduces to the OFDM transmitter structure of Fig. 27.48 for $N = 4$ and $L = 6$.

Prototype analysis filter. We now turn our attention to the receiver side of the transmultiplexer and generalize the OFDM structure of Fig. 27.49. We do so by feeding the received sequence $\bar{y}(n)$ into an analysis filter bank, with N subband filters $\{A_k(z)\}$ followed by downsamplers by a factor of L. This situation is illustrated in Fig. 27.55, where we are denoting the output by $\hat{s}(n-D)$ and D models the amount of delay through the combination transmitter/channel/receiver. In the figure, $A_o(z)$ denotes some low-pass prototype filter. Although possible, we shall not deal with general analysis filter banks. Instead, we shall select the subband filters $\{A_k(z)\}$ to be modulated versions of $A_o(z)$, as explained further ahead (see (27.191)). We will establish later that the OFDM filter bank of Fig. 27.48 is a special case of Fig. 27.54 when we select $A_o(z)$ as:

$$A_o(z) = 1 + z^{-1} + z^{-2} + z^{-3} + \ldots + z^{-(N-1)} \quad \text{(a special case)} \tag{27.186}$$

In this case, the impulse response sequence of $A_o(z)$ corresponds to a rectangular window of duration N. We shall not restrict $A_o(z)$ to the above form. More generally, we assume the impulse response sequence of the prototype filter $A_o(z)$ is real-valued and has length Q; we denote its samples by $a_o(n)$ so that:

$$\boxed{A_o(z) = a_o(0) + a_o(1)z^{-1} + a_o(2)z^{-2} + \ldots + a_o(Q-1)z^{-(Q-1)}} \tag{27.187}$$

We proceed to derive an efficient filter bank implementation for the structure shown in Fig. 27.55 by decomposing the prototype filter into polyphase components of some order $L \geq N$. Using polyphase components of order $L > N$ results in the removal of redundancy from the received data. Thus, let $E_m(z)$ denote the polyphase components of $A_o(z)$ of order $L \geq N$ so that:

$$A_o(z) = \sum_{m=0}^{L-1} z^{-m} E_m(z^L) \tag{27.188}$$

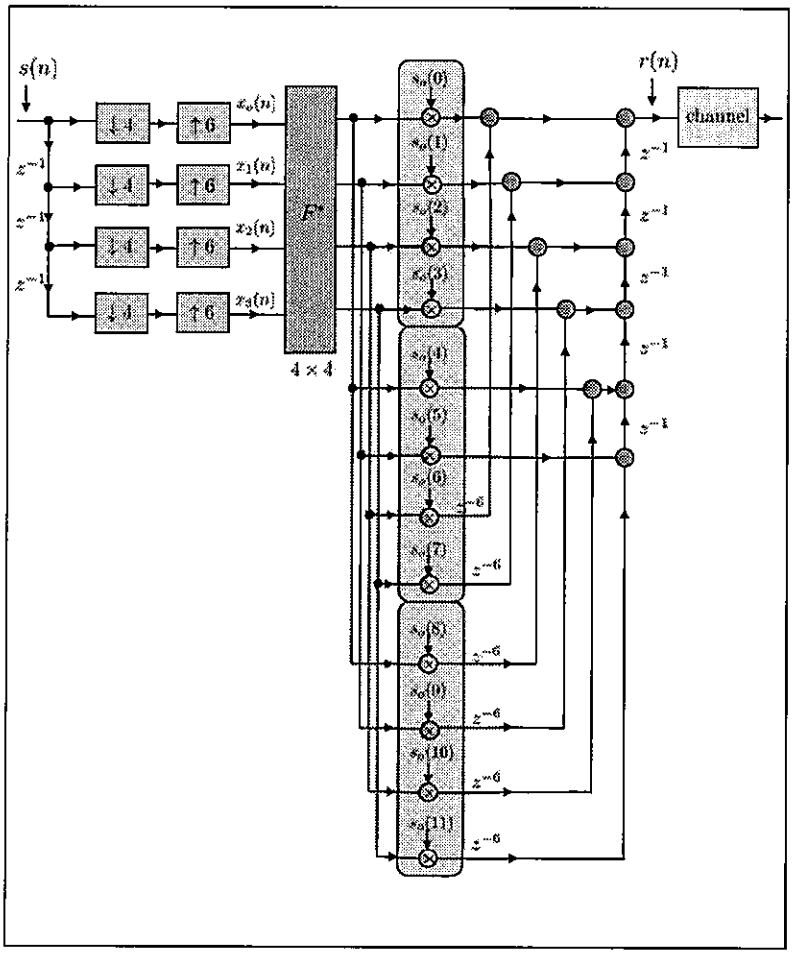

FIGURE 27.53 Transmitter module in a communications transmultiplexer. This is an equivalent filter bank implementation of the structure shown earlier in Fig. 27.52 in terms of an inverse DFT operation for the case $N = 4$, $Q = 12$, and $L = 6$. The samples of the impulse response sequence of the prototype filter $\{s_o(n)\}$ appear multiplying the signals at the output of the F^* operation. The adders and delays to the right of the inverse DFT operation are combined together into a simpler equivalent structure in Fig. 27.54.

We continue to assume that Q is a multiple of both L and N. The polyphase components $E_m(z)$ are defined in terms of the impulse response coefficients $\{a_o(n)\}$ as follows:

$$E_m(z) = \sum_{n=0}^{\frac{Q}{L}-1} a_o(nL+m)z^{-n} \tag{27.189}$$

We can express these polyphase components in terms of the impulse response sequence $\{a_o(n)\}$ through the following matrix-vector relation:

$$\underbrace{\begin{bmatrix} E_o(z) & E_1(z) & \dots & E_{L-1}(z) \end{bmatrix}}_{1\times L \text{ (polyphase components)}} = \tag{27.190}$$

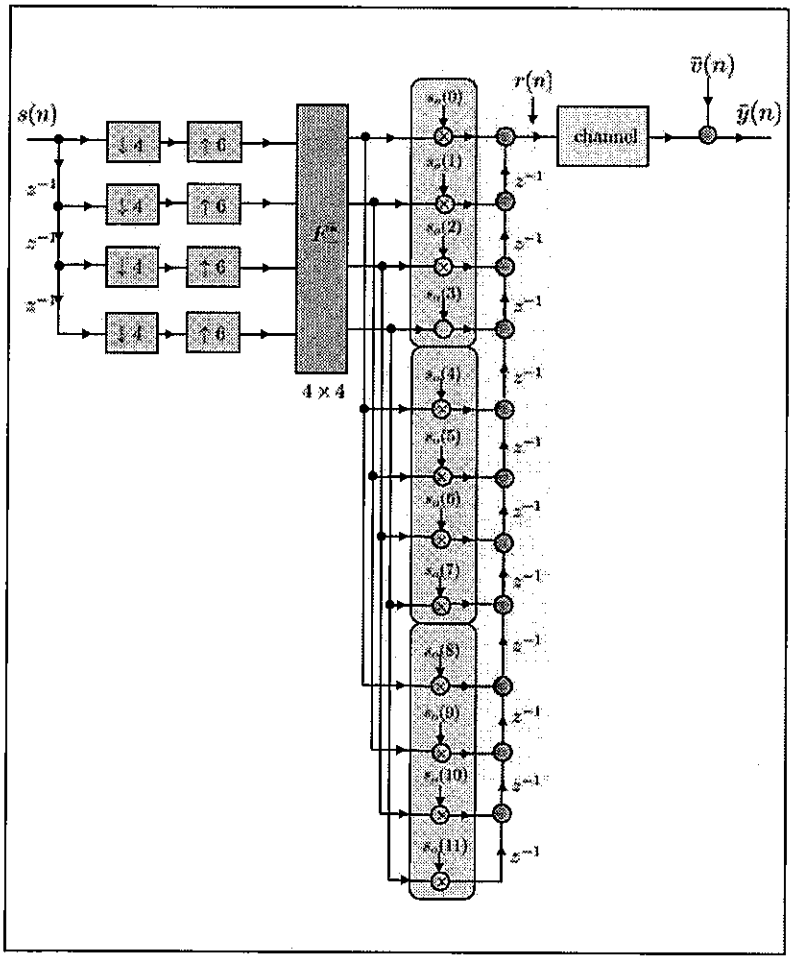

FIGURE 27.54 Transmitter module in a communications transmultiplexer. This is an equivalent filter bank implementation of the structures shown in Figs. 27.52 and 27.53 for the case $N = 4$, $Q = 12$, and $L = 6$. We are now showing the additive noise at the output of the channel.

$$\underbrace{\begin{bmatrix} a_o(0) & a_o(1) & \dots & a_o(Q-1) \end{bmatrix}}_{1\times Q \text{ (impulse response sequence)}} \underbrace{\begin{bmatrix} I_L \\ z^{-1}I_L \\ \vdots \\ z^{-(Q/L)+1}I_L \end{bmatrix}}_{Q\times L\ (\triangleq B(z))}$$

Analysis filter bank. Using the prototype filter $A_o(z)$ in (27.187) we now construct an analysis filter bank consisting of N subband filters $\{A_k(z)\}$ that are chosen as the following modulated versions of $A_o(z)$:

$$\boxed{A_k(z) = A_o\left(ze^{-\frac{j2\pi k}{N}}\right), \quad k = 0, 1, \dots, N-1} \tag{27.191}$$

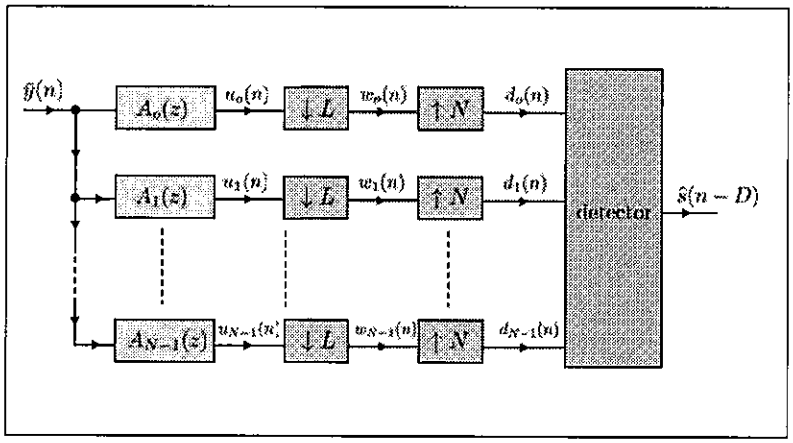

FIGURE 27.55 Receiver module in a communications transmultiplexer. The received sequence $\bar{y}(n)$ is fed into an analysis filter bank with N subband filters, followed by downsamplers by a factor L. The signals are subsequently upsampled by a factor N and fed into a detector or decision device to recover the transmitted data with some delay, $\hat{s}(n-D)$. We are denoting the intermediate signals by $\{u)k(n), w_k(n), d_k(n)\}$ for later reference. The OFDM structure of Figs. 27.48 and 27.50 will be seen to correspond to the special choice (27.186) for the prototype filter $A_o(z)$. In the sequel we show how the subband filters in the above figure can be implemented in terms of a DFT-based structure, which will bring us closer to Fig. 27.48.

The impulse response sequences of the subband filters $A_k(z)$ are then related to the impulse response sequence of the prototype filter $A_o(z)$ as:

$$\boxed{a_k(n) \;=\; W^{kn} \cdot a_o(n), \quad \begin{cases} k = 0, 1, \ldots, N-1 \\ n = 0, 1, \ldots, Q-1 \end{cases}} \tag{27.192}$$

We can express this relation in vector form as follows:

$$\begin{bmatrix} a_k(0) & a_k(1) & \ldots & a_k(Q-1) \end{bmatrix} = \tag{27.193}$$

$$\begin{bmatrix} 1 & W^k & W^{2k} & \ldots & W^{(Q-1)k} \end{bmatrix} \cdot \begin{bmatrix} a_o(0) & & & \\ & a_o(1) & & \\ & & \ddots & \\ & & & a_o(Q-1) \end{bmatrix}$$

As was done earlier to arrive at (27.175), the above relation can be simplified by exploiting the fact that Q is a multiple of N and W is the N-th root of unity to get:

$$\boxed{\begin{bmatrix} a_k(0) & a_k(1) & \ldots & a_k(Q-1) \end{bmatrix} = \underbrace{\begin{bmatrix} 1 & W^k & \ldots & W^{(N-1)k} \end{bmatrix}}_{1 \times N} \cdot \mathcal{J} \cdot \mathcal{A}} \tag{27.194}$$

where

$$\boxed{\mathcal{A} \triangleq \begin{bmatrix} a_o(0) & & & \\ & a_o(1) & & \\ & & \ddots & \\ & & & a_o(Q-1) \end{bmatrix} \quad (Q \times Q)} \tag{27.195}$$

Using (27.194), we can relate the polyphase components of the subband filters $A_k(z)$ to the prototype impulse response sequence $\{a_o(n)\}$, just like we did earlier in (27.190) for the prototype filter. Thus, let $E_{k,m}(z)$ denote the polyphase components of $A_k(z)$ of order L so that:

$$A_k(z) = \sum_{m=0}^{L-1} z^{-m} E_{k,m}(z^L) \tag{27.196}$$

These polyphase components are defined in terms of the impulse response coefficients $\{a_k(n)\}$ as follows:

$$E_{k,m}(z) = \sum_{n=0}^{\frac{Q}{L}-1} a_k(nL+m) z^{-n} \tag{27.197}$$

As was done to arrive at (27.190), it is again straightforward to verify that, for the $k-$th subband filter:

$$\begin{bmatrix} E_{k,o}(z) & E_{k,1}(z) & \ldots & E_{k,L-1}(z) \end{bmatrix} = \begin{bmatrix} a_k(0) & a_k(1) & \ldots & a_k(Q-1) \end{bmatrix} \cdot B(z) \tag{27.198}$$

for the same matrix $B(z)$ as in (27.163). But since we know from (27.192) how to relate the impulse response sequence $\{a_k(n)\}$ to that of the prototype filter, we can rework expression (27.198) into a form that depends on the prototype impulse response sequence. Thus, using (27.192) and (27.198) we can write

$$\begin{bmatrix} E_{k,o}(z) & E_{k,1}(z) & \ldots & E_{k,L-1}(z) \end{bmatrix} = \begin{bmatrix} 1 & W^k & \ldots & W^{(N-1)k} \end{bmatrix} \cdot \mathcal{J} \cdot \mathcal{A} \cdot B(z) \tag{27.199}$$

Collecting relation (27.199) for $k = 0, 1, \ldots, N-1$ gives

$$\begin{bmatrix} E_o(z) & E_1(z) & \ldots & E_{L-1}(z) \\ E_{1,o}(z) & E_{1,1}(z) & \ldots & E_{1,L-1}(z) \\ E_{2,o}(z) & E_{2,1}(z) & \ldots & E_{2,L-1}(z) \\ \vdots & \vdots & & \vdots \\ E_{N-1,o}(z) & E_{N-1,1}(z) & \ldots & E_{N-1,L-1}(z) \end{bmatrix} = F \cdot \mathcal{J} \cdot \mathcal{A} \cdot B(z) \tag{27.200}$$

where F is the $N \times N$ DFT matrix, for example, for $N = 4$:

$$F = \begin{bmatrix} 1 & 1 & 1 & 1 \\ 1 & W_4 & W_4^2 & W_4^3 \\ 1 & W_4^2 & W_4^4 & W_4^6 \\ 1 & W_4^3 & W_4^6 & W_4^9 \end{bmatrix} \tag{27.201}$$

Using (27.196), we conclude that the subband filters $\{A_k(z)\}$ satisfy:

$$\boxed{\begin{bmatrix} A_o(z) \\ A_1(z) \\ A_2(z) \\ \vdots \\ A_{N-1}(z) \end{bmatrix} = F \cdot \mathcal{J} \cdot \mathcal{A} \cdot B(z^L) \cdot \begin{bmatrix} 1 \\ z^{-1} \\ z^{-2} \\ \vdots \\ z^{-(L-1)} \end{bmatrix}} \tag{27.202}$$

Referring to Fig. 27.55, we find that the signals $\{u_k(n)\}$ at the output of the analysis subband filters are given in the z--transform domain by:

$$\begin{bmatrix} U_o(z) \\ U_1(z) \\ \vdots \\ U_{N-1}(z) \end{bmatrix} = \begin{bmatrix} A_o(z) \\ A_1(z) \\ \vdots \\ A_{N-1}(z) \end{bmatrix} \cdot \bar{Y}(z) = F \cdot \mathcal{J} \cdot \mathcal{A} \cdot B(z^L) \cdot \begin{bmatrix} 1 \\ z^{-1} \\ z^{-2} \\ \vdots \\ z^{-(L-1)} \end{bmatrix} \cdot \bar{Y}(z) \tag{27.203}$$

This result indicates that the receiver structure of Fig. 27.55 admits the filter bank implementation shown in Fig. 27.56; in this implementation, we are able to move the upsamplers and downsamplers and place them before the DFT operation as shown in the figure for the case $N = 4$, $Q = 12$, and $L = 6$.

Detector. We explained earlier in Fig. 27.51 the structure of the detector block in the OFDM case: it involved scaling the signals $\{d_k(n)\}$ by $\{1/\lambda_k\}$ and aggregating the result to obtain $\hat{s}(n - P)$. In other words, for OFDM transceivers, equalization can be achieved by means of one-tap equalization (with the scalars $1/\lambda_k$ serving as the equalization coefficients). For more general prototype filters $\{S_o(z), A_o(z)\}$, which need not correspond to rectangular windows, the detection block in Fig. 27.56 will generally be more involved. In Sec. 28.6 we illustrate how the synthesis and analysis filters $\{S_k(z), A_k(z)\}$ in the transmultiplexer structure of Fig. 28.21 can be selected in order to ensure that one-tap equalization is still possible in the general case (see expression (28.162) and the explanation leading to Fig. 28.25). It is again immediate to verify that when $A_o(z)$ is chosen as in (27.186), with $P = 2$ and $a_o(4) = \ldots = a_o(11) = 0$, then the structure of Fig. 28.25 (prior to the detector) reduces to the OFDM receiver structure of Fig. 27.51 for $N = 4$ and $L = 6$.

Practice Questions:

1. Use (27.162) to establish (27.163).
2. Use (27.161) and (27.169) to show that

$$S_k(z) = \sum_{m=0}^{L-1} z^{-m} W_N^{-mk} P_m\left(z^L W^{kL}\right) \tag{27.204}$$

   in terms of the polyphase components of $S_o(z)$.
3. Start from the above expression for $S_k(z)$ and establish (27.184).
4. Assume $N = 4$, $L = 6$, and select the prototype filter as

$$S_o(z) = 1 + z^{-1} + z^{-2} + z^{-3} + z^{-4} + z^{-5} \tag{27.205}$$

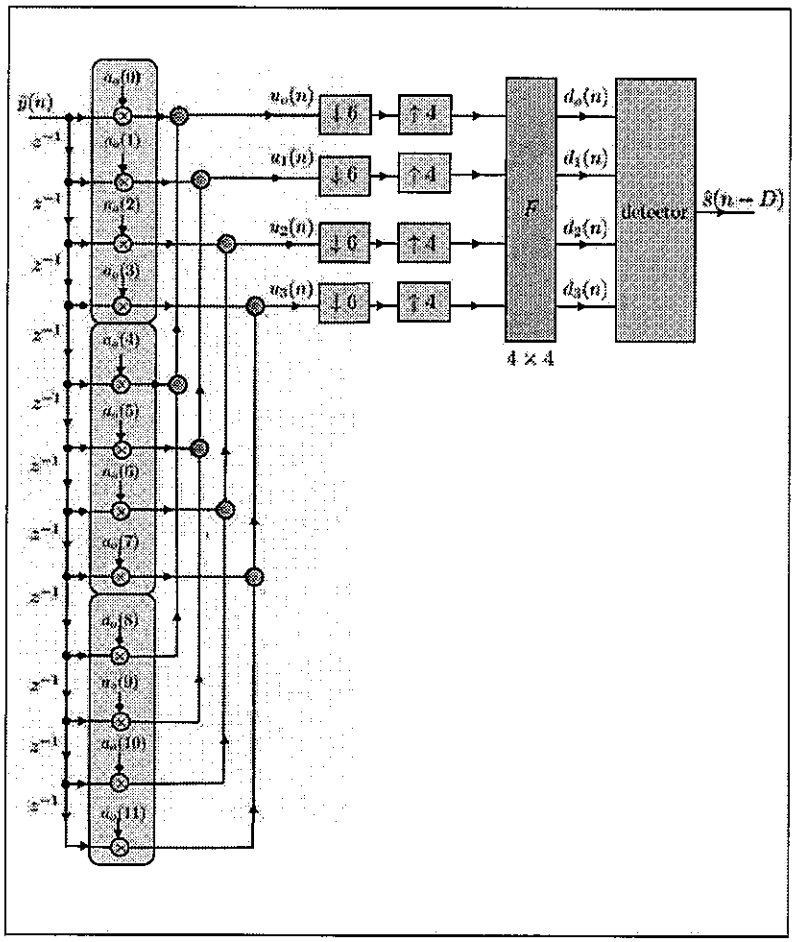

FIGURE 27.56 Receiver module in a communications transmultiplexer. An equivalent filter bank implementation of the structure shown earlier in Fig. 27.54 in terms of the DFT operation for the case $N = 4$, $Q = 12$, and $L = 6$.

Verify that the transmitter structure of Fig. 27.54 reduces to the OFDM transmitter structure of Fig. 27.48.

5. Assume $N = 4$, $L = 6$, and select the prototype filter as

$$A_o(z) = 1 + z^{-1} + z^{-2} + z^{-3} \tag{27.206}$$

Verify that the receiver structure of Fig. 27.56 reduces to the OFDM receiver structure of Fig. 27.51 (apart from the detection module).

◇

27.7 REFERENCES AND COMMENTARIES

Johnston filters (and tables) QMF filters perfect reconstruction filter banks reference for general designs of PR for for than two branches transmultiplexers

27.8 PROBLEMS

P 27.1 Consider the prototype filter

$$A_o(z) = 1 + \frac{1}{2}z^{-1} + \frac{1}{3}z^{-2} + \frac{1}{2}z^{-3} + z^{-4}$$

(a) Draw the corresponding uniform analysis filter bank of Fig. 27.7 assuming $M = 4$. Determine the filters $A_k(z)$.

(b) Repeat using the DFT analysis filter bank of Fig. 27.17. Determine the filters $E_k(z)$.

P 27.2 Consider the prototype filter

$$A_o(z) = 1 - \frac{1}{2}z^{-1} + \frac{1}{4}z^{-2} - \frac{1}{2}z^{-3} + z^{-4}$$

(a) Draw the corresponding uniform analysis filter bank of Fig. 27.7 assuming $M = 5$. Determine the filters $A_k(z)$.

(b) Repeat using the DFT analysis filter bank of Fig. 27.17. Determine the filters $E_k(z)$.

P 27.3 Consider the prototype filter

$$S_o(z) = 1 + \frac{1}{2}z^{-1} + \frac{1}{3}z^{-2} + \frac{1}{2}z^{-3} + z^{-4}$$

(a) Draw the corresponding uniform synthesis filter bank of Fig. 27.22 assuming $M = 4$. Determine the filters $S_k(z)$.

(b) Repeat using the DFT synthesis filter bank of Fig. 27.29. Determine the filters $P_k(z)$.

P 27.4 Consider the prototype filter

$$S_o(z) = 1 - \frac{1}{2}z^{-1} + \frac{1}{4}z^{-2} - \frac{1}{2}z^{-3} + z^{-4}$$

(a) Draw the corresponding uniform synthesis filter bank of Fig. 27.22 assuming $M = 5$. Determine the filters $S_k(z)$.

(b) Repeat using the DFT synthesis filter bank of Fig. 27.29. Determine the filters $P_k(z)$.

P 27.5 Consider the filter bank shown in Fig. 27.57, which is similar to the filter bank we encountered earlier in Fig. 27.19.

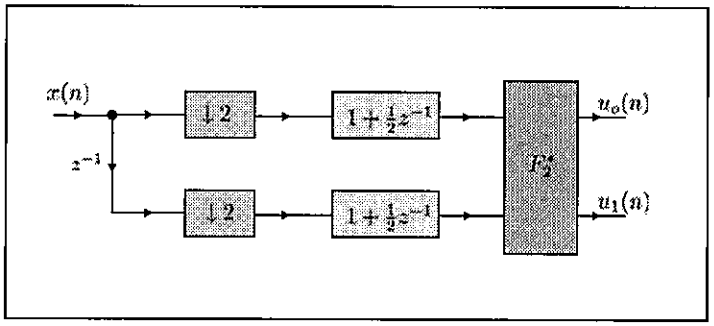

FIGURE 27.57 Analysis filter bank for Prob. 27.5.

(a) Determine the corresponding prototype filter, $A_o(z)$.

(b) Draw the corresponding uniform filter bank structure according to Fig. 27.7.

(c) Find the equivalent DFT analysis filter bank using $M = 4$ (cf. Fig. 27.17).

(d) What are the transfer functions from $x(n)$ to $u_o(n)$ and from $x(n)$ to $u_1(n)$?

P 27.6 Consider the synthesis filter bank shown in Fig. 27.58, which is similar to the filter bank we encountered earlier in Fig. 27.24.

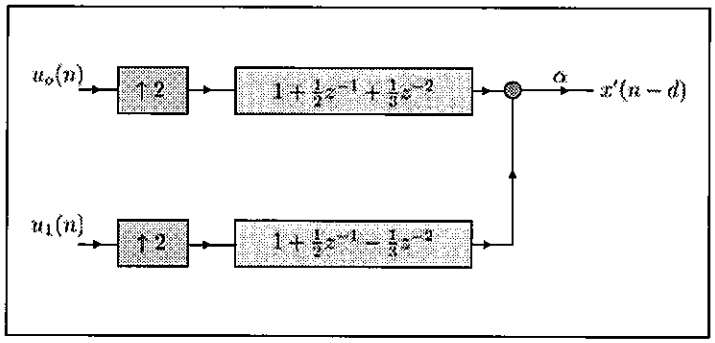

FIGURE 27.58 Synthesis filter bank for Prob. 27.6.

(a) Determine the corresponding prototype filter, $S_o(z)$.

(b) Draw the corresponding uniform filter bank structure according to Fig. 27.22.

(c) Find the equivalent DFT synthesis filter bank using $M = 4$ (cf. Fig. 27.29).

P 27.7 Consider the subband processing structure shown in Fig. 27.59. Let $A_o(z) = 1 + z^{-1}$ and $S_o(z) = 1 + z^{-1}$.

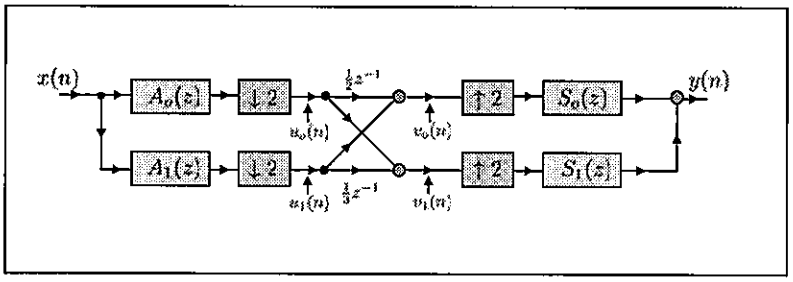

FIGURE 27.59 Subband processing structure for Prob. 27.7.

(a) Draw the corresponding DFT-based structure according to Fig. 27.31.

(b) Express $U_o(z)$ and $U_1(z)$ in terms of $X(z)$.

(c) Express $V_o(z)$ and $V_1(z)$ in terms of $X(z)$.

(d) Express $Y(z)$ in terms of $X(z)$.

P 27.8 Consider the 2-branch filter bank of Fig. 27.37 with $A_o(z) = 1+\frac{1}{2}z^{-1}$, $A_1(z) = 1-\frac{1}{2}z^{-1}$, $S_o(z) = 2 + z^{-1}$, and $S_1(z) = 2 - z^{-1}$.

(a) Is the filter bank alias-free?

(b) Is the filter bank a perfect reconstruction filter?

(c) Is the filter bank a perfect reconstruction filter with analysis and synthesis filters that are FIR?

(d) Is the filter bank a QMF?

(e) It the filter bank an orthogonal reconstruction filter?

(f) What is the transfer function from $x(n)$ to $y(n)$?

P 27.9 Design an orthogonal perfect reconstruction filter with $L = 2$ branches and a prototype filter $A_o(z)$ of duration $N = 8$.

P 27.10 Use (27.20) to show that

$$\begin{bmatrix} E_o(z^M) \\ z^{-1}E_1(z^M) \\ z^{-2}E_2(z^M) \\ \vdots \\ z^{-(M-1)}E_{M-1}(z^M) \end{bmatrix} = \frac{1}{M}F_M \begin{bmatrix} A_o(z) \\ A_1(z) \\ A_2(z) \\ \vdots \\ A_{M-1}(z) \end{bmatrix}$$

This useful result allows the user to determine the $M-$th order polyphase decomposition of an IIR filter, $A_o(z)$, in terms of the filters $A_k(z)$.

P 27.11 Use the result of Prob. 27.10 to determine second and third-order polyphase decompositions of the filter

$$H(z) = \frac{1 - \frac{1}{25}z^{-2}}{1 - \frac{1}{4}z^{-1} - \frac{1}{8}z^{-2}}$$

Draw the decompositions in a manner similar to Fig. 26.24.

P 27.12 Find the second-order type-I polyphase components of the transfer functions

$$A_o(z) = \frac{1}{2}\left(1 + z^{-1}\right), \quad A_1(z) = 1 - z^{-1}$$

Likewise, find the second-order type-II polyphase components of the transfer functions

$$S_o(z) = 1 + z^{-1}, \quad S_1(z) = -\frac{1}{2}\left(1 - z^{-1}\right)$$

P 27.13 Consider the $M-$branch filter bank shown in Fig. 27.60 where the analysis and synthesis filters are not necessarily obtained by uniformly shifting an underlying prototype filter. In the case of a uniform filter bank, we showed in Figs. 27.17 and 27.29 how to obtain efficient DFT-based implementations. In this problem, we assume generic analysis and synthesis filters.

Introduce the $M-$th order type-I polyphase decomposition of the filters $A_k(z)$:

$$A_k(z) = \sum_{m=0}^{M-1} z^{-m}E_{km}(z^M), \quad k = 0, 1, \ldots, M-1$$

and the $M-$th order type-II polyphase decomposition of the filters $S_k(z)$:

$$S_k(z) = \sum_{m=0}^{M-1} z^{-(M-1-m)}R_{mk}(z^M), \quad k = 0, 1, \ldots, M-1$$

Adjust the arguments of Secs. 27.1 and 27.2 to show that the realization of Fig. 27.60 can equivalently be implemented in terms of the polyphase components $E_{mk}(z)$ and $R_{mk}(z)$ as shown in Fig. 27.61, where $\mathcal{E}(z)$ and $\mathcal{R}(z)$ denote $M \times M$ matrices with entries

$$\mathcal{E}(z) = [E_{km}(z)]_{k,m=0}^{M-1}, \quad \mathcal{R}(z) = [R_{mk}(z)]_{k,m=0}^{M-1}$$

P 27.14 Consider the non-uniform filter bank of Prob. 27.13. We say that the filter bank satisfies a perfect reconstruction condition when the output sequence, $y(n)$, is a delayed version of the input sequence, $x(n)$. Show that the filter bank is a perfect construction filter bank when the matrices $\mathcal{E}(z)$ and $\mathcal{R}(z)$ satisfy the condition

$$\mathcal{E}(z)\mathcal{R}(z) = z^{-d}I_M$$

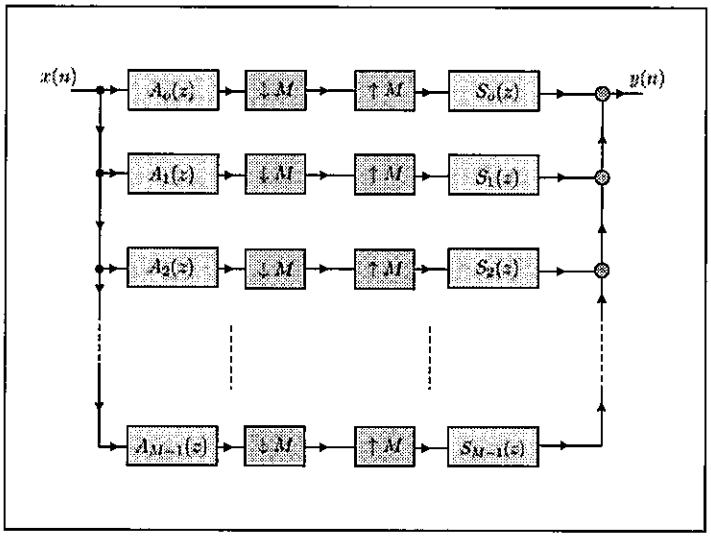

FIGURE 27.60 A non-uniform filter bank with M branches for Prob. 27.13.

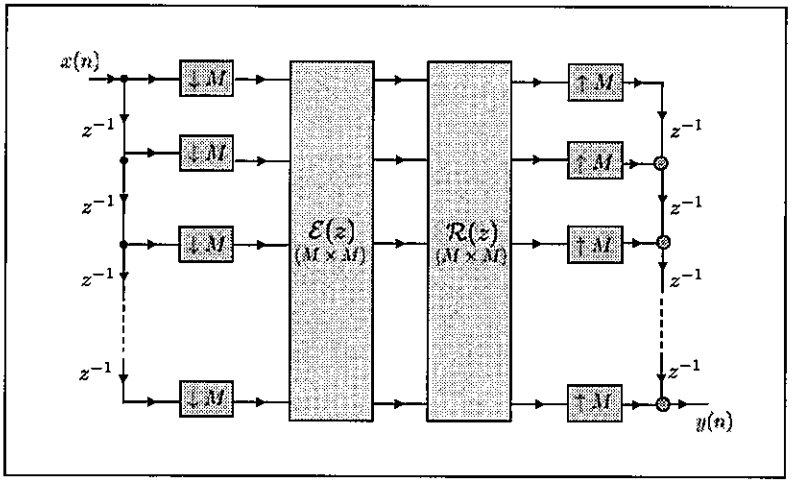

FIGURE 27.61 An equivalent realization of the non-uniform filter bank of Fig. 27.60 in terms of the polyphase components $E_{km}(z)$ and $R_{km}(z)$ for the analysis and synthesis filters, $A_k(z)$ and $S_k(z)$, respectively.

for some delay, d, and where I_M denotes the $M \times M$ identity matrix.

P 27.15 Consider a 2−branch non-uniform filter bank as in Fig. 27.60 with analysis and synthesis filters given by

$$\begin{aligned} A_o(z) &= \left(1+z^{-1}\right)/2, \qquad A_1(z) = 1 - z^{-1} \\ S_o(z) &= 1 + z^{-1}, \qquad\quad S_1(z) = -\left(1 - z^{-1}\right)/2 \end{aligned}$$

(a) Find the corresponding polyphase realization as in Fig. 27.61, i.e., determine the 2×2 matrices $\mathcal{E}(z)$ and $\mathcal{R}(z)$.

(b) Show that the resulting filter bank is a perfect reconstruction filter bank.

(c) Express $y(n)$ in terms of $x(n)$.

(d) Plot the frequency responses of the analysis and synthesis filters.

Remark. This is an example of a filter bank that leads to perfect reconstruction despite the fact that the analysis and synthesis filters are not ideal. The resulting filter bank is known as the Haar filter bank, which we encountered earlier in Sec. 26.5 while discussing subband coding.

P 27.16 Consider the 2−branch filter bank of Fig. 27.37. Let $A_o(z)$ denote a low-pass causal and stable prototype filter with second-order polyphase decomposition given by

$$A_o(z) = E_o(z^2) + z^{-1}E_1(z^2)$$

Assume the other filters are chosen as follows:

$$A_1(z) = A_o(-z), \quad S_o(z) = A_1(-z), \quad S_1(z) = -A_o(-z)$$

Show that the filter bank can be equivalently implemented in terms of the polyphase components of $A_o(z)$ in the manner shown in Fig. 27.62.

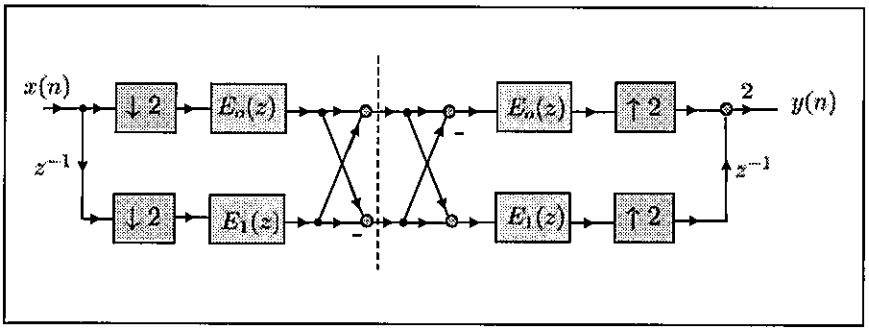

FIGURE 27.62 A polyphase implementation of the quadrature mirror filter bank of Prob. 27.16.